ISSN 0280-5316
ISRN LUTFD2/TFRT--5851--SE

Truck Differential and Rear Axle Modeling

Rikard Bengtsson
Jasper Gundersen

Department of Automatic Control
Lund University
May 2010

Lund University
Department of Automatic Control
Box 118
SE-221 00 Lund Sweden

Document name
MASTER THESIS

Date of issue
May 2010

Document Number
ISRN LUTFD2/TFRT--5851--SE

Author(s)
Rikard Bengtsson and Jasper Gundersen

Supervisor
Edo Drenth and Ola Nockhammar Haldex, Landskrona
Rolf Johansson Automatic Control, Lund (Examiner)

Sponsoring organization

Title and subtitle
Truck Differential and Rear Axle Modeling (Modellering och reglering av drivaxel på lastvagn)

Abstract
Physical modeling of the driveline is crucial in many areas within the commercial vehicle industries. To have an accurate model helps the understanding of physical phenomena and is important when performing computational tests and when designing, for example, traction controllers. The differential gear is often modeled as simple as possible, neglecting more complex behaviour. The main goal with this thesis is to create a model of the differential that takes into account some of these neglected properties. To be able to test and observe the behaviour of the differential, a complete driveline is modeled, extending from the engine to the wheels. The driveline model is then validated using existing measurement data. The results from the tests performed on the model show that there are minor differences on the wheel velocities if the differential is modeled using a more physical approach. Especially the differential behavior have been shown to accurately describe some of the important features, improving model usability. Implementation of a more complex differential model depends on the area of usage of the model. In addition to driveline modeling, a novel traction controller has been developed and implemented, using the model developed. The controller has shown interesting features such as constraints and prediction, however, further investigations are required to achieve desired performance.

Keywords

Classification system and/or index terms (if any)

Supplementary bibliographical information

ISSN and key title
0280-5316

ISBN

Language
English

Number of pages
100

Recipient's notes

Security classification

Acknowledgements

Begin at the beginning and go on till you come to the end - then stop!

At last, it seems, we have come to the end and it is time to stop - our work at Haldex is done. Although, without a doubt, the most interesting, fun and challenging experience during our time at the university, doing our master thesis work has at times been both exhausting and frustrating - the need for support and encouragement has therefore been crucial.

Our sincere thanks to Edo Drenth and Ola Nockhammar, supervising us at Haldex. Their support and profound knowledge in modeling and vehicle dynamics have been truly invaluable. They have constantly challenged us to improve, which has been greatly appreciated, and it has been a privilege to work with them. Further, the support from Dr. Rolf Johansson, LTH, has been of great importance. Though often on the move and involved in a vast number of projects, he has always found time for our questions - thank you! Also, thanks to Anders Widd for his help with the sections on MPC. At last, we would like to thank our friends and families for their never-ending support - you guys are great!

Master thesis - done!

Rikard Bengtsson & Jasper Gundersen, Lund 2010

Contents

1 Introduction

1.1 Problem formulation and objectives

The task is to derive a physical model of the dynamic behaviour of a truck differential and rear axle. The derived model is mainly to be used for traction control development in the simulation environment, i.e. Matlab/Simulink. To further study the model usability, a traction controller on the engine system and the brake system is to be designed and implemented.

1.2 Traction control

The maximum torque generated between wheel and road, without the wheels spinning, is often referred to as *traction*. For the vehicle to be driven forward, the total traction for all wheels must exceed the resistance, i.e. the load torque on the wheels. The load torque is determined by factors such as road inclination and road conditions, vehicle load, the tires used etc. Should the road conditions limit the available traction under one or several of the driven wheels, so that it exceeds the limit traction of the road-tyre interface without exceeding the threshold torque, one or more wheels will spin. As will be explained in the section on wheel dynamics, a spinning wheel has reduced longitudinal traction as well as reduced lateral stability, due to its inability to utilize maximum friction. *Traction control* is the use of mechanisms or control algorithms to prevent loss of traction due to excessive throttle applied by the user in comparison to the threshold torque, thus ensuring control of the vehicle at all times. Loss of traction often occur for "μ-split" conditions, i.e. when the available friction at each wheel causes the load torque of the driven wheels to differ, rapid acceleration causing a burnout or overall friction reduction, e.g. when driving on ice. Typically, μ-split conditions occurs for ice patches or for pools of water causing hydroplaning. Traction control algorithms can control either the engine torque, the brake torque, or, most often, a combination of the two. Control of the brake torque is typically used when a single wheel spins, or when the slip behaviour between wheels differ, while control of the engine torque is typically used when two wheels spin simultaneously. Furthermore, brake torque control is often applied initially and its influence on the total drive torque reduction decreases rapidly over time in favour of engine torque control. Mechanical traction controllers are described in the next section.

1.3 Differential gear

An *open differential gear*, in this thesis simply referred to as a differential, is a mechanical transmitter of torque and rotation. It is used in vehicles on the driving wheels, transmitting equal torque to each wheel and allowing the wheels to turn with different angular velocity. This is necessary when cornering, since the inner wheel rotates with a lower angular velocity than the outer wheel, due to the larger curve radii of the latter. Without a differential, i.e. with a spool, tension would build up due to the inability of the wheels to rotate with different angular velocities, causing one of the wheels to spin, or scrub, on the pavement. This is highly undesirable, since a spinning wheel results in loss of traction and therefore loss of vehicle control. In addition, it would result in increased tire-wear and fatigue as well as driveline resonance vibrations, due to the stick-slip release of the tires, [3]. The splitting of torque is the motive for using a differential in vehicles - in other applications a differential may as well be used to com-

bine two inputs to one output, which is equal to the average or the sum of the inputs.

In Fig. 1.1, the components and structure of a differential gear is illustrated. The propeller shaft, which transfers the torque from the transmission, ends in the *pinion gear* which connects to the *crown wheel*. Mounted on the carrier of the crown wheel, are two *planet gears* which are the essential component of a differential, since these small gears allow for different velocities of the *side gears*, i.e. the drive shafts.

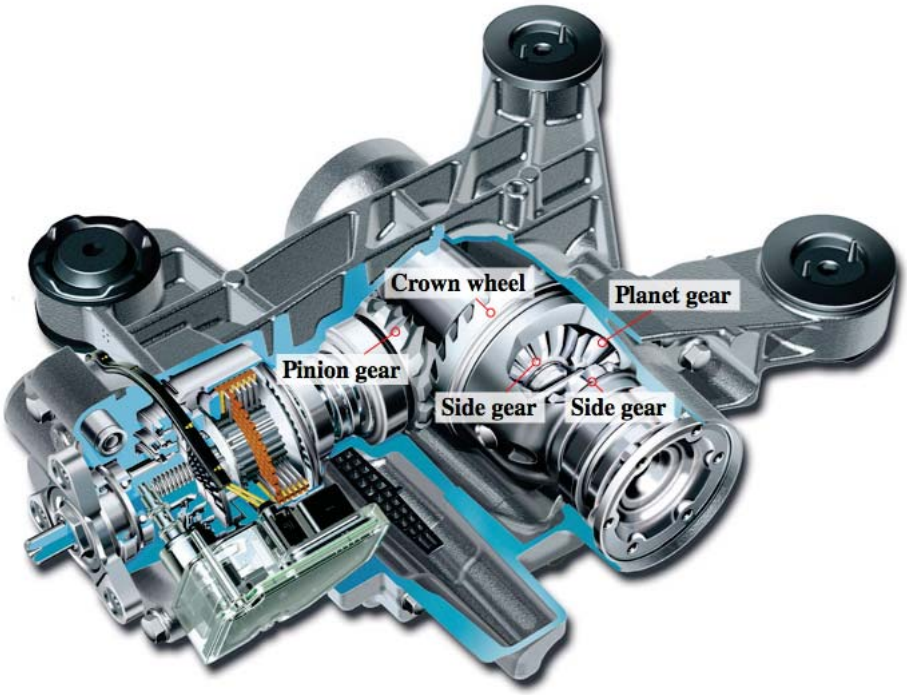

Figure 1.1: Differential gear

The ability to allow the vehicle drive shafts to move with different angular velocities is, however, also one of the major downsides with using a differential. Although equal torque distribution is desirable during normal driving conditions, it is rather unsatisfactory during μ-split conditions. Without a differential, i.e. a spool or a locked differential, maximum traction can be obtained at all wheels resulting in an overall traction equal to the sum of the maximum traction at each driven wheel. Locked differentials are common for off-road vehicles thus enabling maximum traction at all times, while limiting the performance when driving at pavement. However, for a differential driven vehicle, should one of the driving wheels reach its maximum traction and start to spin, the equal distribution of torque will result in the other wheel possibly generating insufficient traction to overcome the threshold torque. The total overall traction is, as with a locked differential, the sum of the traction at each wheel. However, with one wheel spinning and the other not being able to overcome its resistance, the traction is approximately twice that available at the wheel with least friction [3], which may be insufficient to drive the vehicle.

As previously stated, traction control is needed to prevent the loss of traction. In addition to using control algorithms to actively prevent excessive wheel slip, many vehicles are equipped with a mechanical traction control. This is often referred to as a self-acting traction devices, or passive traction devices, since there is no external signal acting upon it, [3]. Self-acting torque control differentials can be of two types, torque sensitive or speed sensitive. An example of the latter is a differential combined with a simple viscous coupling. Of the torque sensitive controllers, a widely used type is the multi-plate clutch. The multi-plate consists of a clutch cage to which a set of pressure plates are attached [4]. The pressure plates are attached so that the clutch cage and plates are forced to rotate together, while the plates can also move in an axial direction. The clutch cage is connected to the input shaft and friction plates attached to the output shaft connects the input shaft and output shaft. When the plates are in contact, a friction torque is generated by the clutch, resisting differential motion. Thus, the difference between the shaft torques must exceed the friction torque for the clutch to differentiate, causing the friction plates to slip resulting in a transfer of torque from the spinning wheel axis to the high friction side [3]. The use of self-acting traction control differentials is however outside the scope of this thesis and an open differential is assumed further on.

1.4 Previous work

Modeling of the driveline is needed to develop traction controllers and focus tend to lie on the latter rather than the former. Publications therefore tend to omit modeling, instead using simplified models assumed to be known from literature such as [5]. However, an extensive approach to model the dynamics of the driveline can be found in [1] and [2], in which several models of various complexity are presented. The more complex models in [1] are developed to capture as much of the dynamics as possible and differ from other approaches in that the influence on overall dynamics of components generally assumed rigid, are investigated. Common for all approaches known to the authors, however, is that the dynamics of the differential gear are omitted. The simplest models available considers the differential as a power distributor, ignoring nonlinear phenomena such as backlash and friction. More complex models take into account the friction, using a rather crude viscous friction model [1, 2].

1.5 Outline

Section 2
Nonlinearity properties are discussed in Section 2, presenting various backlash models as well as friction models.

Section 3
In Section 3, the driveline component models are presented. The section is divided into a driveline part, describing the dynamics from engine to drive shafts, and a wheel dynamics part, describing the wheel and tyre dynamics.

Section 4
Section 4 describes the system properties, simplifications made and expected nonlinearities. The parameter choices used in the model are described as is various simulation problems.

Finally, the validation tests are presented.

Section 5
In Section 5, the details on the control strategy are described.

Section 6
The actual implementation of the control strategy is presented in Section 6, describing both linearization considerations as well as a simplified plant model.

Section 7
In Section 7, the results when validating the model are presented. Also, a presentation of the results when implementing the controller is given.

2 Nonlinearities in driveline

2.1 Backlash

The clearing of mating components, such as gears for example, is called *backlash*. Some backlash is necessary, to allow for thermal expansion and lubrication, though it can also be due to imperfections in the gears. While backlash may be required, it introduces a nonlinearity in the driveline that may cause undesired behaviour. If the process should be reversed when in contact on one side, the backlash must be traversed for the gears to have contact on the other side. This behaviour is called a *hysteresis*, Fig. 2.1, which in its simplest form can be thought of as a delay. Furthermore, since there is no contact while traversing the backlash, there is no contact force to dampen the acceleration of the gears, other than possible viscous friction. Thus, the impact when the gears connect may have a significant effect on the driveline dynamics. Backlash typically introduces oscillations in the driveline and impacts between gears can generate noise and vibrations.

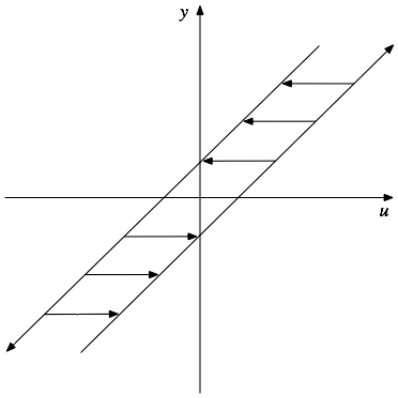

Figure 2.1: Backlash behaviour

There are several components in the driveline in which backlash may occur. Gears are typically found in the transmission, between propeller shaft and differential and in the differential itself. However, since backlash is a known phenomenon, much effort has gone into developing gears that may reduce the effects. An example is bevel gears, where the gear teeth are curved along their length, so that the gears connect gradually in a sliding manner. This reduces both backlash and especially noise and bevel gears can typically be found between the propeller shaft and the differential. The gears in the transmission are generally of high quality, minimizing the imperfections and thus the backlash effects. However, the planet gears in the differential, i.e. the gears that allow for a difference in angular velocity of the driven wheels, are typically of lesser quality. The purpose of the planet gears are not to rotate while driving, but rather to *allow* for a relative rotational difference, e.g. when cornering. Therefore, in this thesis the backlash is assumed to occur between planet gears and side gears.

2.1.1 Dead zone model

Consider a flexible shaft with a backlash gap, Fig. 2.2. The most common model of a backlash is the dead zone model, [6],

$$T = kD_a(\theta_d) \tag{2.1}$$

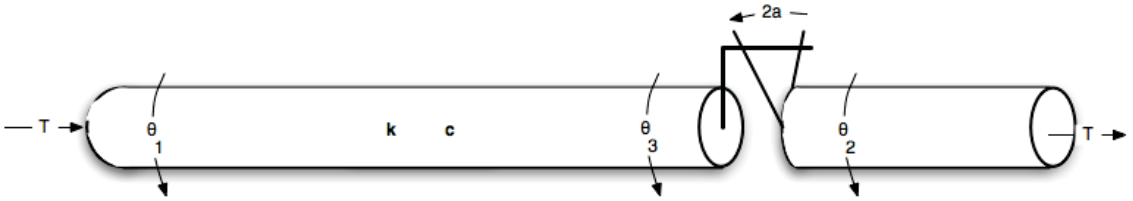

Figure 2.2: Simple backlash model

where

$$D_a(x) = \begin{cases} x - a, & x > a; \\ 0, & |x| \leq a; \\ x + a, & x < -a; \end{cases}$$

and where $\theta_d = \theta_1 - \theta_2$. The flexible shaft is modeled as a spring, inertia-free and without damping. If damping is introduced, the model is often modified as

$$T = \begin{cases} k(\theta_d - a) + c\dot{\theta}_d, & \theta_d > a; \\ 0, & |\theta_d| \leq a; \\ k(\theta_d + a) + c\dot{\theta}_d, & \theta_d < -a; \end{cases}$$

where c is the shaft damping. This modification on the dead-zone model is, however, not physically correct. Should, for instance, the shaft rotate with high velocity through the dead-zone, the damping term would cause a non-physical change of sign of the torque at impact, even though the shafts are in contact. At impact, the shaft may of course bounce back, but this is due to an impact model property rather than a property of the dead-zone. The dead-zone model with damping can be modified as, [6, 7],

$$T = kD_a(\theta_d + c\dot{\theta_d}/k) \tag{2.2}$$

thus including $\dot{\theta}_d$ in the dead zone conditions.

2.1.2 Physical model

A physical model of the backlash can be derived, [6, 7], by introducing an extra state, $\theta_b = \theta_3 - \theta_2$, representing the position of the backlash, Fig. 2.2. The shaft torque can then be derived as

$$T_s = k(\theta_d - \theta_b) + c(\dot{\theta}_d - \dot{\theta}_b) \tag{2.3}$$

assuming inelastic impact when the backlash gap is closed. The case for which $\theta_b > a$, $\dot{\theta}_b = 0$ is referred to as right contact, while the case for which $\theta_b < -a$, $\dot{\theta}_b = 0$ is referred to as left contact. An expression for the backlash angle and the backlash angular velocity can be derived through a phase plane analysis, [6]. However, a simple release condition can be stated using the fact that contact is lost when the sign of the backlash angular velocity is such that it causes the backlash to be traversed, i.e. for right contact, $\dot{\theta}_b < 0$, and for left contact, $\dot{\theta}_b > 0$. By the definition of θ_b, it is clear that for $\theta_b = a$, $\dot{\theta}_b = 0$ (driving

torque) or $\dot{\theta}_b < 0$ (release of contact). For left contact, the conditions are $\dot{\theta}_b = 0$ or $\dot{\theta}_b > 0$. Further, when contact is lost, no torque is transferred, and thus Eq. (2.3) gives

$$0 = T_s = k(\theta_d - \theta_b) + c(\dot{\theta}_d - \dot{\theta}_b) \rightarrow \dot{\theta}_d - \dot{\theta}_b = k/c(\theta_d - \theta_b) \tag{2.4}$$

Using Eq. (2.4) and the conditions for $\dot{\theta}_b$ stated above, θ_b can be expressed as

$$\dot{\theta}_b = \begin{cases} max(0, \dot{\theta}_d + \frac{k}{c}(\theta_d - \theta_b)), & \theta_b = -a; \\ \dot{\theta}_d + \frac{k}{c}(\theta_d - \theta_b) \quad , & |\theta_b| < a; \\ min(0, \dot{\theta}_d + \frac{k}{c}(\theta_d - \theta_b)), & \theta_b = a; \end{cases}$$

The system with backlash is now fully described and the torque is given by Eq. (2.3), using θ_b and $\dot{\theta}_b$ as stated above.

2.2 Friction

Friction is the force that counteracts the relative motion of surfaces and is thus present in every mechanical movement. Considering a vehicle, friction occurs between wheel and ground, the movements inside the engine etc. Since this thesis is concerned with modeling the differential, the friction considered is that between the gears in the differential. To understand the physical effects of friction it is important to have knowledge of some of the phenomena that occur due to friction.

2.2.1 Friction phenomena

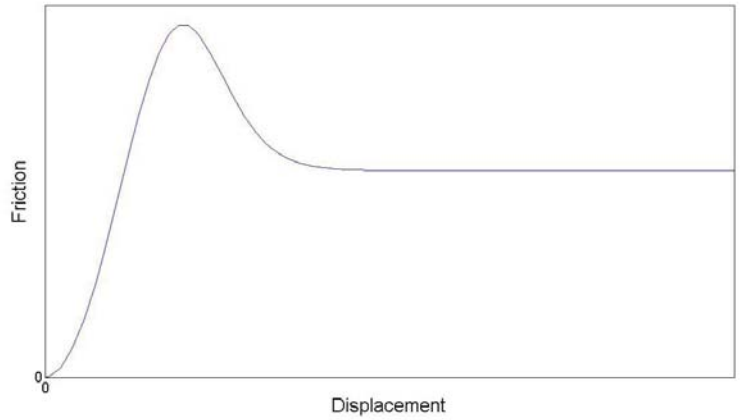

Figure 2.3: Break-away force phenomenon

Friction can be divided into static and dynamic friction. Static friction, also known as stiction, is the friction when objects stick together and dynamic friction is the friction for objects in relative motion. To give objects a relative motion a force needs to be applied that is greater than the static friction, this force is known as the break-away force. Rabinowicz investigated in [14] how friction could be described as a function of displacement, see Fig. 2.3 in which the break-away force results in a peak. As can be seen, there is some displacement before the break-away force is reached. This is known as pre-sliding displacement and is small compared with the displacements when actually in motion. It is, however, worth noting that applying a force and then releasing it before the break-away force is reached give rise to a small permanent displacement. It is also observed that the break-away force is greater than the force needed to keep an object in motion. Frictional lag is another friction phenomena, involving hysteresis. Starting from standstill and increasing the velocity creates a higher frictional force than is generated when decreasing the velocity to standstill.

2.2.2 Classic friction models

Friction is a well investigated area of research and many different friction models have been proposed. Which model to use depends on the importance of different phenomena, and, in addition to recent research, it is worth noting some of the classic models [15].

The most convenient way to handle friction is as, Fig. 2.4(a),

$$F = \mu_C N sign(v) \tag{2.5}$$

where μ_C is the Coulomb friction coefficient and N is the normal load. This description is known as Coulomb friction. The model states that the magnitude of the friction force is independent of parameters such as the velocity and the area of contact between the surfaces. Because of its simplicity, the Coulomb friction is frequently used. A possible problem with the Coulomb friction model is that it is too simple a model to cover friction phenomena such as break-away force and frictional lag, mentioned above.

While the Coulomb friction model only takes into account the friction between dry surfaces, there is also friction referred to as viscous friction, which originates from the viscosity of lubricants. This can be expressed as

$$F = \eta_v v \tag{2.6}$$

where η_v is the viscous friction coefficient. In Eq. (2.6) the viscous friction is proportional to the velocity between the surfaces, but proportionality is not a necessity and more complicated relationships have been presented, [16]. Viscous friction is often combined with Coulomb friction, see Fig. 2.4(a).

Due to the break-away force mentioned in Section 2.2.1, the friction force is higher for $v = 0$ than for small values of v. Applying this to a friction model for $v = 0$ improves the models description of the friction force, see Fig. 2.4(c),

$$F = \begin{cases} F_e, & v = 0 \quad |F_e| < \mu_s N \\ \mu_s N sign(F_e), & v = 0 \quad |F_e| \geq \mu_s N \end{cases} \tag{2.7}$$

where the parameter F_e is the external forces acting on the object. Thus, the break-away force is given by $\mu_s N$, and when $F_e > \mu_s N$ the object will be accelerated, causing $v \neq 0$, i.e. the friction force can be modeled for example by Coulomb friction, Eq. (2.5), see Fig. 2.4(c).

2.2.3 Stribeck effect

The discontinuity visible in Fig. 2.4(c) for zero velocity has been examined thoroughly and Stribeck observed that the velocity dependence is actually continuous, [15]. This can be seen in Fig. 2.4(d), which is known as a Stribeck curve. This yields that a more accurate model of friction is given by

$$F = \begin{cases} F_s, & v \neq 0 \\ F_e, & v = 0, \quad |F_e| < \mu_s N \\ \mu_s N sign(F_e), & v = 0, \quad |F_e| \geq \mu_s N \end{cases} \tag{2.8}$$

where F_s is an arbitrary function that describes the nonlinearity. A common function used is

$$F_s = \mu_C N + (\mu_s - \mu_C) N e^{-|v/v_s|^{\delta_s}} \tag{2.9}$$

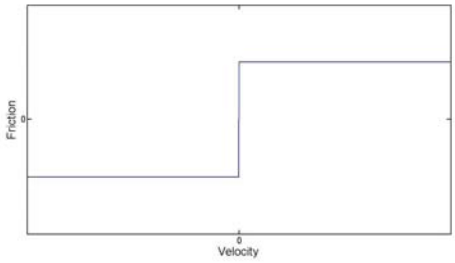

2.4(a) Coulomb friction

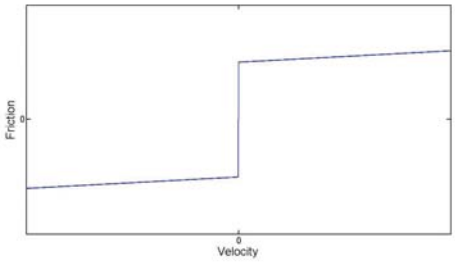

2.4(b) Viscous friction and Coulomb friction

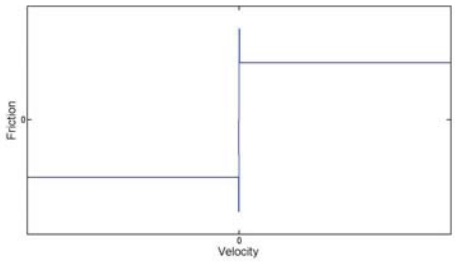

2.4(c) Break away friction

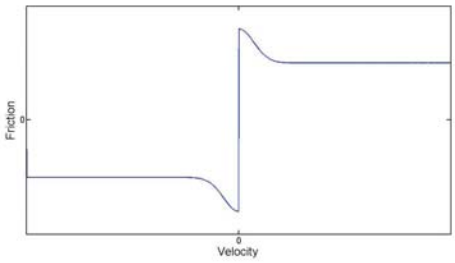

2.4(d) Stribeck friction

Figure 2.4: Different friction models

where v_s is called the Stribeck velocity, indicating how fast the Stribeck effect decreases - a small value results in a fast decrease of the effect, while a large value results in a slow decrease, and where δ_s can be regarded as a shaping factor. This is the arbitrary function used in Fig. 2.4(d).

2.2.4 LuGre model

The friction model named LuGre, an abbreviation of Lund and Grenoble, is one of the most recent contributions within the field of friction research [15, 17]. It was motivated by the lack of complexity of existing models, in that they did not describe the various friction phenomena.

At a microscopic level, surfaces are very irregular and the contact between two surfaces is equivalent to that of many asperities. The LuGre model describes these asperities as elastic bristles that deflects when a tangential force is applied, see Fig. 2.5. However, only a single bristle is observed and so it will have to represent the average behavior for all bristles, see Fig. 2.6. Since only one bristle is used, however, a few aspects need to be taken into consideration. For instance, the bristle can never slip and loose contact, and for constant velocities the bristle will reach a steady-state value. As seen in Fig. 2.6, the average deflection of the bristles is denoted $z$and modeled by

$$\frac{\partial z}{\partial t} = v - \frac{\sigma_0 |v| z}{g(v)} \tag{2.10}$$

where v is the relative velocity between two surfaces and σ_0 is a constant further discussed in Section 2.2.5. The function $g(v)$ accounts for the Stribeck effect and can be

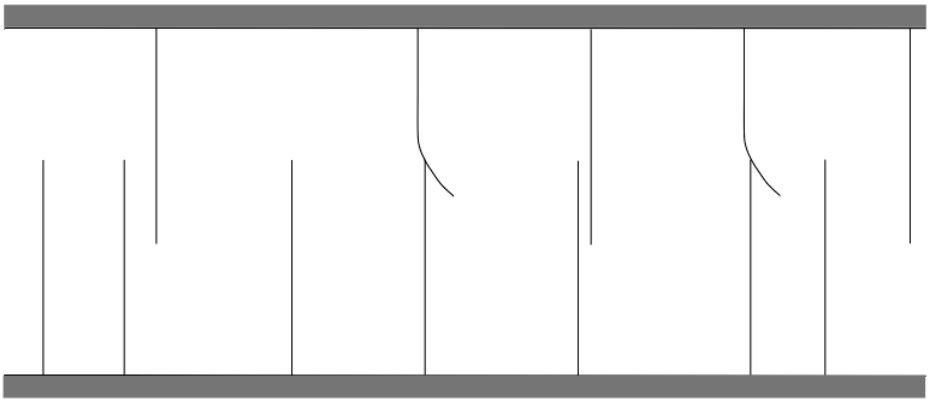

Figure 2.5: Bristles modeling contact asperities

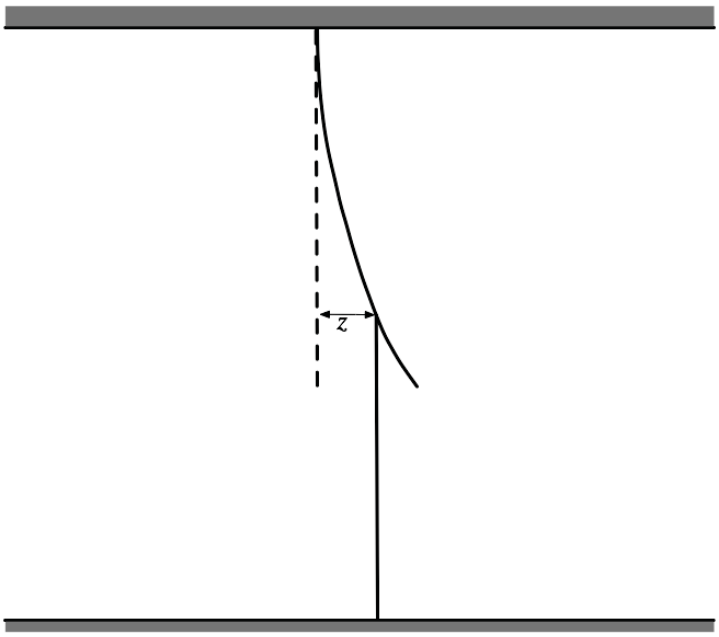

Figure 2.6: Single bristle representing average bristle behaviour

expressed as

$$g(v) = \alpha_0 + \alpha_1 e^{-(v/v_s)^2} \tag{2.11}$$

Comparing equations (2.9) and (2.11) it is clear that α_0 corresponds to $\mu_C N$ and that α_1 corresponds to $(\mu_s - \mu_C)N$, while the shaping factor has been chosen as $\delta_s = 2$. The parameters will be further discussed in Section 2.2.5. The friction force given by the LuGre model is finally derived as

$$F = \sigma_0 z + \sigma_1 \frac{\partial z}{\partial t} + \alpha_2 v \tag{2.12}$$

where $\alpha_2 v$ represents the viscous friction, thus linear to the sliding velocity, and the remaining terms represents dry friction. The LuGre friction model accounts for the fric-

tion phenomena described in Section 2.2.1, as well as for various other phenomena not described further in this thesis. To use the LuGre model efficiently, the parameters $\sigma_0, \sigma_1, \alpha_0, \alpha_1, \alpha_2, v_s$ need to be given proper values.

2.2.5 LuGre Parameters

In total, six parameters need to be analyzed in order to fully understand the dynamics of the LuGre model. To show the impact of these parameters, Fig. 2.7-2.10 are created. Newton's second law of motion is used in the form of Eq. (2.13) for a theoretical case.

$$F - F_{fric} = ma \tag{2.13}$$

Parameter	Value
σ_0	10000 [N/m]
σ_1	200 [Ns/m]
α_0	0.5 [N]
α_1	0.5 [N]
α_2	0.1 [Ns/m]
v_s	1.0 [m/s]

Table 2.1: LuGre friction parameters used in this section

The input force F is defined in Fig. 2.7, where it has been assumed that $m = 10\ kg$ and the parameters for the LuGre friction is set to the values in Table 2.1. The resulting frictional force and velocity can be seen in Fig. 2.8-2.9 respectively.

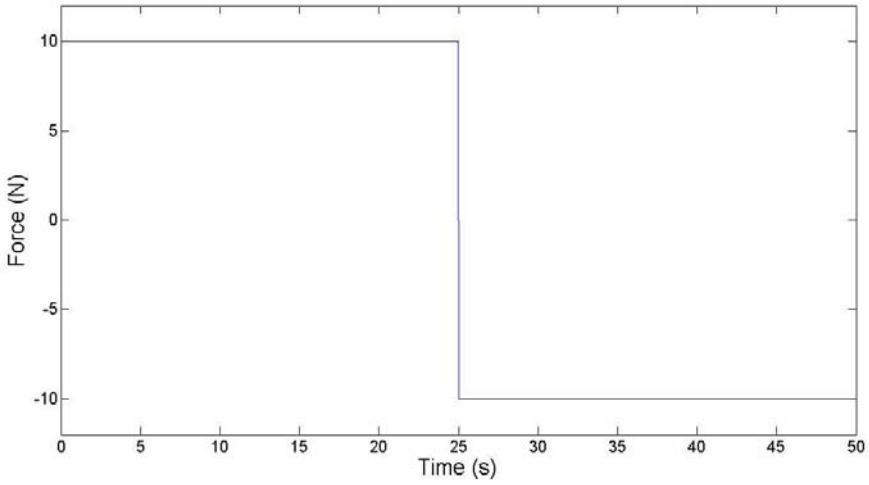

Figure 2.7: Applied force

Considering the resulting figures, the greatest impact seems to appear when the velocity changes sign. To further investigate this impact, the friction force in Fig. 2.8 is considered between $40 - 50\ s$, which is visible in Fig. 2.10. The characteristics of the function $g(v)$,

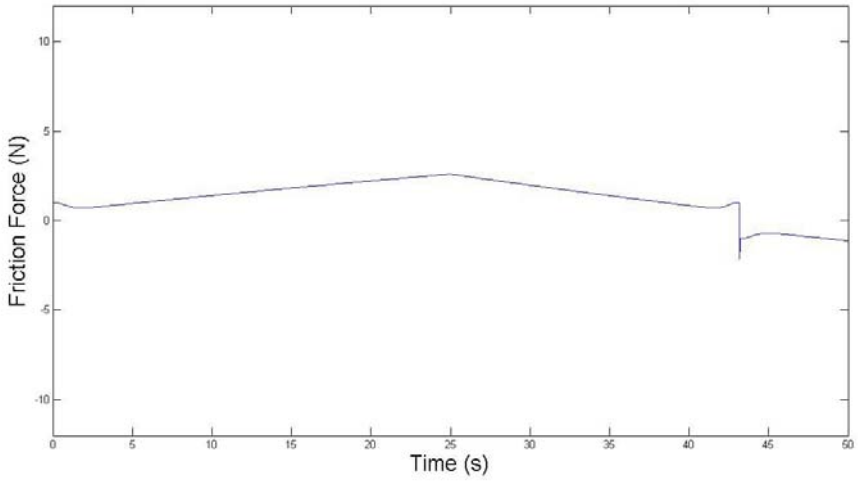

Figure 2.8: Resulting friction force

as well as z and $\frac{\partial z}{\partial t}$ can be seen for the same interval in Fig. 2.11-2.13.

Generally, $\dot{z} = 0\ m/s$, thus, Eq. (2.10) and Eq. (2.12) can be rewritten as

$$z = \frac{g(v)}{\sigma_0} sign(v) \tag{2.14}$$

$$F = \sigma_0 z + \alpha_2 v \tag{2.15}$$

Equation (2.14) shows the $g(v)$ dependency of z. For sufficiently large velocities compared to the Stribeck velocity, $g(v)$ is given by α_0 only, see Eq. (2.11), thus, the friction is only described by the Coulomb friction parameter, α_0, and the viscous friction parameter, α_2. However, when the velocity is in the vicinity of, or lower than, the Stribeck velocity, the value of α_1 has a greater impact. For $v = 0$, the impact of the function $g(v)$ attains its highest value, $\alpha_0 + \alpha_1$, which in this case is equal to $0.5 + 0.5 = 1$, see Fig. 2.11. Due to the velocity sign change, z is subjected to a discontinuity which also has an impact on $\dot{z}$. The value of σ_1 is related to the impact of $\dot{z}$ on the total friction force. Considering Fig. 2.13 and Fig. 2.10 it can be observed that the negative peak is due to $\dot{z}$, i.e. the frictional lag, mentioned briefly in Section 2.2.1, depends on $\dot{z}$.

It is important to study the effects when changes are made in the parameters. Increasing the value of σ_0, for instance, implies a higher bristle deformation resistance, decreasing the values of both z and $\dot{z}$. Changing the value of σ_0 from 10000 N/m to 5000 N/m makes z larger, see Eq. 2.14 but the term $\sigma_0 z$ in the total friction will be unchanged. However, increasing z also increases $\dot{z}$, and if the value of σ_1 is not decreased with regards to σ_0 the frictional lag will be greater, the same response as when increasing σ_1. This relationship should be taken into account when altering either σ_0 or σ_1. The parameters α_0 and α_1 determines the values of the function $g(v)$, see Fig. 2.11. The characteristics of $g(v)$ is also dependent on the Stribeck velocity, v_s. Increasing v_s results in a wider peak in Fig. 2.11, since the impact of α_1 becomes noticeable for larger input velocities, see Eq. (2.11). Thus, the impact of the Stribeck effect on the total friction force spans a wider velocity interval.

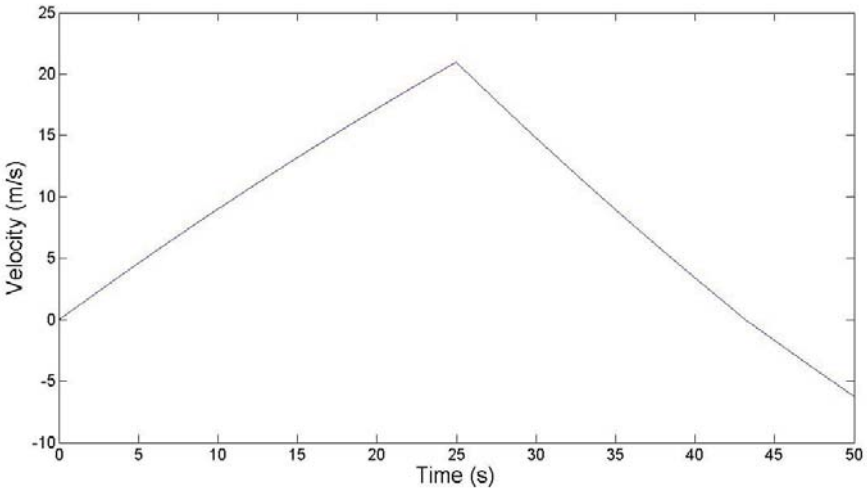

Figure 2.9: Resulting velocity

Lastly, the value of the parameter α_2 determines, as previously mentioned, the impact of viscous friction and is not of great importance for low velocities.

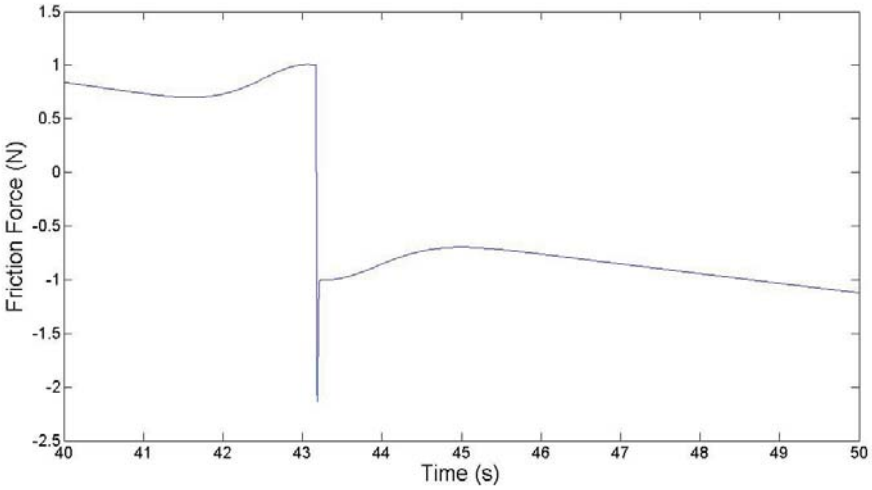

Figure 2.10: Resulting friction force, $40 - 50$ s

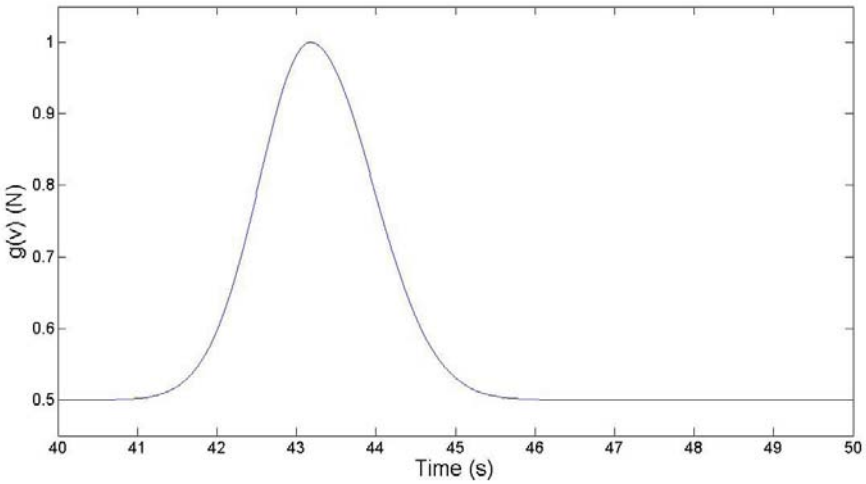

Figure 2.11: The function $g(v)$, $40 - 50$ s

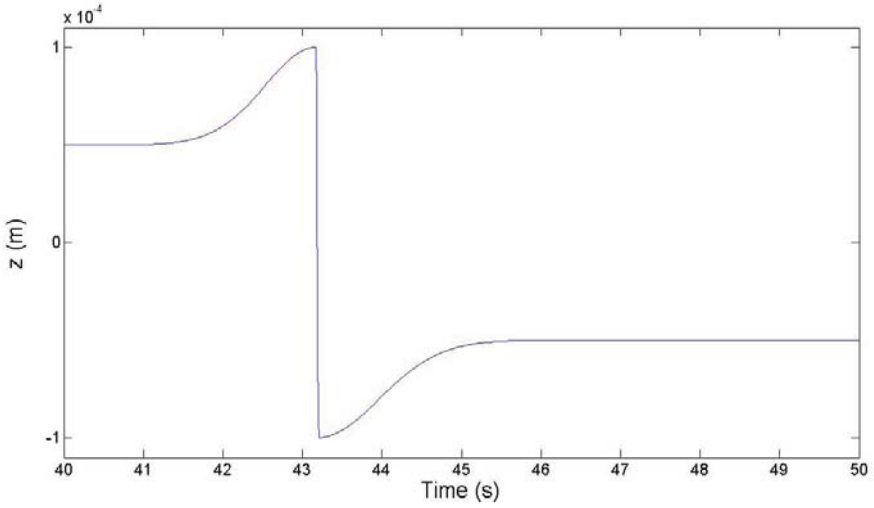

Figure 2.12: Bristle deformation, z, $40 - 50$ s

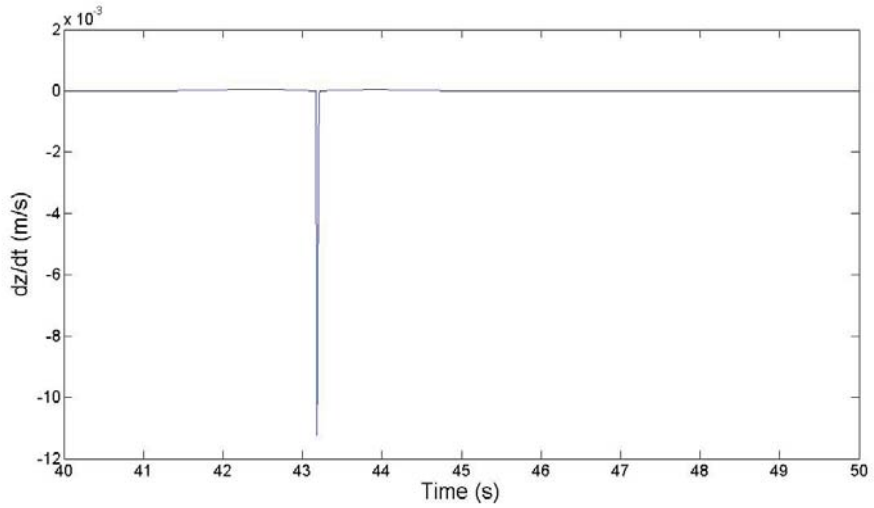

Figure 2.13: Bristle deformation velocity, $\dot{z}$, $40 - 50$ s

3 Driveline modeling

3.1 Introduction

The driveline is modeled as a system of rotating inertias connected by damped, flexible shafts, using Newton's generalized second law of motion. The clutch is assumed to be rigid, as is the transmission. Furthermore, the dynamics of the engine is not considered in this thesis, distinguishing the driveline model from a powertrain model. Rather, the engine is modeled as a flywheel, connected to the transmission. One approach to model the system could be to derive equations for each component in the driveline and combine them to form an overall equation for the lumped system. However, this is not the most practical solution for simulation purposes where it is more intuitive to model each component, combining these models to form the driveline. This is even more practical when considering nonlinearites, such as backlash, for which the lumped equation tends to be somewhat cumbersome.

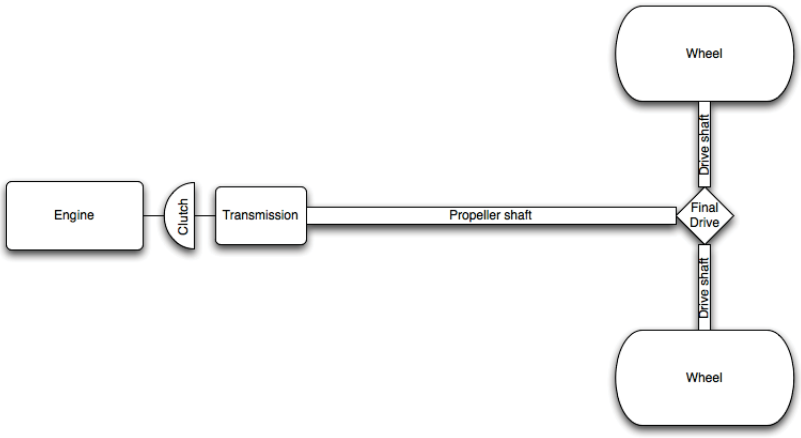

Figure 3.1: Schematic of a basic powertrain

3.2 Driveline components

A schematic of a basic powertrain is depicted in Fig. 3.1 and consists of an engine, a clutch, a transmission, a flexible propeller shaft, a differential gear (often referred to as the final drive), flexible drive shafts and wheels, [1]. The modeling of the system, neglecting the engine dynamics as mentioned above, as rotating inertias can be seen in Fig. 3.2.

3.2.1 Engine

Generally, an engine can be modeled as a flywheel, driven by an engine torque and subject to an internal friction torque load as well as a load torque from the clutch. Thus, according to Newton's second law, the engine model is described by

$$J_e\ddot{\theta}_e = T_e - T_{fr_e} - T_c \tag{3.1}$$

where J_e and $\ddot{\theta}_e$ is the inertia and the angular acceleration of the engine flywheel, respectively, and T denotes the torques, i.e. T_e, T_{fr_e} and T_c corresponds to the torque

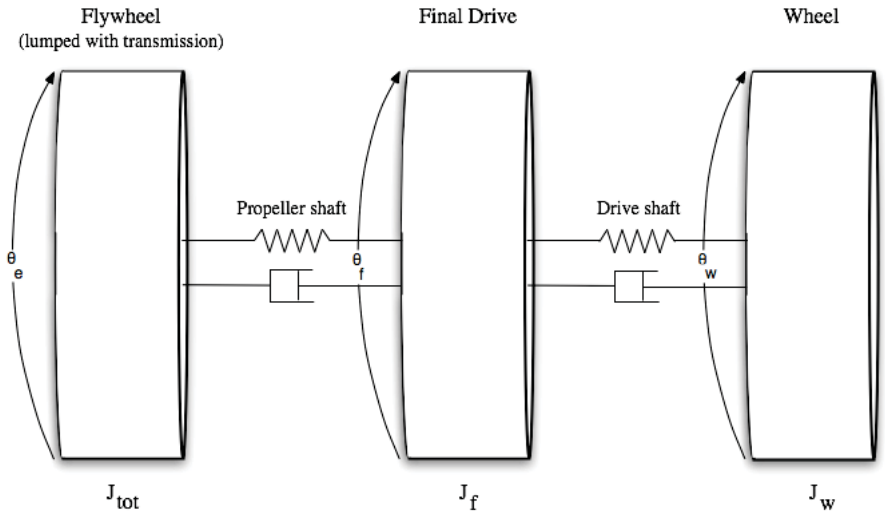

Figure 3.2: Driveline modeled as rotating inertias

of the engine, frictional torque of the engine and clutch torque, respectively. However, modeling of the engine dynamics is outside the scope of this thesis. Instead, a "virtual" torque, calculated by an onboard computer using engine measurements and acting on the flywheel, is used.

3.2.2 Clutch

Under the assumption of a rigid clutch,

$$T_c = T_t, \quad \theta_c = \theta_e \tag{3.2}$$

3.2.3 Transmission

The transmission converts the torque from the clutch, or rather the torque from the engine since the clutch is assumed to be rigid, according to the ratio of the transmission, i_t, i.e. $\theta_e = \theta_t i_t$. Typically, the equation for the transmission is

$$J_t \ddot{\theta}_t \quad = \quad T_t i_t - T_{fr_t} - T_p \tag{3.3}$$

where viscous friction can be assumed for the transmission. However, assuming rigid clutch and not taking transmission friction into account, but rather treating the transmission purely as a scaling factor, the lumped inertia of the flywheel and the transmission inertia, J_{tot}, can be described by

$$J_{tot} = J_e i_t^2 + J_t \tag{3.4}$$

and eq. (3.3) can be written as

$$J_{tot}\ddot{\theta}_t = T_e i_t - T_p \tag{3.5}$$

3.2.4 Propeller shaft

Due to flexibility in the propeller shaft,

$$T_p = k_p(\theta_t - \theta_p) + c(\dot{\theta}_t - \dot{\theta_p}) \tag{3.6}$$

Flexibility such as this induces oscillations in the driveline. According to Petterson, [1], the main flexibility in the driveline is due to the flexibility in the drive shafts rather than in the propeller shaft. However, to ensure model validity, the flexibility of the propeller shaft is included in the simulations.

3.2.5 Final Drive

Typically, the final drive is modeled as a torque distributor with internal friction, scaling the torque from the propeller shaft with a ratio i_f and distributing it between the drive shafts. Thus, the equation for the final drive is

$$J_f\ddot{\theta}_f = T_p i_f - T_{fr_f} - T_d \tag{3.7}$$

with the same notations as for the transmission model given above.

3.2.6 Modified Final Drive

However, the model in Eq. (3.7) model takes into account none of the dynamics of the final drive, i.e. the dynamics of the differential gear.
As previously noted, there are nonlinearities within the differential due to friction (which may be more complex than the viscous friction model) and backlash, and disregarding the impact of these might cause discrepancies in the simulation results. If, instead, the differential is modeled as four inertias, representing the crown wheel, the planet gear and the side gears, these effects can be taken into account. The contact between the end of the propeller shaft, i.e. the pinion gear, and the crown wheel, is assumed to be rigid. Thus, the lumped mass can be expressed in the same manner as the lumped engine mass, Eq. (3.4),

$$J_{tot_2} = J_p i_f^2 + J_c \tag{3.8}$$

The modified driveline, with the extended differential gear model, can be seen in Fig. 3.3. The resulting equations for the four inertias are

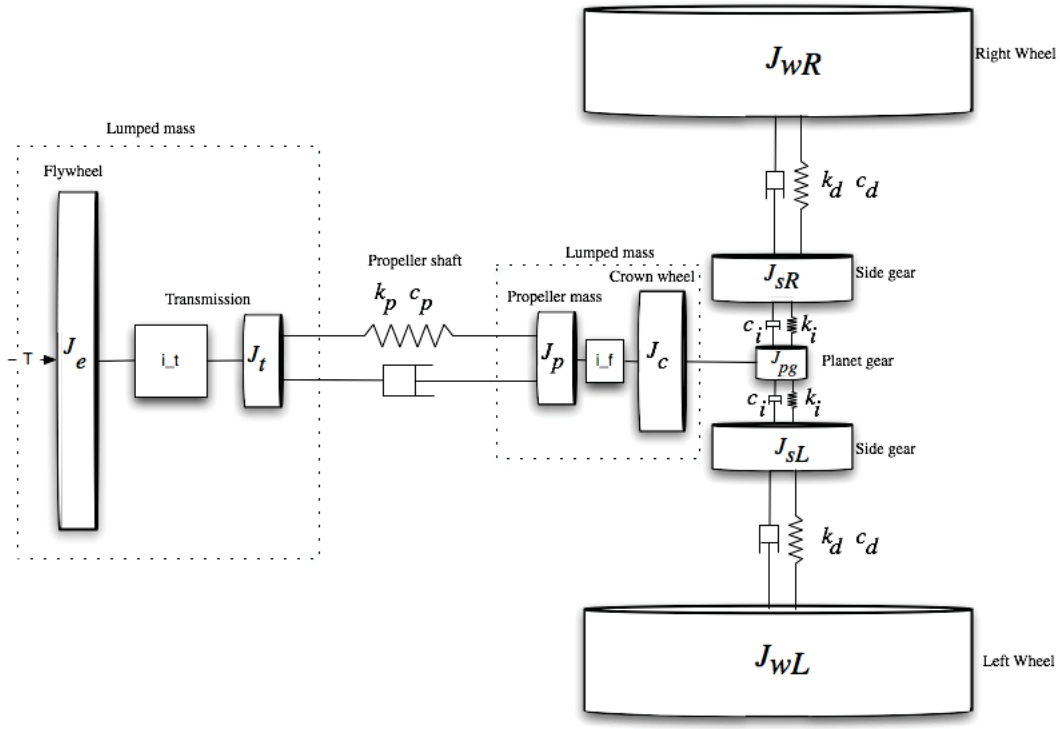

Figure 3.3: Modified driveline model with extended differential gear model.

$$
\begin{aligned}
J_{tot_2}\ddot{\theta}_c &= T_p i_f - T_{diff_L} - T_{diff_R} - T_{fr_c} \\
&= T_p i_f - BL\left[(\theta_c - \theta_{pg}) - \theta_{s_L}\right] - BL\left[(\theta_c + \theta_{pg} - \theta_{s_R}\right] - T_{fr_c} \qquad (3.9)
\end{aligned}
$$

$$
\begin{aligned}
J_{pg}\ddot{\theta}_{pg} &= T_{diff_L} - T_{diff_R} - T_{fr_{pg}} \\
&= BL\left[(\theta_c - \theta_{pg}) - \theta_{s_L}\right] - BL\left[(\theta_c + \theta_{pg}) - \theta_{s_R}\right] - T_{fr_{pg}} \qquad (3.10)
\end{aligned}
$$

$$
\begin{aligned}
J_{s_L}\ddot{\theta}_{s_L} &= T_{diff_L} - T_{d_L} \\
&= BL\left[(\theta_c - \theta_{pg}) - \theta_{s_L}\right] - T_{d_L} \qquad (3.11)
\end{aligned}
$$

$$
\begin{aligned}
J_{s_R}\ddot{\theta}_{s_R} &= T_{diff_R} - T_{d_R} \\
&= BL\left[(\theta_c + \theta_{pg}) - \theta_{s_R}\right] - T_{d_R} \qquad (3.12)
\end{aligned}
$$

where $BL(\Delta\theta)$ denotes the function modeling the backlash and the impact, as previously described.

3.2.7 Drive Shaft

The drive shafts are modeled in the same manner as the propeller shaft,

$$
T_d = k_d(\theta_s - \theta_w) + c_d(\dot{\theta}_s - \dot{\theta}_w) \qquad (3.13)
$$

where the dynamic torque T_d is a model of a torsional spring-damper.

3.3 Wheel modeling

The tyre-road interaction exhibits a complex and highly nonlinear behaviour, which is surface dependent. As will be described later, this results in a complicated control problem, since a spinning wheel looses lateral stability. The tyre-road interaction is of great importance in traction control and developing a model which includes full tyre dynamics is a time consuming process. In this thesis a wheel model containing a tyre module created at Haldex Traction is being used, with a few modifications. This model accounts for various tyre phenomena and uses the Pacejka *Magic Formula*, further described in Section 3.3.5.

3.3.1 Wheel dynamics

The dynamics of the wheel are given by

$$J_w\dot{\omega} = T_d - T_b - r_w F_x \tag{3.14}$$

where J_w is the inertia of the wheel, T_d is the dynamic drive shaft torque, T_b is the brake torque, r_w is the effective rolling radius of the wheel and F_x is the force acting in the longitudinal direction.

Evaluating the longitudinal force equilibrium gives

$$F_x - F_{res} = m_{veh}\dot{v}_{veh} \tag{3.15}$$

where F_{res} represents the combination of resistive forces on the vehicle,

$$F_{res} = F_{air} + F_{roll} + F_{slope} \tag{3.16}$$

The resistive forces are discussed in the next section.

The longitudinal force, often referred to as the adhesive force or traction force, is given by

$$F_x = \mu N \tag{3.17}$$

where μ is the friction coefficient of the road surface and N is the normal load. The main focus in traction control, is to maximize the traction force throughout the acceleration.

3.3.2 Resistive Forces

For the vehicle to move forward, the traction force needs to overcome the resistive forces. Those discussed in this section are the rolling resistance, the slope resistance and the resistance due to air drag of which the rolling resistance and the slope resistance were accounted for in the provided wheel model.

The rolling resistance is surface dependent - it is, for example, higher if a tire is driven on sand than when driving on asphalt. The rolling resistance can be expressed as

$$F_{roll} = N(q_{init} + q_{vel}\frac{|V_x|}{|V_0|}) \tag{3.18}$$

where N is the normal load, q_{init} is the initial level of resistive force and q_{vel} is a velocity dependent parameter. The parameters q_{init} and q_{vel} varies with the road surface, [8, 10].

The slope resistance is given by

$$F_{slope} = m_{veh}g \cdot sin\alpha \tag{3.19}$$

where m_{veh} is the vehicle mass and α is the road inclination angle.

Finally, the air drag resistance, not accounted for in the provided wheel model, can be expressed as

$$F_{air} = \frac{1}{2}\rho v_{veh}^2 c_w A \tag{3.20}$$

where ρ is the air density, A is the frontal area of the vehicle and c_w is the aerodynamic drag coefficient, [1, 8].

3.3.3 Haldex Wheel Model

The wheel model provided by Haldex consists of a tyre module, with numerous inputs due to the complexity of a tyre. For calculating tyre slip and various forces and torques, a single file consisting of 250 variables was supplied along with the tyre module. Apart from these variables, the module uses the drive shaft torque, the brake torques and the velocity of the wheel center as inputs. There is also a variety of outputs from the module, however, in this thesis only the traction force and the angular velocity of the tyre are considered.

3.3.4 Wheel Slip

Applying torque to a wheel, causes the tyre to deform slightly, see Fig. 3.4. The deformation is a result of the compliance of the deflected tyre treads, see Fig. 3.5, and regarding the tread as a spring, the energy stored in the spring generates a tractive force .
The deformation of the tyre causes a driven wheel to travel a shorter distance than a free-rolling wheel, thus, the angular velocity of a driven wheel is higher than that of a free-rolling wheel. The velocity difference between a driven wheel and the vehicle is called *slip* and can be defined as

$$\lambda = \frac{\omega r - v_{veh}}{v_{veh}} \tag{3.21}$$

where ω is the angular velocity of the wheel. Clearly, $\lambda = 0$ for a free-rolling wheel, while a spinning wheel implies high slip values. The surface friction coefficient has a high slip dependence, which is often described by the so called *Magic Formula*, further described below.

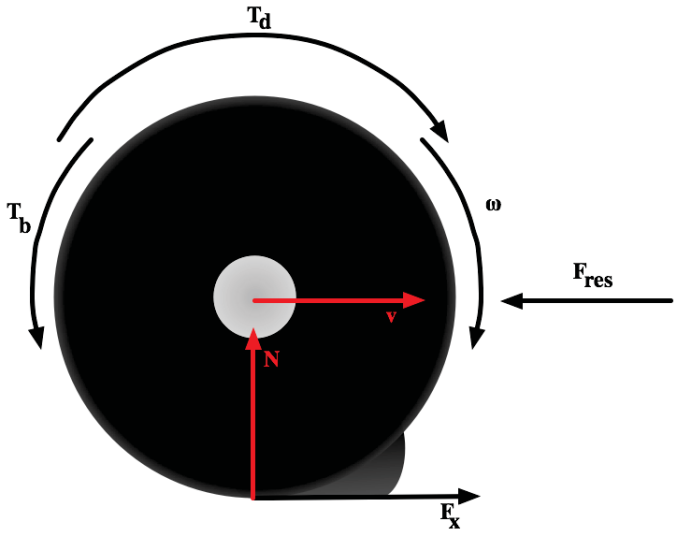

Figure 3.4: Driven wheel, with (exaggerated) deformation

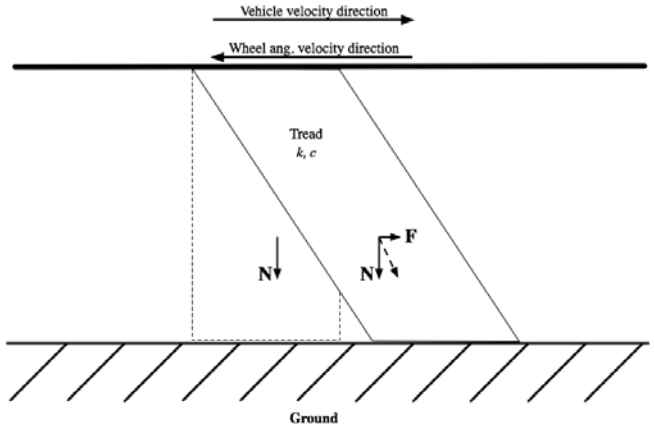

Figure 3.5: Model of deflected tyre tread, microscopic view

3.3.5 Pacejka *Magic Formula*

A commonly used model describing the tyre-road interaction, is the *Magic Formula*, Eq. (3.23), which describes the interaction during steady-state conditions [**?**],

$$Y(x) = D\sin(C\arctan(Bx - E(Bx - \arctan(Bx)))) \tag{3.22}$$

The formula has various applications in that it adequately describes forces, torques and friction coefficients. The formula is easily modified to describe the surface friction coefficient as a function of slip,

$$\mu(\lambda) = D\sin(C\arctan(B\lambda - E(B\lambda - \arctan(B\lambda)))) \tag{3.23}$$

as shown in Fig. 3.6 for different surfaces.

The constants in the Magic Formula denoted B, C, D and E have different meanings, which can be understood by graphically examining Fig. 3.6, [9].

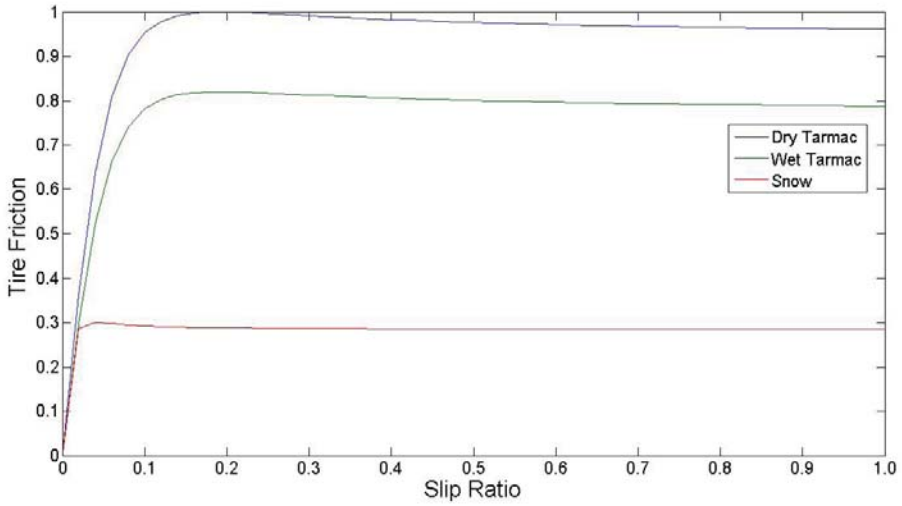

Figure 3.6: Pacejka's Magic Formula, generating the function $\mu(\lambda)$, for different surface conditions

- D is the peak coefficient and determines the maximum value of the curve (since the remaining part of the Magic Formula is a sine function and can thus never be larger than 1)
- C is the shape factor and determines the value of the sine function and has the highest impact on the shape of the curve. A value larger than 1 generates a peak and by increasing the value, the peak takes on a more defined form
- B is the stiffness factor, affecting the initial slope of the curve and thus determines the position of the peak
- E is the curvature factor, the curve flattens with decreasing values

The slip dependency of the surface friction utilization coefficient μ, and due to Eq. (3.17) the traction force, is clearly seen in Fig. 3.6, as is the large difference in the friction coefficient for the various surface conditions. As previously stated, this thesis considers only longitudinal forces, however, for the traction control problem the lateral stability has to be taken into account. The lateral forces decreases rapidly with increasing slip, i.e. to achieve maximum longitudinal acceleration while maintaining lateral stability, the slip should never exceed the value for which the friction coefficient attains its maximum value. This is not quite true, however, with regards to the absence of a well defined peak when driving on snow or ice, in which case the slip should not be allowed to exceed the value marking the beginning of the plateau. The left side of the peak is for obvious reasons denoted *stable*, while the right side is denoted *unstable*. In the absence of a well defined peak, the plateau is denoted unstable. The choice of an optimal slip value, λ_{opt} is important within traction control, as will be discussed further in Section 5.

4 System modeling

4.1 System

The complete system is a driveline for a heavy-duty truck. The weight of the truck is assumed to be 12200 kg, of which only 2000 kg is distributed on the rear axle, i.e. the truck is unloaded. These parameters match those of the test vehicle used in the measurements provided by Haldex.

The parameters for the provided tyre module were those of a standard car tyre and thus not directly applicable in the developed drivetrain model, due to the difference in properties for a heavy-duty truck tyre - i.e. some changes needed to be made, such as increasing the radius, the mass and the inertia of the wheel. Also, four wheels are attached to the drive shaft, two on each side, on the real vehicle while the tyre module only describes one tyre. This could be solved by using four tyre modules i.e. four wheel models, one for each wheel. However, since the wheels are paired together on the drive shaft, it is more convenient to use two wheel models, one for the right side and one for the left side. Thus, the inertia and the adhesive force of the wheels need to be doubled, as well as adjusting the displacement parameters and the rolling resistance parameters for each wheel accordingly. Also, additional wheels decreases the normal load on each wheel. Thus, Eq. (3.14) can be modified as

$$2 \cdot J_w \dot{\omega} = T_d - T_b - r_w \cdot 2 \cdot F_x(\frac{F_z}{2}, \lambda) \tag{4.1}$$

4.2 Simplifications

Proper modeling is of great importance to account for complex behaviour of the real system, however, simplifications are often introduced to increase model usability while maintaining model simplicity. While these simplifications might not affect the system dynamics, it is important to declare where they have been introduced.

As mentioned in Section 3, the clutch is assumed rigid, i.e. it transfers the torque without altering it. Clutch dynamics is further investigated in, for example, [1]. Also the contact between the pinion gear, at the end of the propeller shaft, and the crown wheel is modeled as rigid. It has been shown, [1], that a major part of the driveline dynamics are captured using a model for which the drive shaft is the main flexibility, however, this thesis also accounts for flexibility in the propeller shaft to ensure model validity.

4.3 Nonlinearities

This thesis focuses on developing an accurate model of the differential and rear axle behaviour, thus, the nonlinearities considered in the model are backlash between planet gear and side gears, and friction. The friction modeling of the differential is based on two different approaches. The contact friction between the planet gear and the side gears in the differential is modeled using the LuGre friction model while the contact friction between the pinion gear, at the end of the propeller shaft, and the crown wheel is modeled as a combination of Coulomb friction and viscous friction. Though backlash and friction are present in other parts of the driveline as well, the influence of these on the differential

dynamics can be neglected, e.g. by assuming a rigid clutch and transmission as described above.

4.4 Choice of parameters

4.4.1 Compliance and Damping

To model the flexible shafts as spring-dampers connecting rotating inertias, the parameters k and c need to be determined. The parameters could be determined using a dynamometer, which would require the shafts to be dismounted. However, an easier approach is to estimate the values using straightforward mechanics of materials. Since the propeller shaft connects the engine with the final drive and therefore is of considerable length, a hollow shaft is usually used to minimize the weight of the shaft while maintaining desirable strength. The weight is not an issue for the drive shaft, therefore it can be assumed to be solid. In steady state, i.e. at constant load torque T, the displacement angle can be expressed as

$$\theta_d = \frac{T}{k} = \frac{T \cdot L}{G \cdot K} \Rightarrow k = \frac{G \cdot K}{L} \tag{4.2}$$

where k is the stiffness parameter, L is the length of the shaft, G is the shear modulus and K is a parameter dependent on the cross section of the shaft. The cross section dependent parameter K for a hollow shaft with outer diameter D and inner diameter d, is given by

$$K = \frac{\pi}{32}(D^4 - d^4) \tag{4.3}$$

A solid shaft is simply a special case of a hollow shaft for which $d \to 0$, thus, K is given by

$$K = \frac{\pi}{32}D^4 \tag{4.4}$$

Introducing damping in the shaft leads to a harmonic oscillator,

$$J\ddot{\theta} = -k\theta - c\dot{\theta} \Rightarrow (Js^2 + cs + k)\theta = 0 \Rightarrow (s^2 + \frac{c}{J}s + \frac{k}{J})\theta = 0 \tag{4.5}$$

where the natural frequency ω_0 is given by

$$\omega_0 = \sqrt{\frac{k}{J}} \tag{4.6}$$

and where k is the stiffness of the spring and J is the inertia. Defining the damping ratio, ζ, as

$$\zeta = \frac{c}{2\sqrt{Jk}} \tag{4.7}$$

the harmonic oscillator can be expressed as

$$(s^2 + 2\zeta\omega_0 s + \omega_0^2)\theta = 0 \tag{4.8}$$

Thus, by estimating the damping ratio, the damping coefficient c of the shaft can be obtained through Eq. (4.7).
The parameter values for the compliance and damping used in this thesis, are presented in Table (4.1)

Parameter	Value	
k_p	$90 \cdot 10^3$	[Nm/rad]
c_p	127	[Nms/rad]
k_d	$16 \cdot 10^3$	[Nm/rad]
c_d	16	[Nms/rad]

Table 4.1: Compliance and damping parameters

4.4.2 Friction

The main issue with using the LuGre friction model is the difficulty in parameter choice, described in Section 2.2.5. The LuGre friction is used in the model for the contact between the planet gears and the side gears, i.e. making it harder for the planet gear to move. For longitudinal motion during stable conditions, e.g. when the left and right wheels have the same velocity, the planet gears do not move. Therefore, friction between planet gear and side gears occurs only when one of the wheels have higher angular velocity than the other, i.e. when one or both wheels are spinning or when turning. Thus, when the planet gears do not move, only Coulomb friction and viscous friction between pinion gear and crown wheel is present, described by

$$T_{fr_c} = \mu_{C_m} T_p i_f + \eta_{v_m} \dot{\theta}_c \tag{4.9}$$

where μ_{C_m} is the Coulomb friction coefficient, and the parameter for the viscous friction, η_{v_m}, is given in Nms. The parameters of this friction model should therefore be determined first, which can be accomplished using simulations with measurement data and comparing the stable parts. Thereafter, the LuGre parameters can be determined, using the same approach as above but rather examining the unstable parts, i.e. when one wheel is spinning, setting the parameters so that the friction model counteracts the motion of the planet gears.

The LuGre friction model has been discussed thoroughly in Section 2.2.5 as a model used to calculate a friction force that is velocity dependent. However, the friction is also dependent on the acting torque. Thus, instead of calculating a friction force the model can be rewritten to calculate a friction coefficient, f, which, multiplied with the acting torque, gives the friction torque. The six parameters σ_0, σ_1, α_0, α_1, α_2 and v_s must be chosen accordingly. Firstly, the viscous parameter α_2 is neglected since it should not be accounted for when calculating the friction coefficient. The relative velocity between the planet gears and the side gears is calculated, in m/s and used as input velocity. Due to low relative velocity, the friction present is mainly dry friction. Assuming the same value for the LuGre model as for the Coulomb friction in the friction model describing the contact friction for the pinion gear and the crown wheel, gives a rough estimation of the LuGre model parameters. Using model tests and plausible results, while confirming an accurate description of the friction phenomena, a set of values for σ_{0_m}, σ_{1_m}, α_{0_m}, α_{1_m} and v_{s_m} is given, where the index m denotes the modified parameters. Thus, the LuGre model provides a friction coefficient rather than a friction force. Adding viscous friction, the total LuGre friction is given as

$$T_{fr_{pg}} = T_{diff_L} f_L + \alpha_2 v_{rel_L} - (T_{diff_R} f_R + \alpha_2 v_{rel_R}) \tag{4.10}$$

4.5 Simulation problems

When implementing the model of the driveline in Matlab/Simulink, a few problems occur, mainly due to the complexity and stiffness of the differential model.

In Simulink, there are a few things that need consideration. There exists, for example, different solvers since the main purpose of Simulink is solving differential equations. The first solver tried was ode45 which is the default choice in Simulink. It is a one-step solver, based on an explicit Runge-Kutta formula. The main issue with ode45 is the simulation time, which tend to increase for stiff system, since the solver is non-stiff. Using a stiff solver, for example the ode23s which is based on a modified Rosenbrock formula of second order, decreases simulation time but with slightly less accuracy. In this thesis, the ode23s solver with a relative tolerance of 0.001 is being used.

When evaluating the model using the measurement data provided, some problems occured when the wheels started to spin - the wheels velocities increased to unreasonably high values. By using the vehicle velocity obtained from measurement data as input to the wheel models and themeasurements of flywheel velocity as an observer this problem was solved.

As expected, the most problems for the model occurred when implementing the nonlinearities, i.e. the backlash and the friction, in the final drive. Both the backlash and the friction slowed down the simulation and occasionally forced Matlab to shut down. For the friction, these problems are due, in part, to the problem of choosing the right values for the parameters, as a poor choice of parameters might cause the friction to increase beyond reasonable values. For backlash, a problem is, in part, the use of look-up tables, which can cause problems in Simulink due to the introduction of discontiuities. In addition, the compliance of the spring-damper modeling the contact between planet gears and side gears is very high, and numerical problems can arise for small variations in angular difference between gears. The problems arising when introducing nonlinearities were solved, to some extent, by changing solver to ode23s.

4.6 Validation

The model is validated using measurement data provided by Haldex. The data is collected at the test site in Arjeplog, Sweden, and features test runs with an unladen truck on ice, i.e. in low-μ and split-μ conditions.

Three series of measurement data are used. These series of measurement data will hereafter be referred to as Test 1, 2 and 3. Each of the measurement data series contains 288 different measurements obtained from the CAN-bus on the truck. Since this thesis considers a driveline model without engine dynamics, the engine torque applied to the flywheel is used as input. The wheel velocities generated by the model are compared with those of the measurement data. Also, the brake measurement data is used, as inputs to the wheel models. The three tests includes some gear shifting and each gear has its own ratio that needs to be accounted for. Thus, the model compares the velocity of the flywheel to the velocities of the rear wheels, to calculate the driveline scaling factor. The flywheel velocity is also used as an observer when calculating the angular velocity of the transmission.

4.6.1 Test 1

The first test spans 65 seconds. The initial vehicle velocity is approximately 20 km/h with a low initial acceleration, and the vehicle is then kept at almost constant velocity before the brakes are used at the end of the test. During the test, only one gear shift is performed. Since the acceleration is low, there is not much wheel spin.

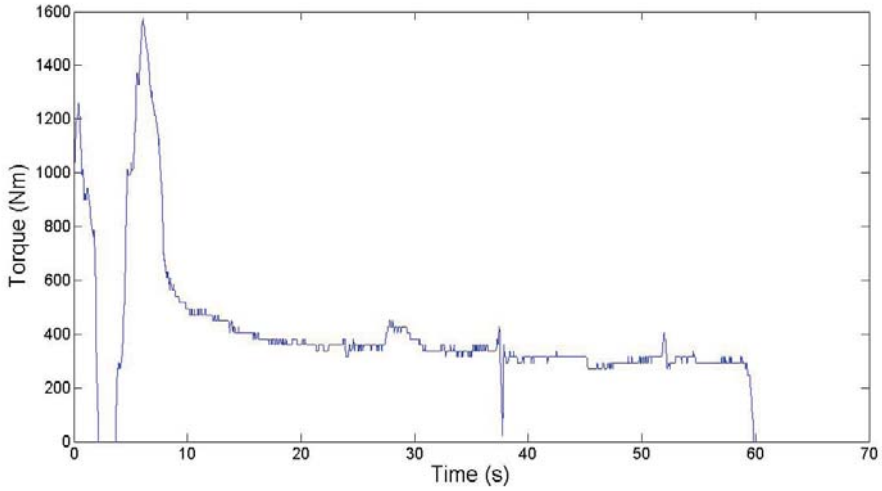

Figure 4.1: Engine torque, Test 1

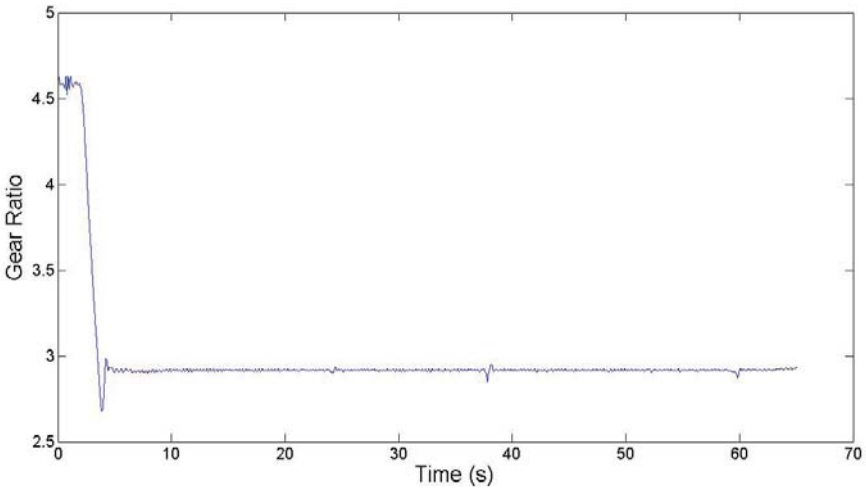

Figure 4.2: Gear ratio, Test 1

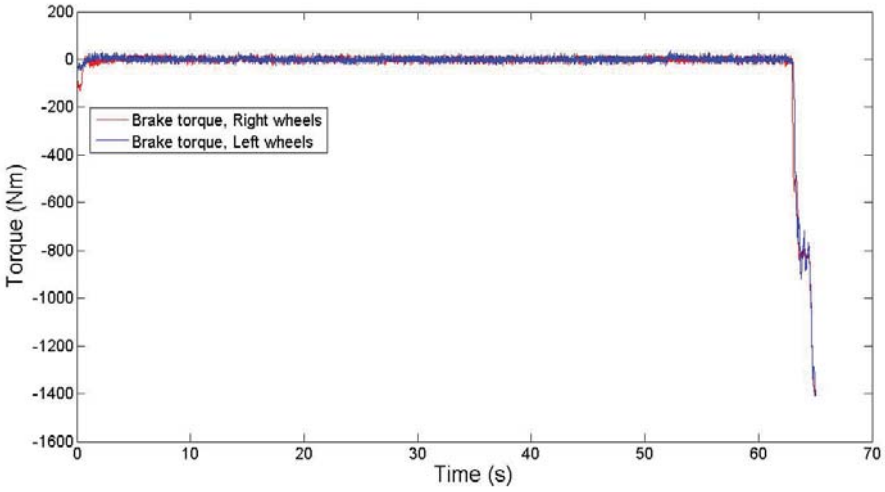

Figure 4.3: Brake torques, Test 1

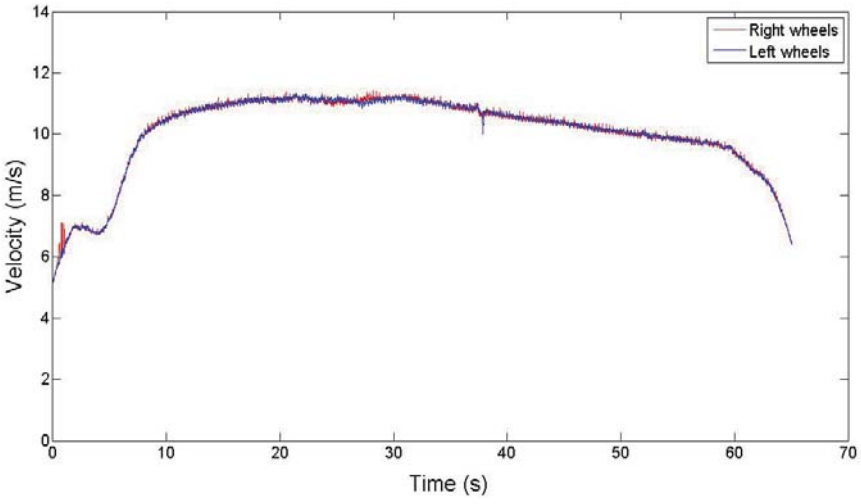

Figure 4.4: Wheel velocities, Test 1

4.6.2 Test 2

This test is almost the same as Test 1, with one important difference - initially, the vehicle velocity is almost zero, i.e. the vehicle is accelerating from standstill, to a constant velocity, similar to Test 1. Wheel spin is frequently occuring during the acceleration for both left and right wheels.

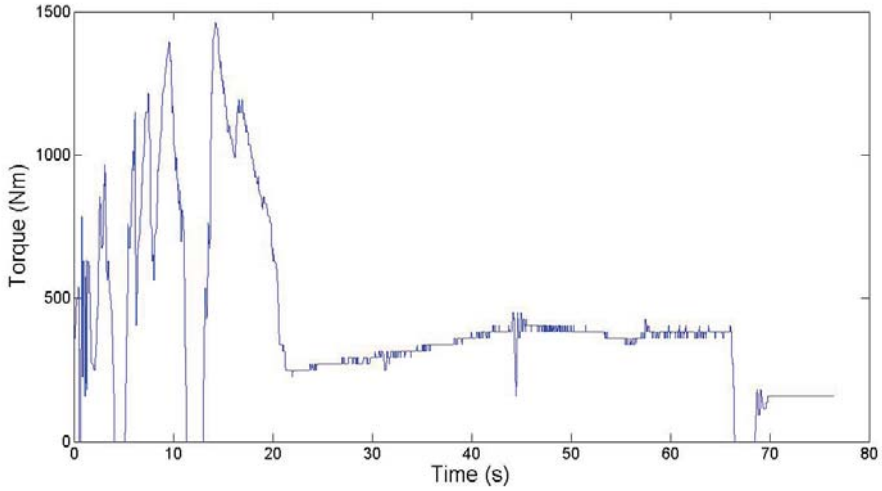

Figure 4.5: Engine torque, Test 2

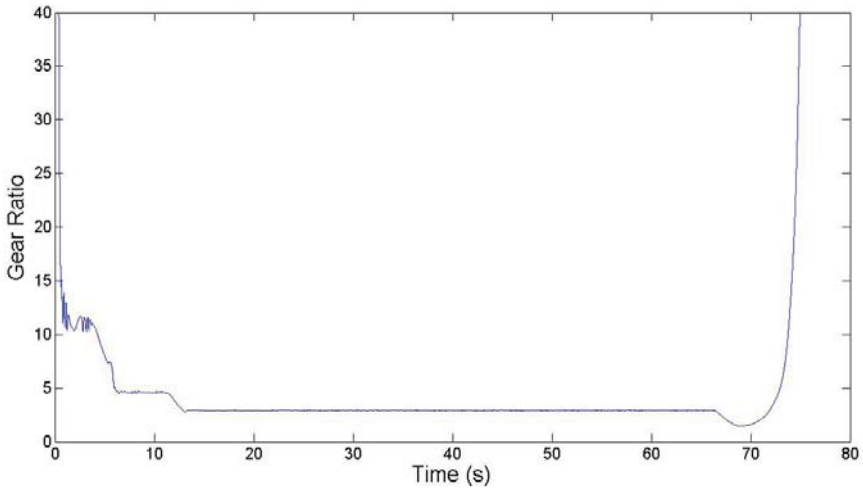

Figure 4.6: Gear ratio, Test 2

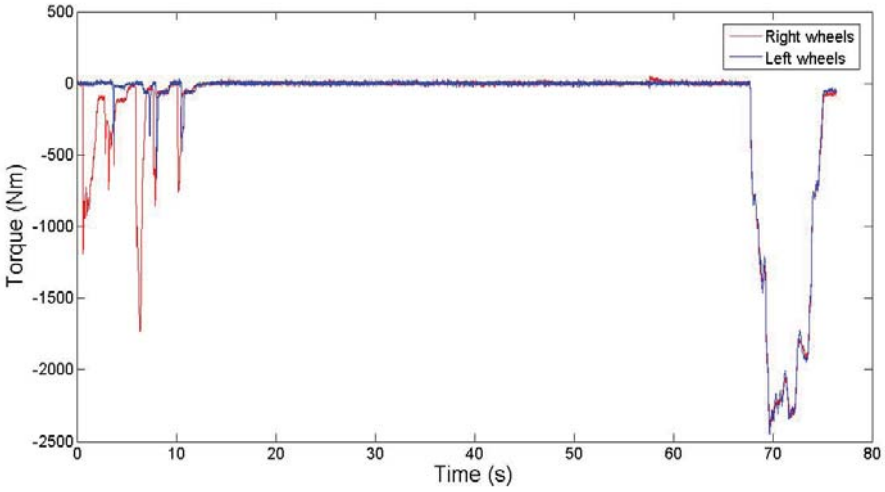

Figure 4.7: Brake torques, Test 2

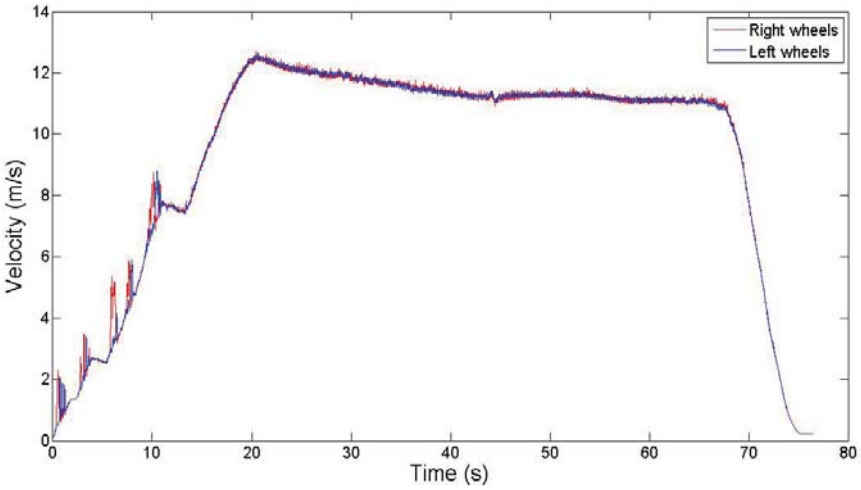

Figure 4.8: Wheel velocities, Test 2

4.6.3 Test 3

The third test is the most complex with gear shifting both up and down. There is fast acceleration both initially and after a time period of 60 seconds. During both accelerations, the wheels start to spin. Notice that the duration of the test is 190 seconds, which is the longest of the three tests. During the test, the brakes are used frequently.

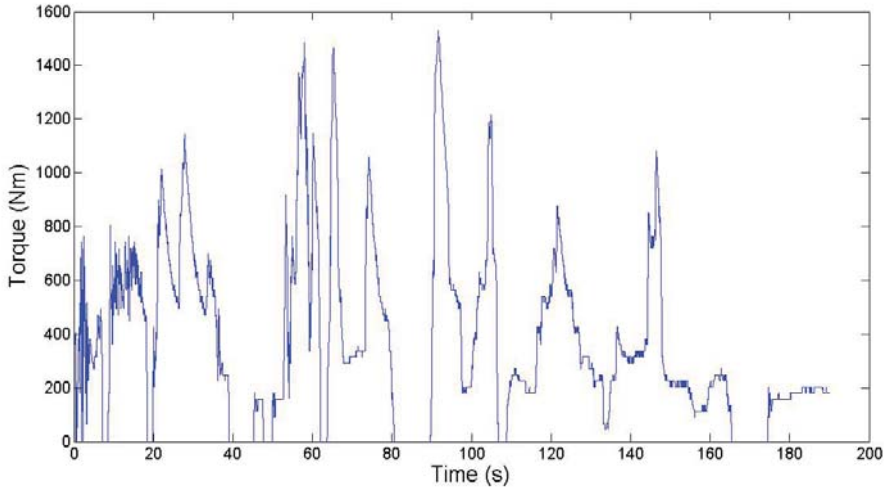

Figure 4.9: Engine torque, Test 3

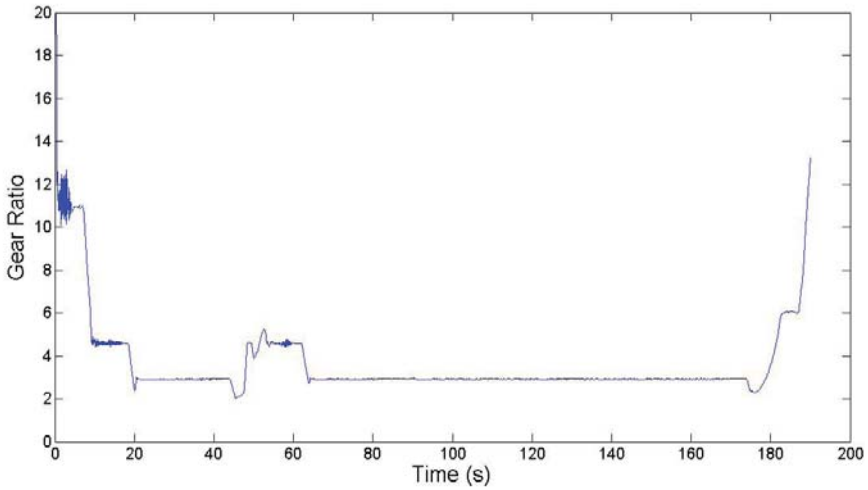

Figure 4.10: Gear ratio, Test 3

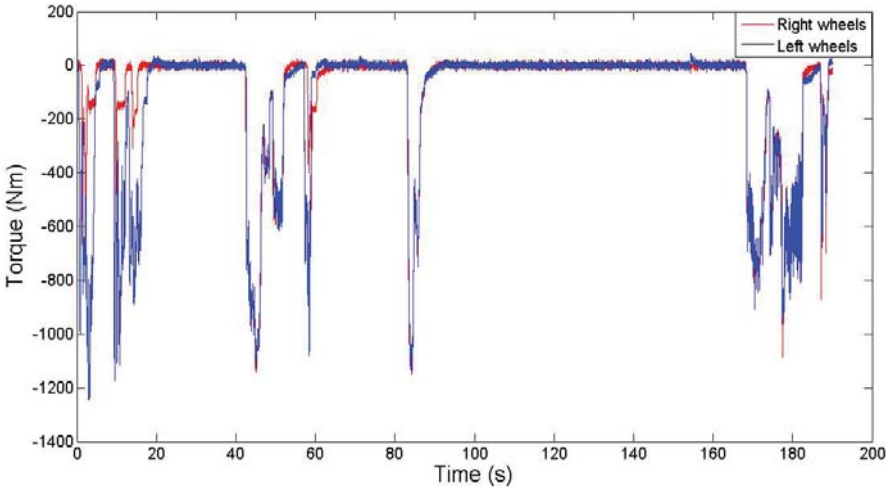

Figure 4.11: Brake torques, Test 3

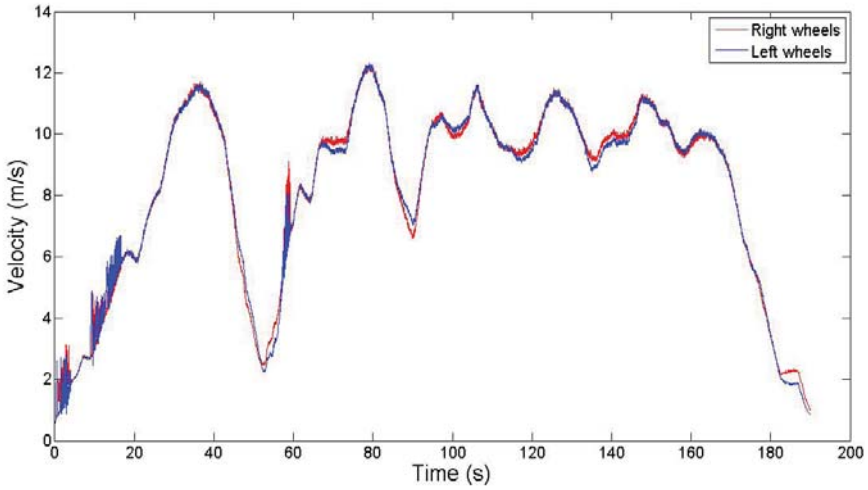

Figure 4.12: Wheel velocities, Test 3

4.6.4 Step responses

Besides the validation using measurement data, the model was also tested with various inputs, such as steps. The problem with using these tests is that the model requires secondary inputs apart from the primary engine torque input.

For the engine torque, different step functions were defined. An instantaneous change in engine torque from 0 Nm can cause large changes in the wheel accelerations and therefore the steps will be taken from a constant value of 300 Nm.

The secondary inputs to the model are the brake torques, the engine velocity, the velocities of the wheels and the velocity of the vehicle. The velocities of the wheels are used in the model as comparison with the model outputs and for calculation of the transmission ratio. For simplicity, constant gear ratio is assumed for all steps. The engine velocity is also used for the ratio calculations, though it is also used as an observer when calculating the velocity of the propeller shaft. Without the use of the engine velocity there is no feedback to the engine and the velocities of the driveline can therefore attain unreasonably high values. However, the purpose of the step responses is to observe system dynamics rather than absolute values. The braking torques are also neglected, i.e. the brakes are not used. Finally, the velocity of the vehicle has been obtained from measurements in the validations, however, for the step responses it is calculated in the model. Since the wheel models calculate the adhesive traction force of the wheels, Newton's second law of motion can be used

$$m_{veh}a_{veh} = F_{x_L} + F_{x_R} - F_{air} \tag{4.11}$$

where F_{air} is the resistive force due to air drag, see Section 3.3.2. The constant value for the gear ratio is set to 2.9 for the step responses, which approximately corresponds to the third gear. The engine torque used in the step responses can be seen in Fig. 4.13-4.14.

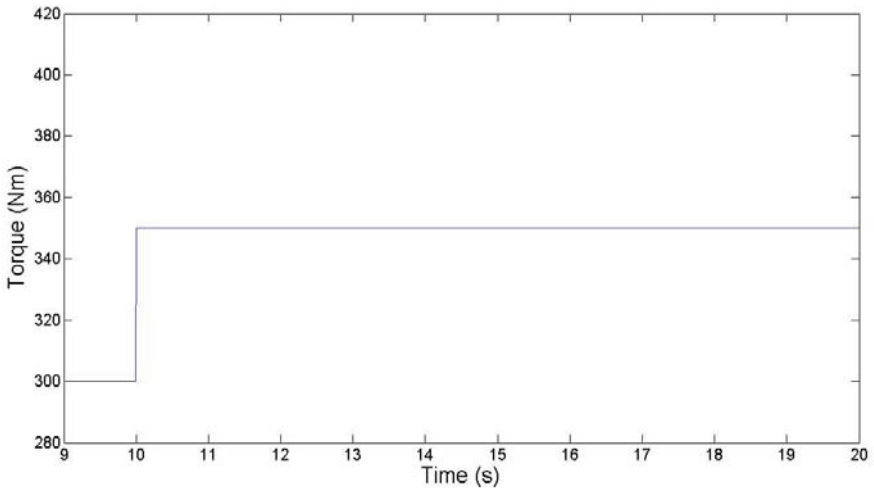

Figure 4.13: Step in engine torque, 300-350 Nm

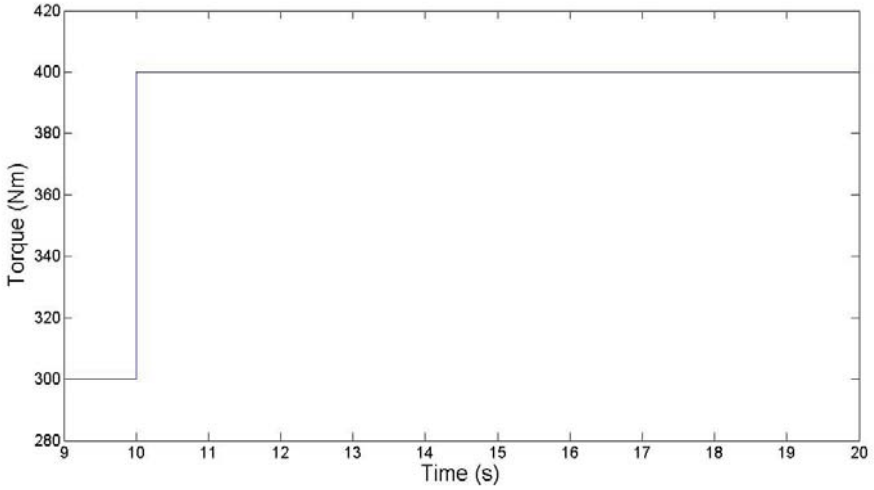

Figure 4.14: Step in engine torque, 300-400 Nm

5 Control theory

When reviewing previous work on traction control, a number of options regarding the choice of control strategy are presented. Since this thesis does not consider turning or cornering, i.e. only longitudinal motion, the control problem is reduced to obtain optimal traction in the longitudinal direction while maintaining stability in the lateral direction. As described in the section on wheel dynamics, over all stability is a trade-off between longitudinal traction and lateral stability. Often, an optimal slip trade-off value is in the slip peak, λ_{max}, vicinity, on the stable side. For larger slip values, $\lambda > \lambda_{max}$, the system becomes unstable as the lateral friction decreases. Thus, with regards to Fig. 3.6, the control problem can be vaguely formulated as

"to control the slip to values close to the peak on its stable side, while not exceeding λ_{max}*"*

Evidently, due to the nonlinear behaviour of the slip curve, the control problem itself is highly nonlinear. Since the traction control is actuated by brake torque and/or by changing the engine torque, a multivariable controller, with robust properties due to the nonlinear slip behaviour, is required. The control problem is further complicated due to the varying nature of the friction-slip curve. Since the curve varies depending on the surface, so does the optimal slip value. Some controllers, e.g. gain scheduling or fuzzy control, can be designed to control the slip to a value for which the friction curve attains a maximum instead of controlling it to a fixed reference value, while other controllers require an algorithm for estimation of the optimal slip value.

A proper controller should include some form of method to determine surface conditions, i.e. the current μ-value. This can be done in several different ways, e.g.

- via slip-based estimations, [11]
- using optical sensors to detect reflections from the surface, [12]
- using acoustic sensors to analyze noise from the tyres, [12]
- using sensors attached to the wheel threads to measure stress and strain, [13]

However, proper evaluation of such methods is outside the scope of this thesis, and it is therefore assumed that the road surface conditions are known.

As mentioned above, a number of controllers would be suitable for the traction control. Most research has been devoted to the use of fuzzy control or sliding mode controllers, often motivated by the nonlinear road-tire friction behaviour. This thesis, however, investigates the use of a model-based, predictive controller, an approach proposed only, to the authors knowledge, by one previous research group.

5.1 Model Predictive Control

In Model Predictive Control (MPC), an on-line, open-loop finite-horizon optimal control problem is solved to obtain an optimal control sequence, of which only the first control action is applied to the process. The algorithm uses current measurements as initial states and at each new measurement the optimization problem is recalculated over the prediction

horizon. Applying the first control action of the proposed optimal control sequence to the process, new measurements are obtained. The iterative behaviour moves the prediction horizon ahead, often referred to as receding horizon control. While originally developed for industrial process control, typically with slow plant dynamics, MPC has proven efficient also for faster systems, e.g. in automotive and aerospace control.

MPC differs from other control methods involving predictive control, e.g. Linear Quadratic (LQ) and Linear Quadratic Gaussian (LQG) control, in that it considers constraint on inputs, states and outputs. The prediction is provided by an approximate, linear model (most often a state-space formulation) of the plant. The capacity to handle contraints, for singlevariable (SISO) systems as well as for multivariable (MIMO) systems is one of the many advantages with using MPC, making it possible to achieve robust set-point tracking with the possibility, for example, to minimize actuator costs or to restrict rapid variations in inputs etc. The optimization problem consists of minimizing a cost function of the type

$$J(u) = \sum_{i=0}^{p}(y_{k+i} - y^r_{k+i})^T Q_y (y_{k+i} - y^r_{k+i}) + \sum_{i=0}^{m}(\Delta u_{k+i})^T Q_u (\Delta u_{k+i}) \tag{5.1}$$

where $Q_y > 0$, $Q_u > 0$ and y^r_k is a reference value, over the prediction horizon p with the control horizon m. In the cost function above, Q_y and Q_u represents weights on the states and on the inputs, respectively.

In the following sections, the plant is assumed to be described by the linear state-space formulation

$$\begin{aligned} x_{k+1} &= Ax_k + B_u u_k + B_v v_k + B_{v^*} v^*_k \\ y_k &= Cx_k + D_v v_k + D_w w_k \end{aligned} \tag{5.2}$$

5.2 Prediction Algorithms

As stated above, the prediction of future plant outputs with regard to a series of control actions, is, as the name suggests, one of the important features of MPC. Consider the plant dynamics given by Eq. (5.2). The predictions of future plant outputs, starting at time k and with the prediction horizon p, can be described as

$$\begin{aligned} y_{k+p} &= C(A^p x_k + \sum_{j=0}^{p-1} A^j B_u (u_{k-1} + \sum_{i=0}^{j} \Delta u_i)) \\ &+ C\sum_{j=0}^{p-1} A^j B_v v_{k+j} + D_v v_p + C\sum_{j=0}^{p-1} A^j B_w w_{k+j} + D_w w_p \end{aligned} \tag{5.3}$$

Thus, all predicted outputs during the prediction horizon can be summarized as

$$\begin{bmatrix} y_{k+1} \\ y_{k+2} \\ \vdots \\ y_{k+p} \end{bmatrix} = S_x x_k + S_{u-1} u_{k-1} + S_u \begin{bmatrix} \Delta u_k \\ \Delta u_{k+1} \\ \vdots \\ \Delta u_{k+p-1} \end{bmatrix} + S_v \begin{bmatrix} v_k \\ v_{k+1} \\ \vdots \\ v_{k+p-1} \end{bmatrix} + S_w \begin{bmatrix} w_k \\ w_{k+1} \\ \vdots \\ w_{k+p-1} \end{bmatrix} \tag{5.4}$$

where

$$S_x = \begin{bmatrix} CA \\ CA^2 \\ \vdots \\ CA^p \end{bmatrix} \in \Re^{pn_y \times n_x} \tag{5.5}$$

$$S_{u-1} = \begin{bmatrix} CB_u \\ CAB_u + CB_u \\ \vdots \\ \sum_{j=0}^{p-1} CA^j B_u \end{bmatrix} \in \Re^{pn_x \times n_y} \tag{5.6}$$

and

$$S_u = \begin{bmatrix} CB_u & 0 & \dots & 0 \\ CB_u + CAB_u & CB_u & \dots & 0 \\ \vdots & & \ddots & \vdots \\ \sum_{j=0}^{p-1} CA^j B_u & \sum_{j=0}^{p-2} CA^j B_u & \dots & CB_u \end{bmatrix} \in \Re^{pn_y \times n_x} \tag{5.7}$$

$$S_v = \begin{bmatrix} CB_v & D_v & 0 & \dots & 0 \\ CAB_v & CB_v & D_v & \dots & 0 \\ \vdots & & & \ddots & \vdots \\ CA^{p-1}B_v & CA^{p-2}B_v & CA^{p-3}B_v & \dots & D_v \end{bmatrix} \in \Re^{pn_y \times (p+1)n_v} \tag{5.8}$$

$$S_w = \begin{bmatrix} CB_w & D_w & 0_v & \dots & 0 \\ CAB_w & CB_w & D_w & \dots & 0 \\ \vdots & & & \ddots & \vdots \\ CA^{p-1}B_w & CA^{p-2}B_w & CA^{p-3}B_w & \dots & D_w \end{bmatrix} \in \Re^{pn_y \times (p+1)n_w} \tag{5.9}$$

5.3 Optimization

With m denoting the control horizon, the free control moves can be expressed as

$$z = \begin{bmatrix} z_k \\ z_{k+1} \\ \vdots \\ z_{m-1} \end{bmatrix}, \qquad \begin{bmatrix} \Delta u_k \\ \Delta u_{k+1} \\ \vdots \\ \Delta u_{k+p-1} \end{bmatrix} = J_m \begin{bmatrix} z_k \\ z_{k+1} \\ \vdots \\ z_{m-1} \end{bmatrix} \tag{5.10}$$

where J_m is a blocking matrix, introducing possible restrictions on sample-to-sample moves, i.e. with the control signal fixed over consecutive samples, a concept not further explained in this thesis.

Optimization variables can be introduced according to

$$e_u = \begin{bmatrix} u_k \\ u_{k+1} \\ \vdots \\ u_{k+p-1} \end{bmatrix} - \begin{bmatrix} u_k^r \\ u_{k+1}^r \\ \vdots \\ u_{k+p-1}^r \end{bmatrix}, \; e_{\Delta u} = \begin{bmatrix} \Delta u_k \\ \Delta u_{k+1} \\ \vdots \\ \Delta u_{k+p-1} \end{bmatrix}, \; e_y = \begin{bmatrix} y_{k+1} \\ y_{k+2} \\ \vdots \\ y_{k+p} \end{bmatrix} - \begin{bmatrix} r_{k+1} \\ r_{k+2} \\ \vdots \\ r_{k+p} \end{bmatrix} \tag{5.11}$$

Considering the unconstrained case, i.e. with no constraints on inputs or outputs, the cost criterion to be minimized is

$$J(z,\varepsilon) = e_y^T W_y^2 e_y + e_{\Delta u}^T W_{\Delta u}^2 e_{\Delta u} + e_u^T W_u^2 e_u \tag{5.12}$$

where W denotes weighting matrices according to

$$W_u = diag\left[w_{k,1}^u \; w_{k,2}^u \; \dots \; w_{k,n_u}^u \; \dots \; w_{k+p-1,1}^u \; w_{k+p-1,2}^u \; \dots \; w_{k+p-1,n_u}\right] \tag{5.13}$$

$$W_{\Delta u} = diag\left[w_{k,1}^{\Delta u} \; w_{k,2}^{\Delta u} \; \dots \; w_{k,n_{\Delta u}}^{\Delta u} \; \dots \; w_{k+p-1,1}^u \; w_{k+p-1,2}^{\Delta u} \; \dots \; w_{k+p-1,n_{\Delta u}}^{\Delta u}\right] \tag{5.14}$$

$$W_y = diag\left[w_{k,1}^y \; w_{k,2}^y \; \dots \; w_{k,n_y}^y \; \dots \; w_{k+p-1,1}^y \; w_{k+p-1,2}^y \; \dots \; w_{k+p-1,n_y}\right] \tag{5.15}$$

with w_{ij}^x being a non-negative weight coefficient for the variable x_j at time i. Small weights w implies low importance of the behaviour of corresponding variable to overall performance. In eq. (5.12), the first term represents the setpoint tracking,

$$E_y(k) = \sum_{i=1}^{p} \sum_{j=1}^{n_y} \{w_j^y [y_j(k+i) - r_j(k+i)]\}^2 \tag{5.16}$$

i.e. how much an output will deviate from its reference value. The weights, as defined in eq. (5.15), determines the most important reference value to track, i.e. the tracking of an output with a low weight may be sacrificed in order to improve tracking of an output with a high weight. However, focusing strictly on setpoint tracking might cause the controller to make large actuator changes, which is often undesired since it may lead to system instability. To this purpose, move suppression is introduced through the second term of eq. (5.12) as

$$E_{\Delta u}(k) = \sum_{i=1}^{m} \sum_{j=1}^{n_{mv}} \{w_j^{\Delta u} \Delta u(k+i-1)\}^2 \tag{5.17}$$

where the weights, defined in eq. (5.14), causes the controller to make more cautious changes in actuator input. This is often, yet not always, done at the expense of setpoint tracking degradation. However, the benefit is a more robust controller, that is less sensitive to prediction inaccuracies.

Finally, the last term of eq. (5.12) is introduced as an attempt of trying to maintain the manipulated variables of the controller at a fixed point (within a constrained region, for the constrained case),

$$E_u(k) = \sum_{i=1}^{m} \sum_{j=1}^{n_{mv}} \{w_j^u [u_j(k+i-1) - u_j^r]\}^2 \tag{5.18}$$

This might, as when introducing move suppression, cause a degradation in output setpoint tracking. However, should a plant have an excess of manipulated variables with regards to the number of outputs, allowing the manipulated variables to move freely would result in a non-unique set of actuator input values. This, in turn, would cause the manipulated variables to drift within the region of operation.

Introducing constraints on inputs and outputs, according to

$$\begin{bmatrix} (y_{k+1})_{min} - \varepsilon(V^y_{k+1})_{min} \\ \vdots \\ (y_{k+p})_{min} - \varepsilon(V^y_{k+p})_{min} \\ (u_k)_{min} - \varepsilon(V^u_k)_{min} \\ \vdots \\ (u_{k+p-1})_{min} - \varepsilon(V^u_{k+p-1})_{min} \\ (\Delta u_k)_{min} - \varepsilon(V^{\Delta u}_k)_{min} \\ \vdots \\ (\Delta u_{k+p-1})_{min} - \varepsilon(V^{\Delta u}_{k+p-1})_{min} \end{bmatrix} \leq \begin{bmatrix} y_{k+1} \\ \vdots \\ y_{k+p} \\ u_k \\ \vdots \\ u_{k+p-1} \\ \Delta u_k \\ \vdots \\ \Delta u_{k+p-1} \end{bmatrix} \leq \begin{bmatrix} (y_{k+1})_{max} + \varepsilon(V^y_{k+1})_{max} \\ \vdots \\ (y_{k+p})_{max} + \varepsilon(V^y_{k+p})_{max} \\ (u_k)_{max} + \varepsilon(V^u_k)_{max} \\ \vdots \\ (u_{k+p-1})_{max} + \varepsilon(V^u_{k+p-1})_{max} \\ (\Delta u_k)_{max} + \varepsilon(V^{\Delta u}_k)_{max} \\ \vdots \\ (\Delta u_{k+p-1})_{max} + \varepsilon(V^{\Delta u}_{k+p-1})_{max} \end{bmatrix}$$

where ε is the slack-variable, introduced to relax the constraints on y, u and Δu given by $y_{min}, y_{max}, u_{min}, u_{max}, \Delta u_{min}$ and Δu_{max}. The relaxation vectors V^y_{min}, V^y_{max}, V^u_{min}, V^u_{max}, $V^{\Delta u}_{min}$ and $V^{\Delta u}_{max}$, with non-negative entries, indicates the cost of relaxing the corresponding constraint - large values of V implies a soft constraint which may, though matematically discouraged, be violated, while small values of V implies a hard constraint, that must not be violated. Typically, input constraints are hard, since these are often specified by physical constraints of the plant. Hard constraints on outputs may cause infeasibility of the optimization problem, e.g. due to model mismatch or unpredicted disturbances. Thus, output constraints are generally soft. The cost function to be minimized for the constrained case is, with constraints as stated above,

$$J(z, \varepsilon) = e_y^T W_y^2 e_y + e_{\Delta u}^T W_{\Delta u}^2 e_{\Delta u} + e_u^T W_u^2 e_u + \rho_\varepsilon \varepsilon^2 \tag{5.19}$$

where ρ_ε is the weight on ε, penalizing violations of constraints - large ρ_ε with respect to input and output weights, implies a high penalty on constraint violations. Clearly, in eq. (5.19), $\rho_\varepsilon \varepsilon^2$ indicates a quadratic penalty on violating the constraints of the system.

Summarizing the equations above, the MPC optimization problem can be formulated as

$$\begin{aligned} \min_u J(u) \quad &= \quad \min_{\Delta u_{k|k} \ldots \Delta u_{m-l+k|k},\ \varepsilon} \{ \sum_{i=0}^{p-1} (\sum_{j=1}^{n_y} |w^y_{i+1,j} (y_{k+i+1|k} - r^j_{k+j+1})|^2 \\ &+ \quad \sum_{j=1}^{n_u} |(w^{\Delta u}_i)^j \Delta u_{k+i|k}|^2 + \sum_{j=1}^{n_{n_u}} |(w^u_i)^j (u^j_{k+i|k} - (u^r_{k+i})^j)|^2) + \rho_\varepsilon \varepsilon^2 \} \end{aligned} \tag{5.20}$$

subject to

$$(u^j_i)_{min} - \varepsilon(V^u_j)_{min} \leq u^j_{k+i|k} \leq (u^j_i)_{max} + \varepsilon(V^u_j)_{max} \tag{5.21}$$

$$(y^j_i)_{min} - \varepsilon(V^y_j)_{min} \leq y^j_{k+i+1|k} \leq (y^j_i)_{max} + \varepsilon(V^y_j)_{max} \tag{5.22}$$

$$(\Delta u^j_i)_{min} - \varepsilon(V^{\Delta u}_j)_{min} \leq \Delta u^j_{k+i|k} \leq (\Delta u^j_i)_{max} + \varepsilon(V^{\Delta u}_j)_{max} \tag{5.23}$$

$$\Delta u_{k+h|k} = 0, h = m, \ldots, p-1 \tag{5.24}$$

$$\varepsilon \geq 0, i = 0, 1, \ldots, p \tag{5.25}$$

6 Control design

6.1 Slip Linearization

Since MPC uses an approximate *linear* model of the plant to provide the prediction, the nonlinear slip behaviour must be linearized. A typical slip behaviour, for different surface conditions, can be seen in Fig. 3.6. In the following sections, all controllers are designed for ice surfaces, i.e. $\mu = 0.2$.

As stated previously, the model provided in the MPC design, is most often in state-space formulation. However, since slip is, according to eq. (3.21), dependent of the vehicle velocity, this would result in a combination of states. The problem when considering a suitable model of the plant for MPC design is thus twofold - the slip behaviour must be linearized, while avoiding combination of states.

Considering the problem of state combinations, this is solved by assuming model validity for specified velocity regions, i.e. when calculating the slip curves, the velocity is assumed constant. In this thesis, only low vehicle velocity is assumed, since low velocities poses the largest traction control problems. The slip can then be defined as

$$\lambda^* = \frac{\omega r - v_{veh}}{v^*_{veh}} \tag{6.1}$$

where v^*_{veh} denotes the assumed constant vehicle velocity. Assuming a velocity region of $1 - 10\ km/h$, v^*_{veh} can be calculated as

$$\frac{\frac{1}{1} - \frac{1}{10}}{2} = \frac{1}{v^*_{veh}} \rightarrow v^*_{veh} = \frac{20}{9}\ km/h = \frac{50}{81}\ m/s \approx 0.62\ m/s \tag{6.2}$$

The resulting slip curve, when using v^* from Eq. (6.2), can be seen in Fig. 6.1. The nonlinear slip curve can be linearized by assuming linear behaviour on each side of the peak, i.e. on the stable and unstable side respectively. In Fig. 6.1, linear curves are shown, indicating also the switch point λ_{max}.The result is thus two linear functions

$$T_L \ = \begin{cases} \kappa_1 \lambda^*, & \lambda^* \leq \lambda^*_{max} \\ (\kappa_1 + \kappa_2)\lambda^*_{max} + \kappa_2 \lambda^*, & \lambda^* > \lambda^*_{max} \end{cases} \tag{6.3}$$

where T_L denotes the tyre-road friction torque load on the wheel, and where κ_1 and κ_2 is the derivative of the stable and unstable linear function respectively.

The controller is designed to accelerate the vehicle from standstill, assuming the role of both driver and traction controller. This could cause problems since the behaviour of an accelerating controller and a traction controller with the purpose of preventing excessive slip, might be different. An accelerating controller should have fast response, in order to accelerate the vehicle to desired velocity within a reasonable time frame, while a traction controller preventing excessive slip should be more robust with regards to disturbances, e.g. changes in surface conditions. An alternative to the controller designed and implemented above, would be a controller only activated when the wheel slip is in the vicinity of the peak, λ^*_{max}, an approach not further investigated in this thesis.

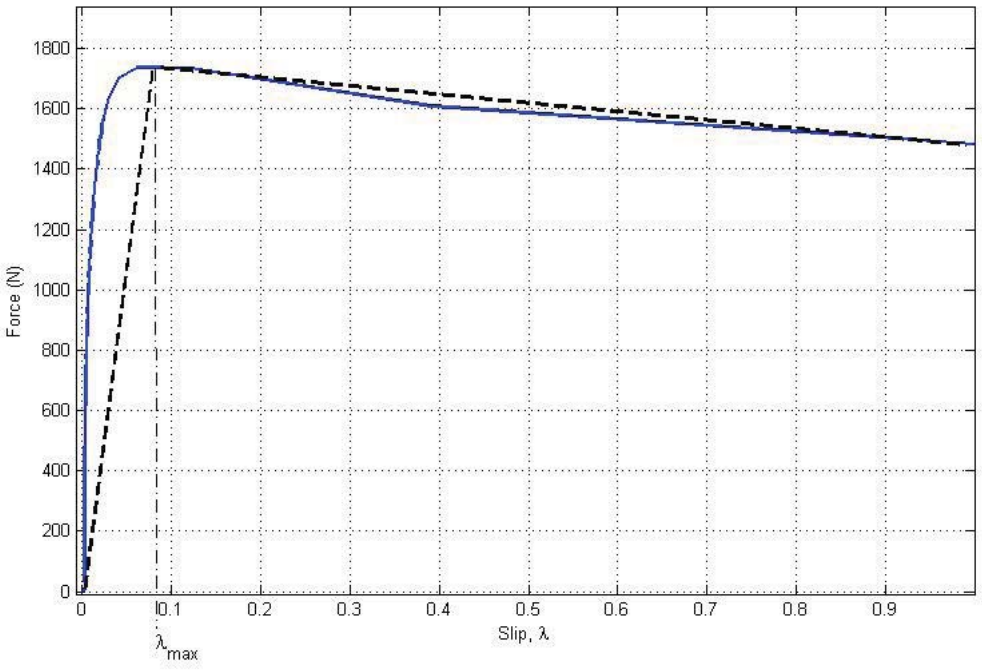

Figure 6.1: Slip curve when using v^*_{veh} for $\mu = 0.2$

Considering Fig. 6.1, it is clear that the linear parameters varies depending on the linearization points. For the stable linear curve, for instance, the parameters may be chosen with regards to the slip curve in the vicinity of the peak - they may, however, be chosen with regards to the initial behaviour of the slip curve instead. In Section 7.2, the importance of the linearization parameters are shown, and the problem discussed above is examined with regards to these parameters, as well as with regards to controller weights.

6.2 State-Space Formulation

Since the controller is designed for a given model and then implemented, the model can not be modified without re-designing the controller. Thus, different slip scenarios must be defined as models, for which separate controllers are designed. The scenarios considered are

- Both wheels are stable, i.e. $\lambda^*_L \leq \lambda^*_{max}$ and $\lambda^*_R \leq \lambda^*_{max}$
- The left wheel have excessive slip, i.e. $\lambda^*_L > \lambda^*_{max}$ and $\lambda^*_R \leq \lambda^*_{max}$
- The right wheel have excessive slip, i.e. $\lambda^*_L \leq \lambda^*_{max}$ and $\lambda^*_R > \lambda^*_{max}$
- Both wheels have excessive slip, i.e. $\lambda^*_L > \lambda^*_{max}$ and $\lambda^*_R > \lambda^*_{max}$

Thus, four models are defined, requiring four separate controllers. An approximate model of the differential gear dynamics, can be expressed as

$$
\begin{aligned}
J_c\ddot{\theta}_c &= T_p - c(\dot{\theta}_{s_L} - \dot{\theta}_{w_L}) - k(\theta_{s_L} - \theta_{w_L}) - c(\dot{\theta}_{s_R} - \dot{\theta}_{w_R}) - k(\theta_{s_R} - \theta_{w_R}) && (6.4)\\
J_{pg}\ddot{\theta}_{pg} &= -c(\dot{\theta}_{s_L} - \dot{\theta}_{w_L}) - k(\theta_{s_L} - \theta_{w_L}) + c(\dot{\theta}_{s_R} - \dot{\theta}_{w_R}) + k(\theta_{s_R} - \theta_{w_R}) && (6.5)\\
J_w\ddot{\theta}_{w_L} &= c(\dot{\theta}_{s_L} - \dot{\theta}_{w_L}) + k(\theta_{s_L} - \theta_{w_L}) - T_{L_L} - T_{B_L} && (6.6)\\
J_w\ddot{\theta}_{w_R} &= c(\dot{\theta}_{s_R} - \dot{\theta}_{w_R}) + k(\theta_{s_R} - \theta_{w_R}) - T_{L_R} - T_{B_R} && (6.7)
\end{aligned}
$$

where c denotes the drive shaft damping and k denotes the drive shaft compliance, and state notations from Section 3.7, Eq. (3.9) - (3.12). Also, for the side gears

$$
\begin{aligned}
\theta_{s_L} &= \theta_c + \frac{1}{2}\theta_{pg} && (6.8)\\
\theta_{s_R} &= \theta_c - \frac{1}{2}\theta_{pg} && (6.9)
\end{aligned}
$$

Inserting Eq. (6.8) and Eq. (6.9) in Eq. (6.4) - (6.7),

$$
\begin{aligned}
J_c\ddot{\theta}_c &= T_p - c(\dot{\theta}_c + \frac{1}{2}\dot{\theta}_{pg} - \dot{\theta}_{w_L}) - k(\theta_c + \frac{1}{2}\theta_{pg} - \theta_{w_L})\\
&- c(\dot{\theta}_c - \frac{1}{2}\dot{\theta}_{pg} - \dot{\theta}_{w_R}) - k(\theta_c - \frac{1}{2}\theta_{pg} - \theta_{w_R})\\
&= T_p - 2c\dot{\theta}_c + c\dot{\theta}_{w_L} + c\dot{\theta}_{w_R} - k(\theta_c + \frac{1}{2}\theta_{pg} - \theta_{w_L}) - k(\theta_c - \frac{1}{2}\theta_{pg} - \theta_{w_R}) && (6.10)
\end{aligned}
$$

$$
\begin{aligned}
J_{pg}\ddot{\theta}_{pg} &= c(\dot{\theta}_c - \frac{1}{2}\dot{\theta}_{pg} - \dot{\theta}_{w_R}) + k(\theta_c - \frac{1}{2}\theta_{pg} - \theta_{w_R})\\
&- c(\dot{\theta}_c + \frac{1}{2}\dot{\theta}_{pg} - \dot{\theta}_{w_L}) - k(\theta_c + \frac{1}{2}\theta_{pg} - \theta_{w_L})\\
&= c\dot{\theta}_{W_L} - c\dot{\theta}_{W_R} - c\dot{\theta}_{pg} + k(\theta_c - \frac{1}{2}\theta_{pg} - \theta_{W_R}) - k(\theta_c + \frac{1}{2}\theta_{pg} - \theta_{W_L}) && (6.11)
\end{aligned}
$$

$$
\begin{aligned}
J_w\ddot{\theta}_{w_L} &= c(\dot{\theta}_c + \frac{1}{2}\dot{\theta}_{pg} - \dot{\theta}_{w_L}) + k(\theta_c + \frac{1}{2}\theta_{pg} - \theta_{w_L}) - T_{L_L} - T_{B_L} && (6.12)\\
J_w\ddot{\theta}_{w_R} &= c(\dot{\theta}_c - \frac{1}{2}\dot{\theta}_{pg} - \dot{\theta}_{w_R}) - k(\theta_c - \frac{1}{2}\theta_{pg} - \theta_{w_R}) - T_{L_R} - T_{B_R} && (6.13)
\end{aligned}
$$

By linearizing the wheel dynamics as described in Eq. (6.3), the tyre-road friction load torque on the wheels can be expressed as

$$
T_{L_L} = \frac{\kappa_1}{v^*_{veh}/r}(\dot{\theta}_{w_L} - v/r) \tag{6.14}
$$

and

$$
T_{L_R} = \frac{\kappa_1}{v^*_{veh}/r}(\dot{\theta}_{w_R} - v/r) \tag{6.15}
$$

for the left and right wheel during stable surface conditions, respectively. During unstable surface conditions, the linearized tyre-road friction load torque can be expressed as

$$T_{L_L} = (\kappa_1 + \kappa_2)\lambda_{max} + \frac{\kappa_2}{v^*_{veh}/r}(\dot{\theta}_{w_L} - v/r) \tag{6.16}$$

and

$$T_{L_R} = (\kappa_1 + \kappa_2)\lambda_{max} + \frac{\kappa_2}{v^*_{veh}/r}(\dot{\theta}_{w_R} - v/r) \tag{6.17}$$

as described above.

The system of equations can thus be described using state-space form, as

$$\begin{bmatrix} J_c\ddot{\theta}_c \\ J_{pg}\ddot{\theta}_{pg} \\ J_w\ddot{\theta}_{w_L} \\ J_w\ddot{\theta}_{w_R} \\ (\dot{\theta}_c + \frac{1}{2}\dot{\theta}_{pg} - \dot{\theta}_{w_L}) \\ (\dot{\theta}_c - \frac{1}{2}\dot{\theta}_{pg} - \dot{\theta}_{w_R}) \\ m_{veh}\dot{v} \end{bmatrix} = \begin{bmatrix} -2c & 0 & c & c & -k & -k & 0 \\ 0 & -c & c & -c & -k & k & 0 \\ c & c/2 & -c & 0 & k & 0 & 0 \\ c & -c/2 & 0 & -c & 0 & k & 0 \\ 1 & 1/2 & -1 & 0 & 0 & 0 & 0 \\ 1 & -1/2 & 0 & -1 & 0 & 0 & 0 \\ 0 & 0 & 0 & 0 & 0 & 0 & 0 \end{bmatrix} \begin{bmatrix} \dot{\theta}_c \\ \dot{\theta}_{pg} \\ \dot{\theta}_{w_L} \\ \dot{\theta}_{w_R} \\ (\theta_c + \frac{1}{2}\theta_{pg} - \theta_{w_L}) \\ (\theta_c - \frac{1}{2}\theta_{pg} - \theta_{w_R}) \\ v \end{bmatrix}$$

$$+ \begin{bmatrix} 1 & 0 \\ 0 & 1 \\ 0 & 0 \\ 0 & 0 \\ 0 & 0 \\ 0 & 0 \\ 1/r & 1/r \end{bmatrix} \begin{bmatrix} T_{L_L} \\ T_{L_R} \end{bmatrix} + \begin{bmatrix} 1 & 0 & 0 \\ 0 & 0 & 0 \\ 0 & -1 & 0 \\ 0 & 0 & -1 \\ 0 & 0 & 0 \\ 0 & 0 & 0 \\ 0 & 0 & 0 \end{bmatrix} \begin{bmatrix} T_p \\ T_{B_L} \\ T_{B_R} \end{bmatrix}$$

$$y = \begin{bmatrix} 0 & 0 & 1 & 0 & 0 & 0 & -1/r \\ 0 & 0 & 0 & 1 & 0 & 0 & -1/r \end{bmatrix} \begin{bmatrix} J_p\dot{\theta}_c \\ J_d\dot{\theta}_{pg} \\ J_w\dot{\theta}_{w_L} \\ J_w\dot{\theta}_{w_R} \\ (\theta_c + \frac{1}{2}\theta_{pg} - \theta_{w_L}) \\ (\theta_c - \frac{1}{2}\theta_{pg} - \theta_{w_R}) \\ m_{veh}v \end{bmatrix}$$

where the states $(\theta_c + \frac{1}{2}\theta_{pg} - \theta_{w_L})$ and $(\theta_c - \frac{1}{2}\theta_{pg} - \theta_{w_R})$ have been introduced to ensure full model observability, and where T_{L_L} and T_{L_R} are defined in Eq. (6.14)-(6.17).

6.3 Constraints and Weights

As previously discussed, one of the main difficulties with using MPC, is the choice of weights. There is no method providing optimal weights, rather, these are determined upon knowledge of the system and the experience of the control designer.

Consider the control problem at hand. As discussed in Section 6.2, four controllers are needed. These will in the following sections be denoted as SS, US, SU and UU, where S denotes stable behaviour and U denotes unstable slip behaviour, and where the order is taken as $[Left\ wheel, Right\ wheel]$. Naturally, the highest weight should be on set point tracking, i.e. the weights on λ_L and λ_R should be significantly higher than the

other weights, for all controllers. Should the weights be too high in relation to the others, however, other weights may become insignificant and not affect the controller in the desired manner. Further on, on the stable side of the slip curve (SS), the brake force should be conservative since excessive use of brake force can increase brake wear. The rate weights, should be low to allow for higher accelerations while limiting bang-bang behaviour.

On the unstable side of the slip curve (UU), the brake force should have no weights since slowing down spinning wheels is important and the brakes should be allowed to use as much brake power as is required. However, too low rate weights on the brake force may cause high-frequent braking and unwanted bang-bang behaviour. The engine torque should have a rather high weight, to account for the fact that engine torque should be significantly reduced to slow down the spinning wheels. In order for the engine torque to be reduced rapidly when entering the unstable side of the slip curve, the rate weight should be kept low. Also, slightly lower weights on set point tracking might increase the impact of the other weights favourably.

The split controllers (US and SU) should have the same weights, since the model is symmetric. There should be a moderate weight on engine torque, since it is not desired to have high engine torque when one of the wheels is spinning. The rate weight on the engine torque could be kept slightly lower, to allow for faster changes in torque. Regarding the brake force weights, it would be natural to assume low weight on the brake force on the wheel experiencing high slip, while increasing the weight on the other wheel. However, the differential dynamics causes the wheels to affect one another, as discussed previously. Thus, increasing the weight on the wheel currently on the stable side of the slip curve, would most likely cause it to spin when brake force is actuated on the spinning wheel. To account for the differential gear dynamics, there should be no weights on the brake torques and low weights on the rate weights, since the brakes should be engaged rapidly once one of the wheels start to spin.

The system is subject to actuator constraints, which should be defined when designing the controllers. The constraints on the engine and on the brakes, are listed in Table (6.1).

Name	Minimum	Maximum	Max Down Rate	Max Up Rate
Engine Torque	0	2250	2000	2000
Brake Force, left	0	50000	50000	50000
Brake Force, right	0	50000	50000	50000

Table 6.1: Actuator constraints

Also, the weights are, as previously discussed, of great importance when designing the controllers. The implementation of controllers, with varying weights, are presented in Section 7.2 - thus, specific choice of weights are not presented here.

7 Results

7.1 Validation of model

7.1.1 Test 1

As previously stated, Test 1 have negligible slip as well as a large offset in wheels velocities. Thus, Test 1 has initially been used to get an accurate model without implemented nonlinearities. The resulting wheel velocities for the model are shown in Fig. 7.1.

Figure 7.1 should be compared with the actual velocities from measurement data, see Section 4.6.1. For convenience, the actual velocities for the left wheel and the right wheel are paired with the respective wheel velocity from the model in Fig. 7.2-7.3.

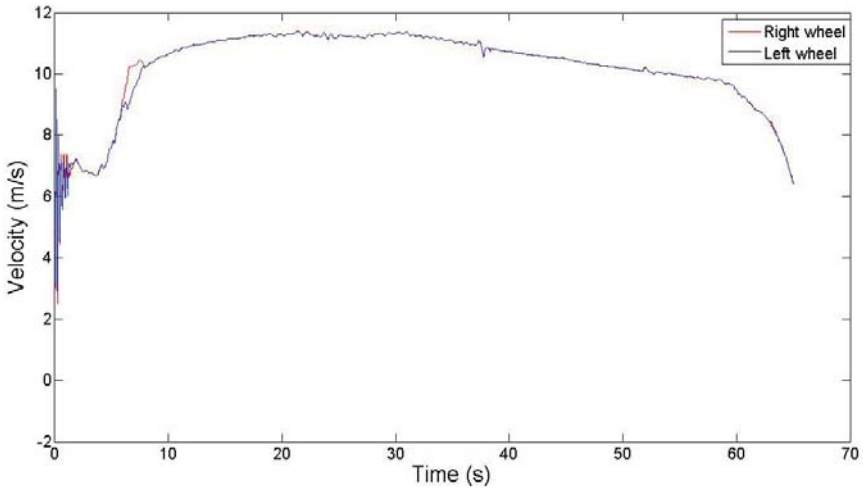

Figure 7.1: Model wheel velocities

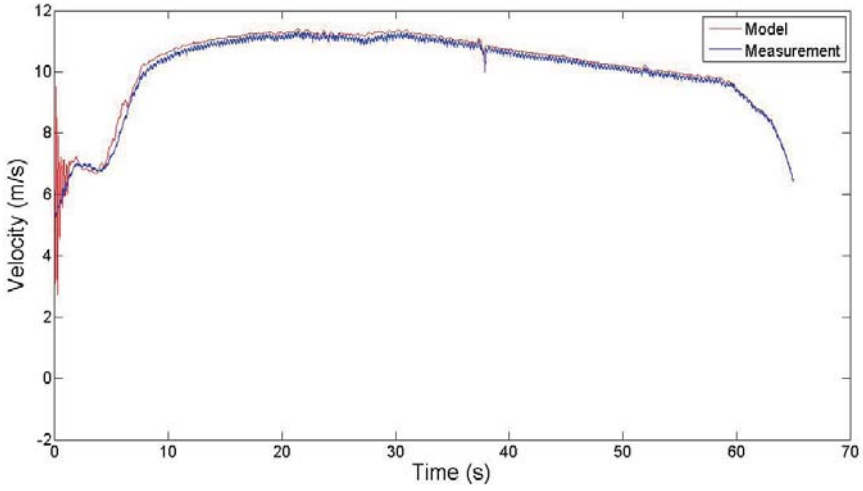

Figure 7.2: Model and actual left wheel velocities

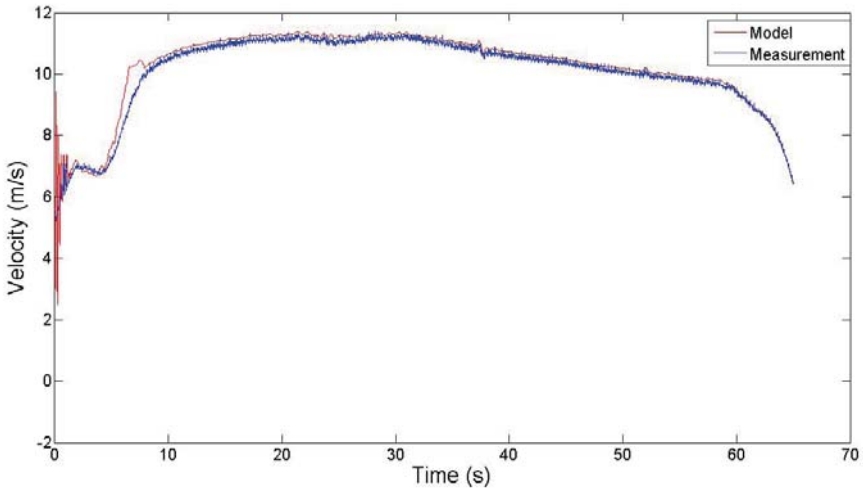

Figure 7.3: Model and actual right wheel velocities

Implementing friction and adjusting the parameters until the results are satisfactory, as suggested in Section 4.4.2, causes the friction to attain values higher than physically plausible. Rather, the difference in velocities is likely due to imperfections in the wheel dynamics and will therefore not be further examined.

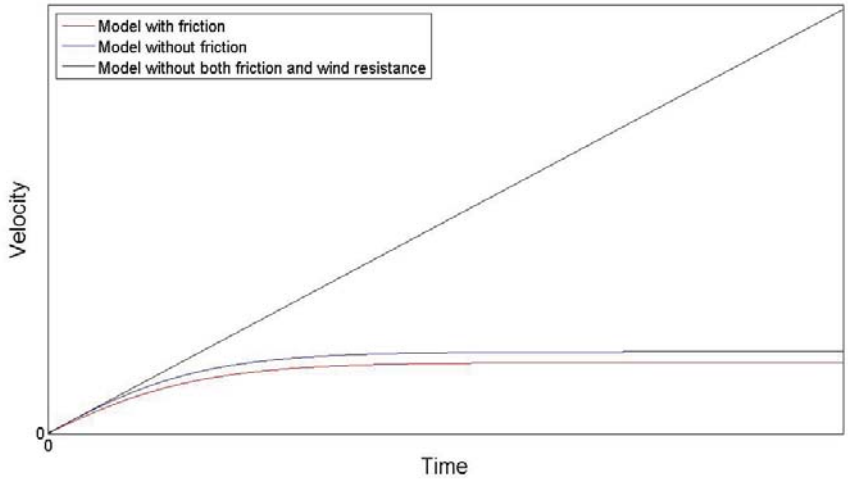

Figure 7.4: Friction effects on wheel velocities

Since the measurements could not be used for finding the friction parameters for the Coulomb friction and the viscous friction, another approach was necessary. Discussions with the supervisors and testing of the effect of the friction rendered values roughly chosen as $T_C = 300\ Nm$ and $\eta_{visc} = 10\ Nms$. The effect when implementing the friction, when the input engine torque is constant and no brake torque is actuated, can be seen in Fig. 7.4 .

A comparison between measurement data and model results, with and without friction implemented, for Test 1, can be seen in Fig. 7.5. The figure depicts the simulation between

$10 - 20s$, where the velocities are stable and sufficiently high. Since there is little difference for the velocities on the left and right side only the left wheels are considered.

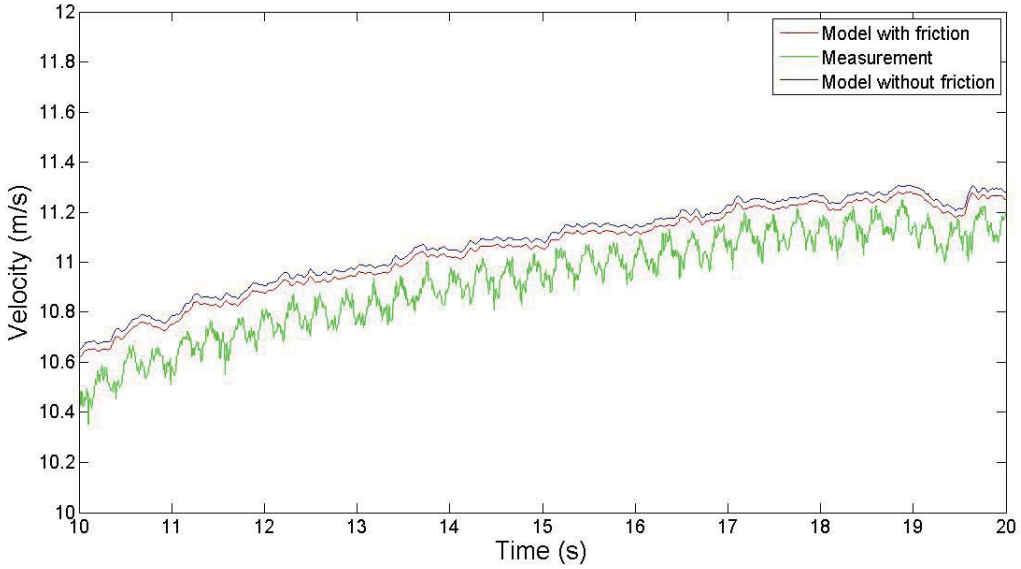

Figure 7.5: Friction effects on left wheel velocities compared with actual left wheel velocities

7.1.2 Test 2

The resulting wheel velocities when simulating the model using measurement data from Test 2, see Section 4.6.2, can be seen in Fig. 7.6.

As for Test 1, the left and right wheel velocities are also plotted separately paired with the corresponding wheel velocities from measurement data, see Fig. 7.7-7.8. In the same manner as with Test 1, neither the backlash nor friction was implemented in the model initially.

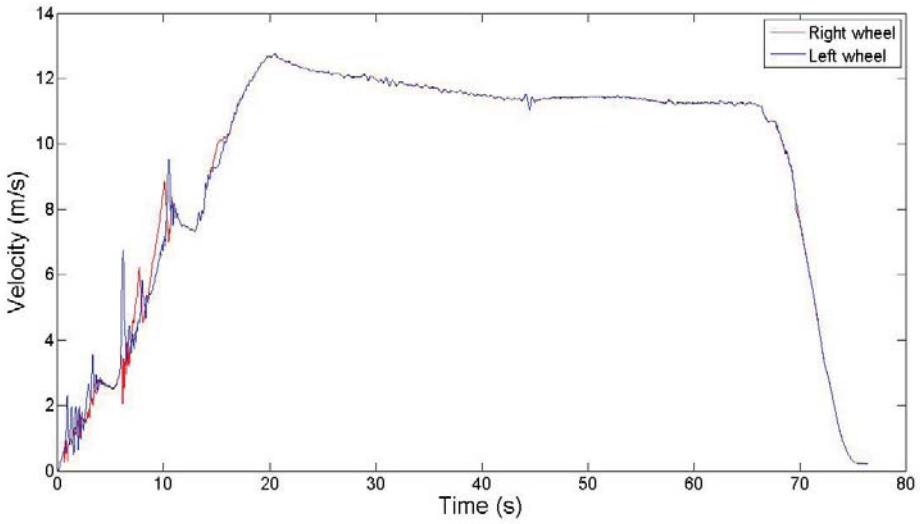

Figure 7.6: Model wheel velocities

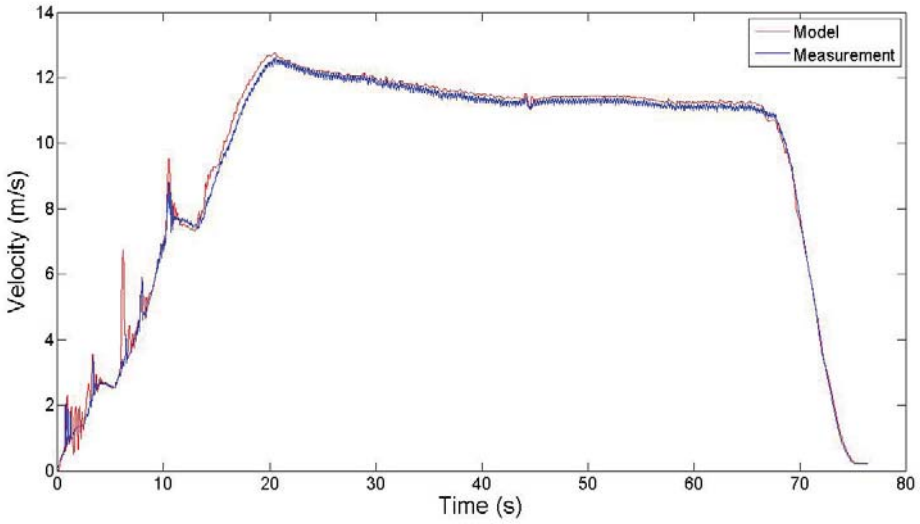

Figure 7.7: Model and actual left wheel velocities

The most interesting interval is between $0-15$ s where there is excessive wheel slip on both wheel sides. In Fig. 7.9 the model wheel velocities for the left and right side are shown in

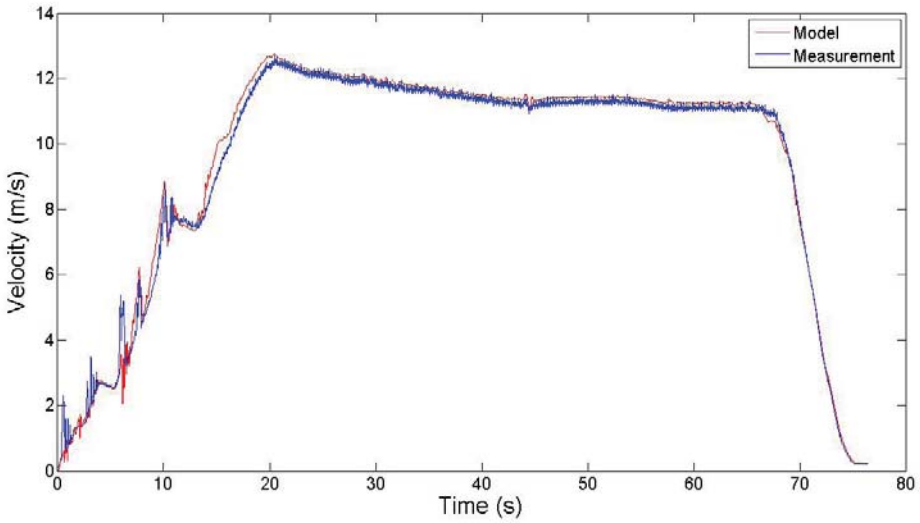

Figure 7.8: Model and actual right wheel velocities.

this interval, while the actual wheel velocities from measurement data are shown in Fig. 7.10.

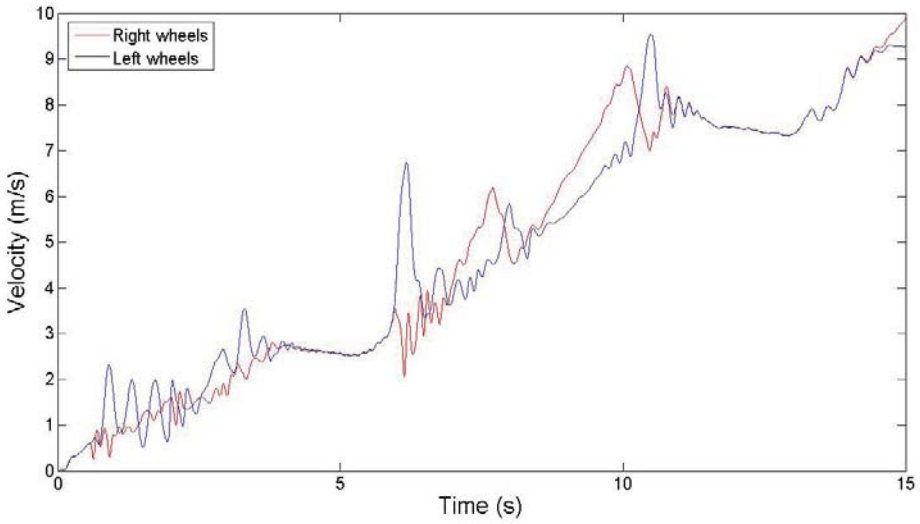

Figure 7.9: Model wheel velocities, $0 - 15$ s

After the initial simulation, the nonlinearities discussed in Section 2, were implemented, starting with the friction models. The friction between pinion gear and crown wheel, used in Test 1, results in a decrease of the wheel velocities for sufficiently high velocities similar to the behaviour in Fig. 7.5. The effects when the LuGre friction model was implemented, can be seen in Fig. 7.11-7.12 for the interval $0 - 15$ s and for the left and right wheels respectively.

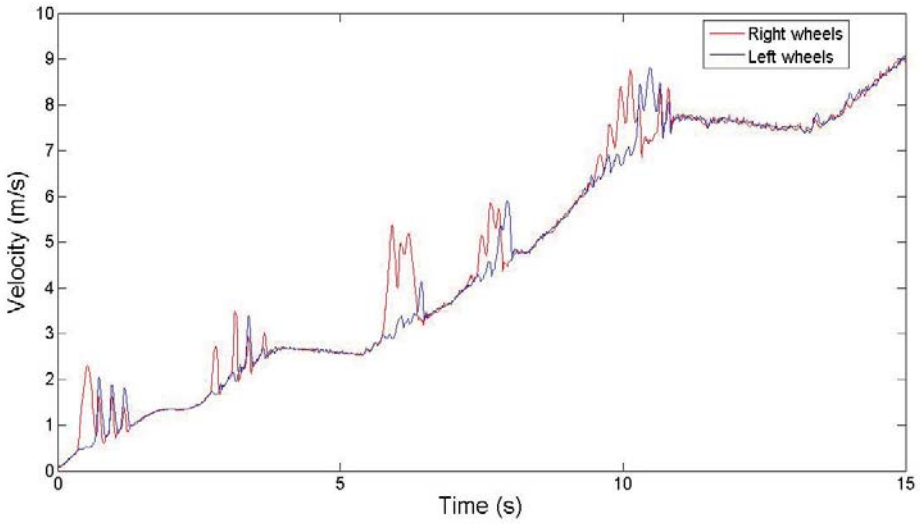

Figure 7.10: Actual wheel velocities, $0 - 15$ s

It is interesting to note the effect of the LuGre friction on the velocities of the planet gears since the friction is present between planet gears and side wheels, see Fig. 7.13.

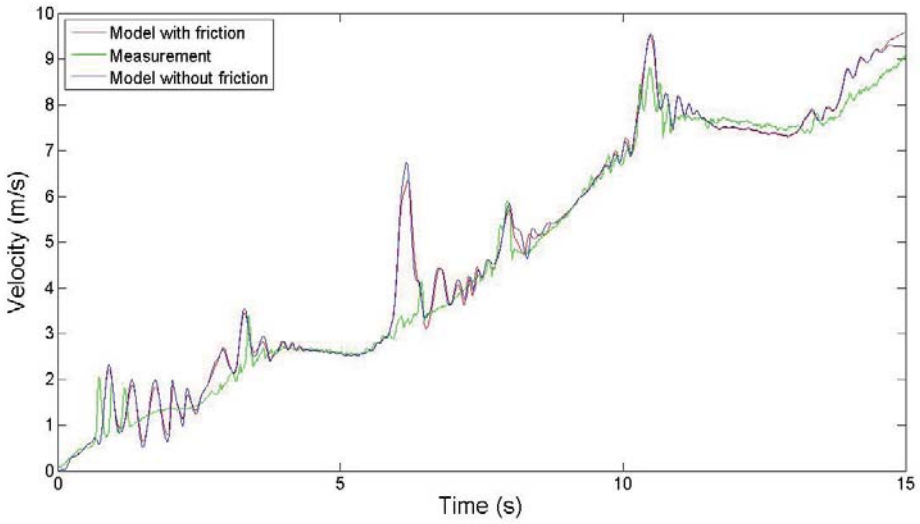

Figure 7.11: Model with and without friction, and actual left wheel velocities, $0 - 15$ s

Apart from the friction, backlash was implemented, initially using the frictionless model, see Fig. 7.16-7.18.

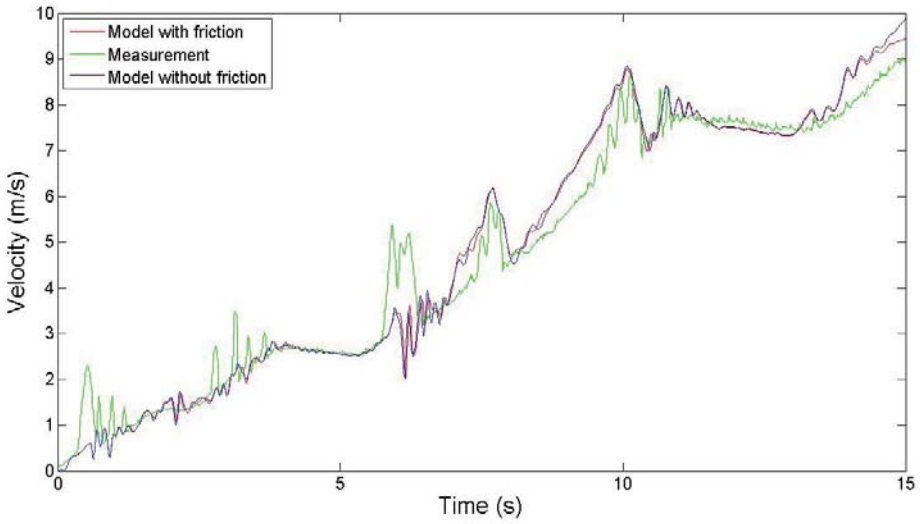

Figure 7.12: Model with and without friction, and actual right wheel velocities, $0 - 15\ s$

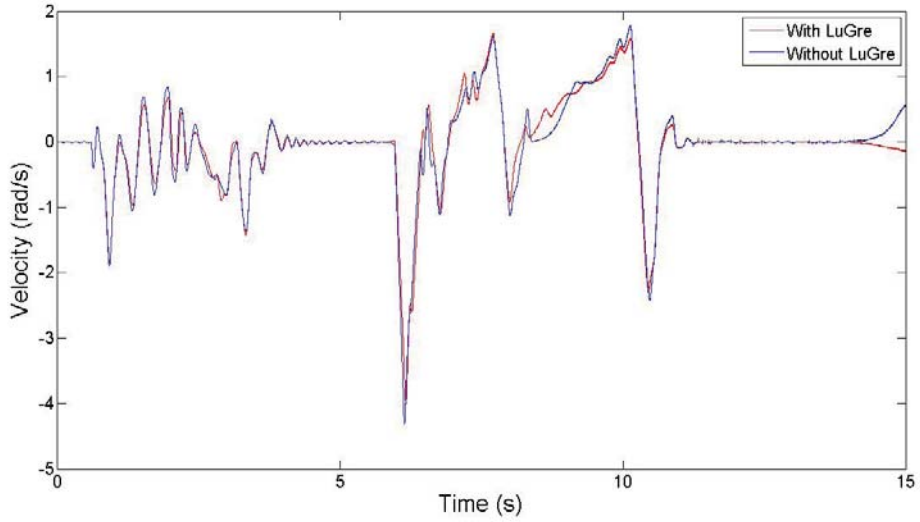

Figure 7.13: Planet gear velocities, with and without friction, $0 - 15\ s$

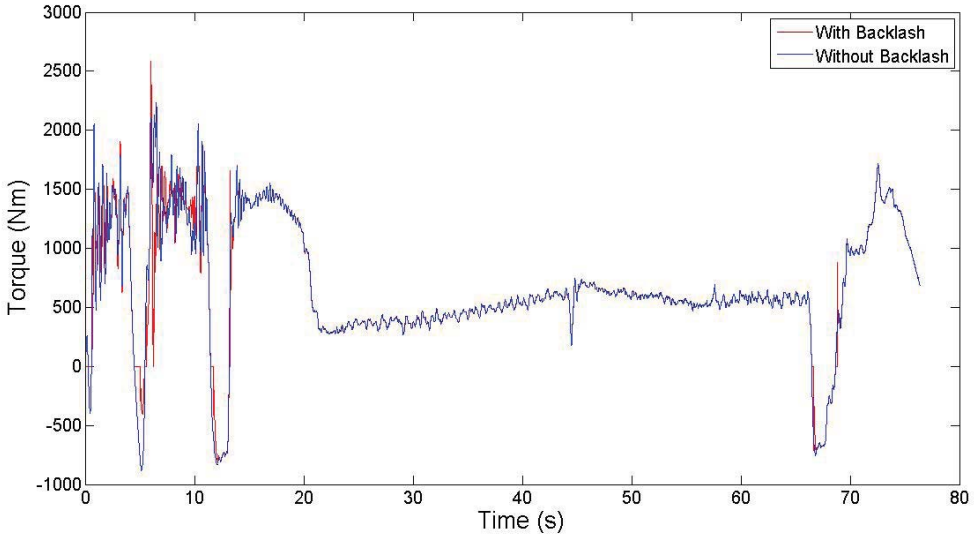

Figure 7.14: Contact torque between planet gears and left side gear,with and without backlash

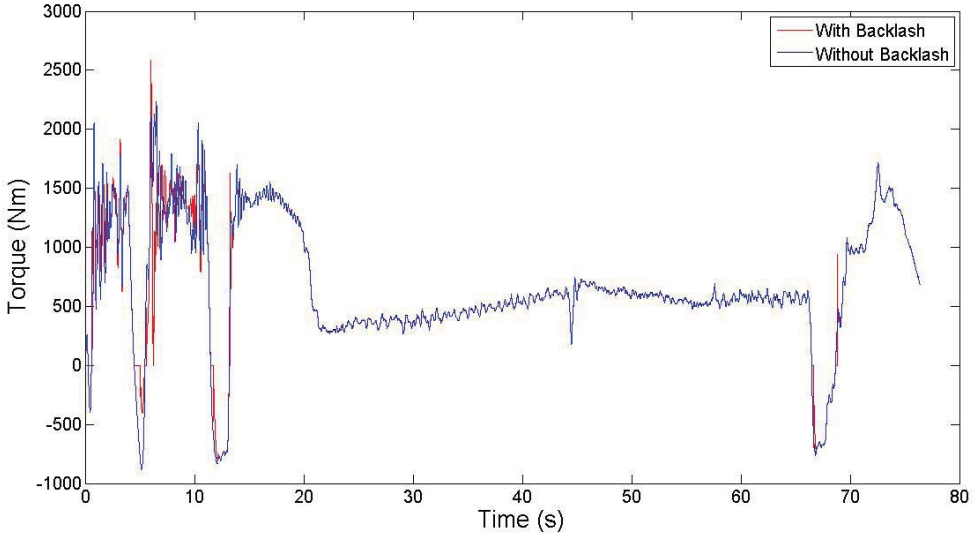

Figure 7.15: Contact torque between planet gears and right side gear,with and without backlash

It is of interest to regard the impact of the backlash on the wheel velocities. The greatest differences were found during the first 15 s, thus, only this interval will be considered. Plotting the velocities for the left and right wheels with and without backlash, yields Fig. 7.17 and Fig. 7.19. For comparison, the respective contact torques are plotted for the same interval.

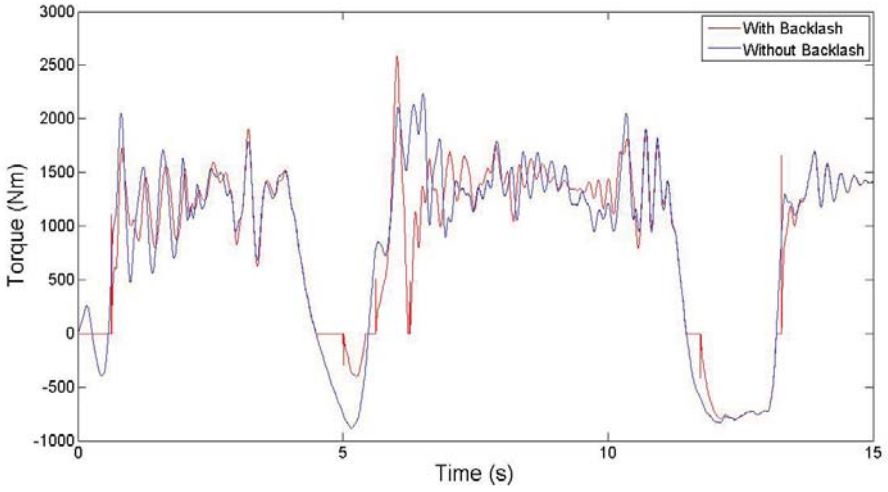

Figure 7.16: Contact torque between planet gears and left side gear, with and without backlash, $0 - 15$ s

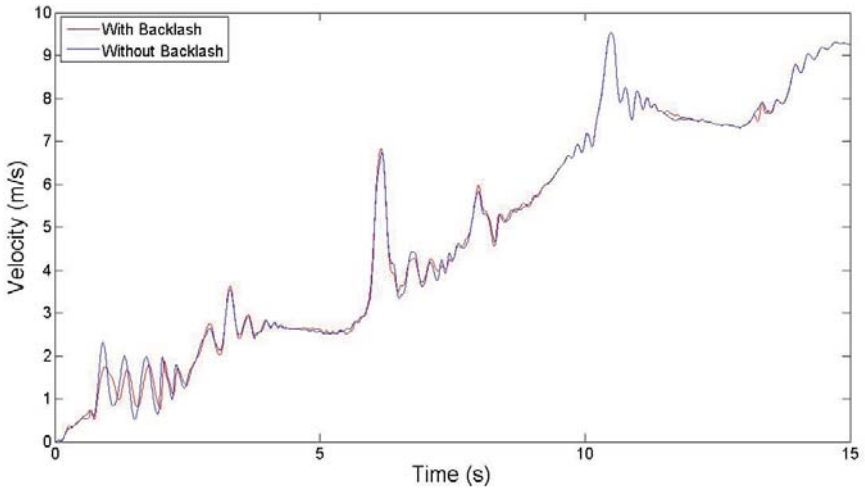

Figure 7.17: Model left wheel velocities, with and without backlash, $0 - 15$ s

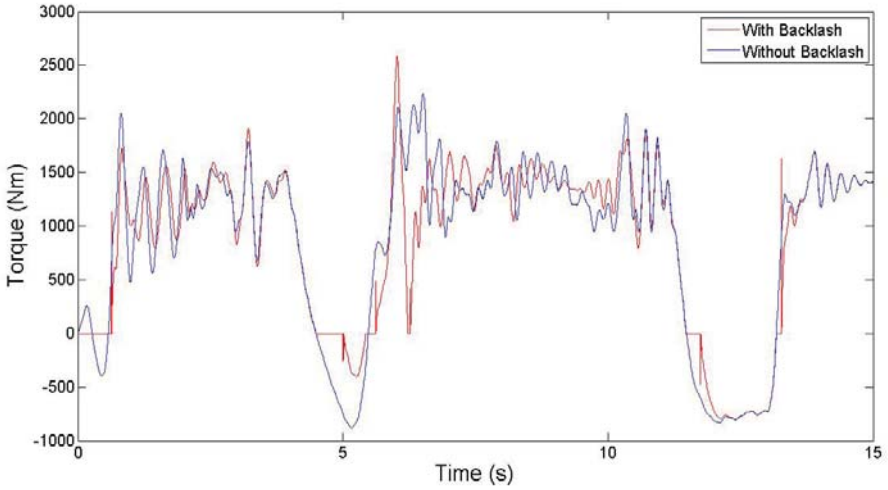

Figure 7.18: Contact torque between planet gears and right side gear, with and without backlash, $0 - 15$ s

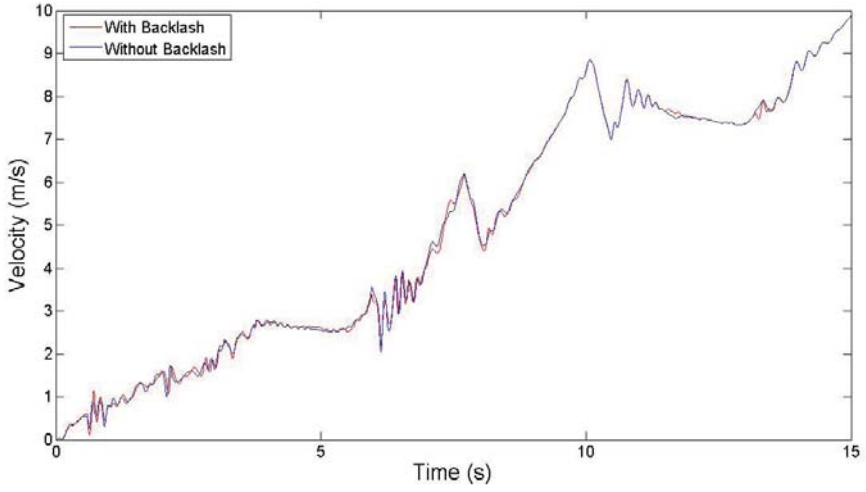

Figure 7.19: Model right wheel velocities, with and without backlash, $0 - 15$ s

The model behaviour with both friction and backlash implemented was also studied. The simulation results when implementing both friction and backlash, can be seen in Fig. 7.20-7.21 for the interval $0 - 15$ s.

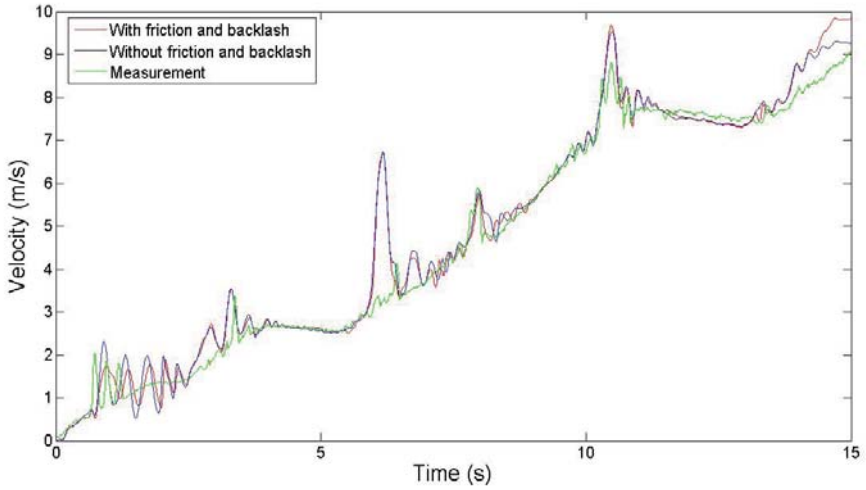

Figure 7.20: Model left wheel velocities, with and without backlash and friction, compared to actual velocities, $0 - 15$ s

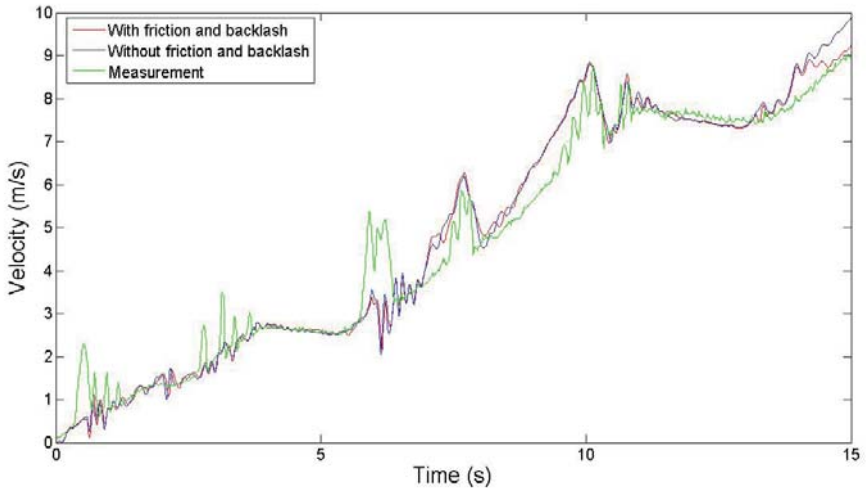

Figure 7.21: Model right wheel velocities, with and without backlash and friction, compared to actual velocities, $0 - 15$ s

Adjusting the values for both the left and right wheels leads to wheel velocity differences. To compare the wheel velocities from the model with adjusted friction coefficient to the actual wheel velocities, these are plotted together in Fig. 7.22.

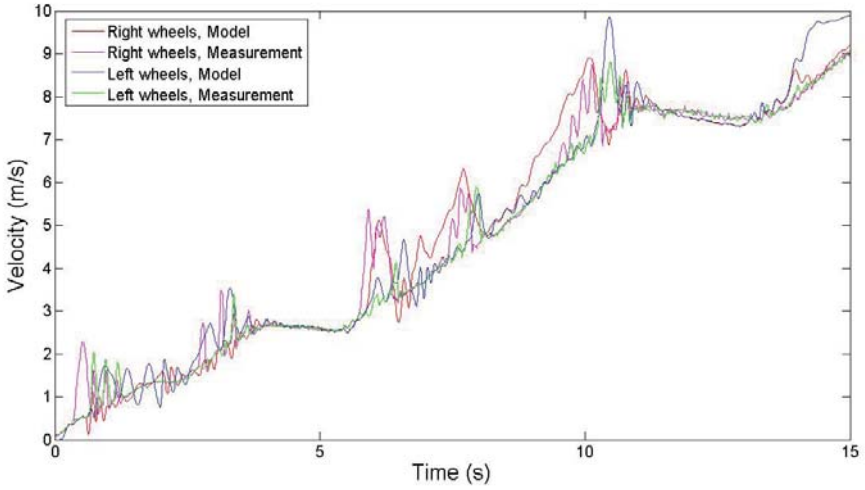

Figure 7.22: Model wheel velocities, with adjusted road friction coefficient, compared to actual velocities, $0 - 15$ s

7.1.3 Test 3

The validation against Test 3, used the model with parameters derived from validation against Test 1 and Test 2, hence both friction and backlash were implemented. As discussed in Section 4.6.3, there are two separate intervals for which there is excessive wheel slip. The first interval is $0 - 18\ s$ and the other interval is $55 - 60\ s$. It should be noted that the road surface friction coefficient has been adjusted which results in wheel velocity differences.

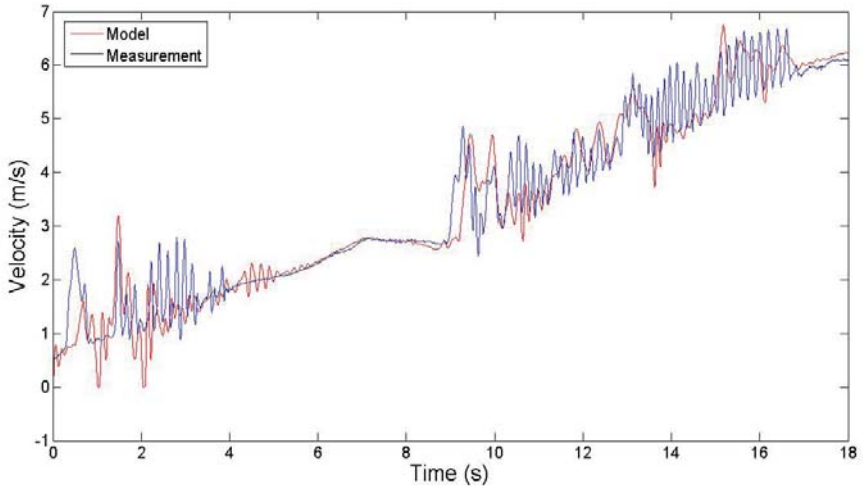

Figure 7.23: Model left wheel velocities, with adjusted road friction coefficient, compared to actual velocities, $0 - 18\ s$

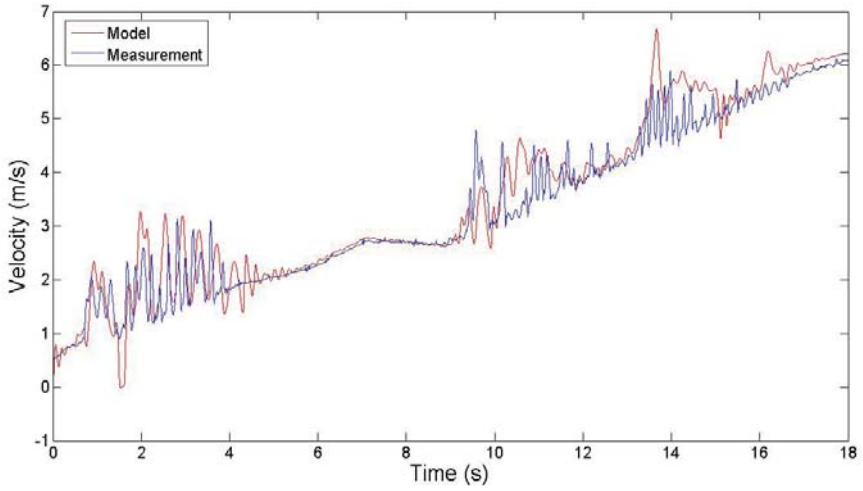

Figure 7.24: Model right wheel velocities, with adjusted road friction coefficient, compared to actual velocities, $0 - 18\ s$

Figure 7.25 shows the wheel velocities for both the left wheels and the right wheels, during the second interval, $55 - 60\ s$, for which the road surface friction coefficient is the same for

both wheel sides.

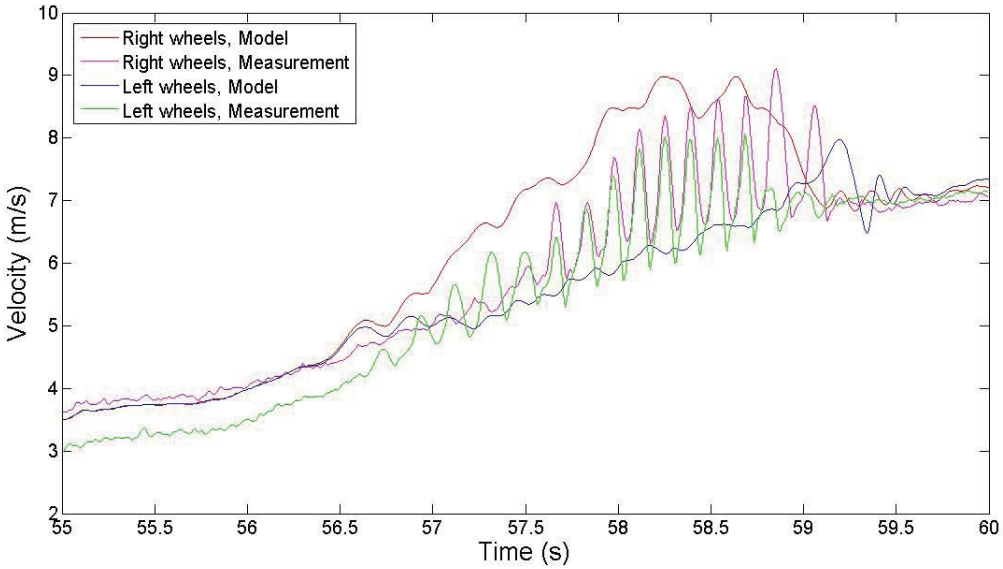

Figure 7.25: Model and actual wheel velocities, $55 - 60$ s

7.1.4 Step response

The first step simulated was from 300 Nm to 350 Nm, as described in Section 4.6.4.

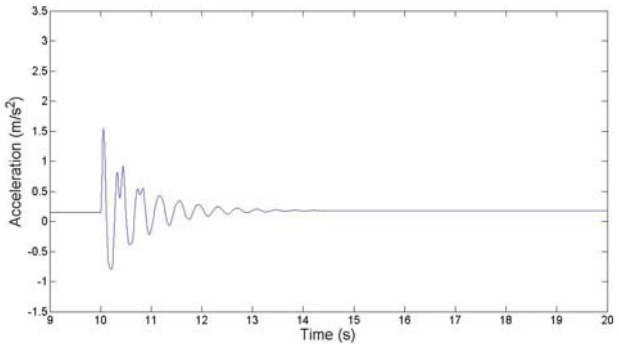

7.26(a) Wheel accelerations (m/s^2)

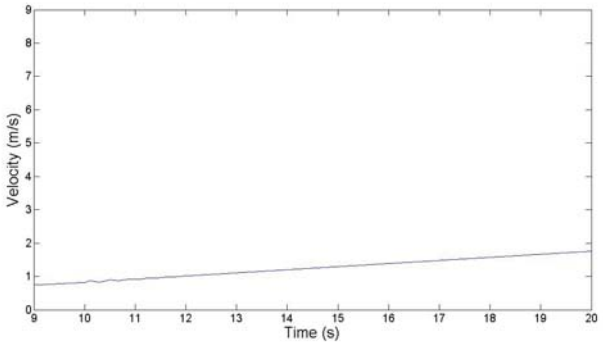

7.26(b) Wheel velocities (m/s)

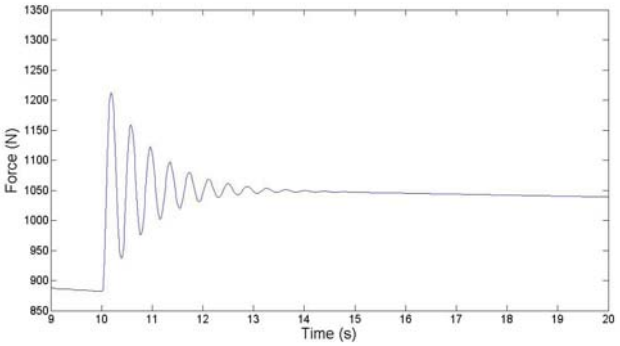

7.26(c) Adhesive force (N)

Figure 7.26: Step response, 300-350 Nm

The second step was from 300 Nm to 400 Nm, see Fig. 4.14.

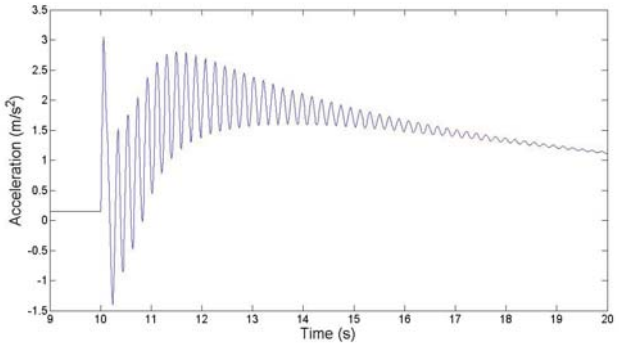

7.27(a) Wheel accelerations (m/s^2)

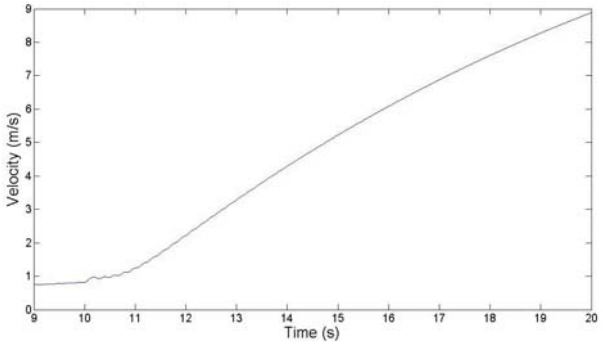

7.27(b) Wheel velocities (m/s)

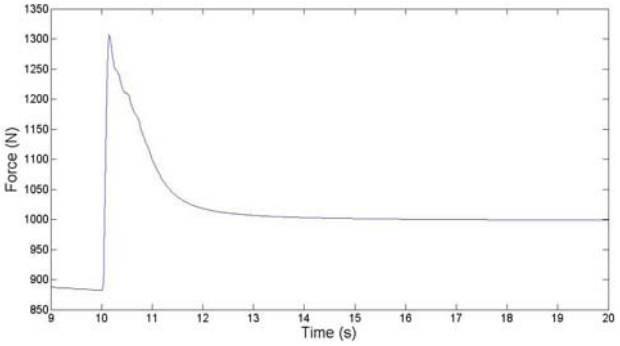

7.27(c) Adhesive force (N)

Figure 7.27: Step response, 300-400 Nm

7.2 Results when implementing MPC

The controllers simulated in this thesis are implemented using the Model Predictive Control Toolbox in Matlab. The toolbox contains a graphical interface for controller design, where the weights and constraints are easily defined. An additional overall weight can also be defined and provides a smooth adjustment of all weights, and can be used to make a controller showing adequately performance more robust or faster. Bumpless transfer between the controllers are ensured using the manipulated variables to update each controllers states.

7.2.1 Choice of control horizon and prediction horizon

The choice of prediction horizon is important in MPC, since it determines the controllers ability to act on, for example, future constraint violations. A long prediction horizon has a better chance to cope with constraint violations, however, since all states are calculated over the prediction horizon, at each sample, too long a horizon would require too much computer capacity. A short prediction horizon, on the other hand, may not act as well on future constraint violations, resulting in a less robust controller. A rule of thumb is to choose the sampling time so that the system settling time is approximately $20-30$ sampling intervals, and to choose the predicition horizon to the number of periods used to determine the sampling time. The control horizon is typically chosen low, between $3-5$ intervals.

In the controllers designed as part of this thesis, a standard sampling time, suggested by Haldex, of $0.01s$ is used. Thus, the prediction horizon is set on the premises that the controller should have long enough prediction horizon to adequately counter act possible constraint violations, while short enough as to not cause to high increase in simulation time. Other concerns, for example the choice of prediction and control horizon with regards to plant time delays, are for obvious reasons not considered in this thesis.

7.2.2 Choice of linearization points

In Section 6.1, the choice of linear parameters where discussed. How the parameters are chosen evidently affects the behaviour of the controllers, since the linearized tyre model will be accurate only in the vicinity of the linearization point. Thus, while linearizing the slip curve with parameters chosen to fit the initial part of the nonlinear curve may describe the slip behaviour adequately when accelerating from standstill, it will not be an accurate model of the slip curve in the vicinity of the peak. In the same sense, linearizing the curve as to fit the slip curve in the vicinity of the peak results in high inaccuracy during the initial part of the curve.

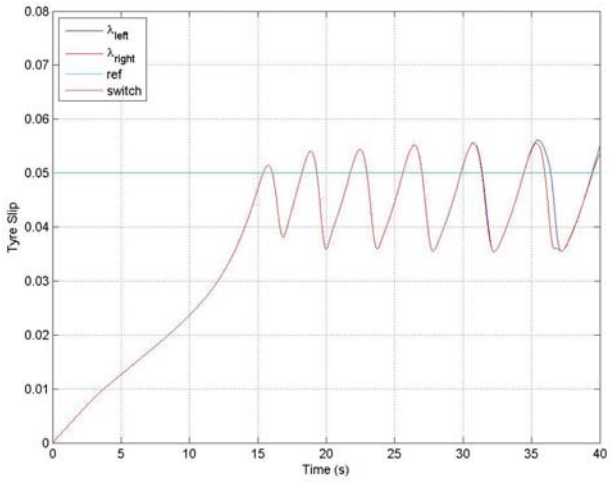

7.28(a) Model generated tyre slip

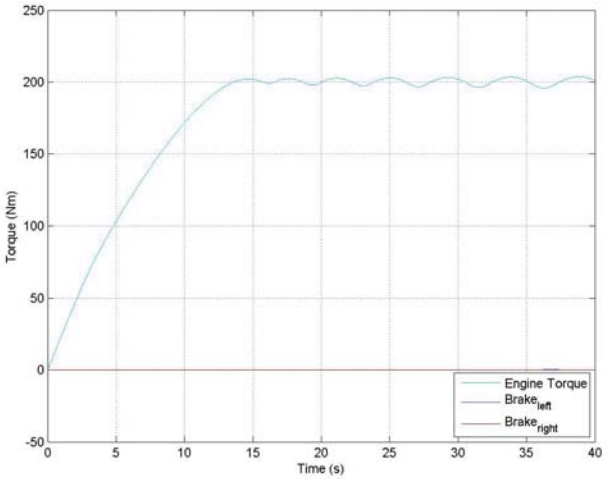

7.28(b) Manipulated variables

Figure 7.28: Simulation of controller with $\lambda_{ref_L} = \lambda_{ref_R} = 0.05$, with model linearized in the vicinity of the slip peak.

Consider Fig. 7.28-7.29, which represents a controller designed with regards to the slip be-

haviour in the vicinity of the peak. The controller is simulated with reference values set to $\lambda_{ref_L} = \lambda_{ref_R} = 0.05$, representing a reference point on the stable side of the slip peak. It should be noted that the controller used in Fig. 7.28-7.29 was designed solely to investigate the properties of the stable side of the peak, and is not used further in the following sections

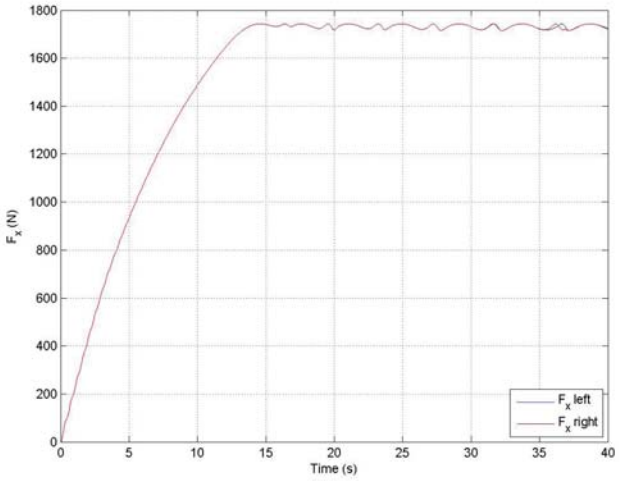

7.29(a) Tyre-road friction force

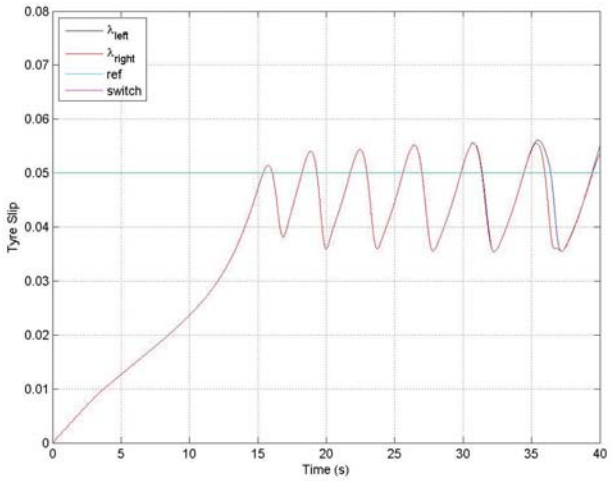

7.29(b) Model generated tyre slip

Figure 7.29: Simulation of controller with $\lambda_{ref_L} = \lambda_{ref_R} = 0.05$, with model linearized in the vicinity of the slip peak.

The results when using the same controller as used in Fig. 7.28-7.29, for a model linearized in the beginning of the slip curve, can be seen in Fig. 7.30-7.31, where it should be noted that the scales differ from the other figures in this section, to properly show the amplitude of the slip. Naturally, the weights would need to be reconfigured to some extent, to provide a well-tuned controller, thus, this example is instructive solely as an example of the importance of choosing linearization parameters. In the following examples, linearization

with regards to the slip peak behaviour is considered.

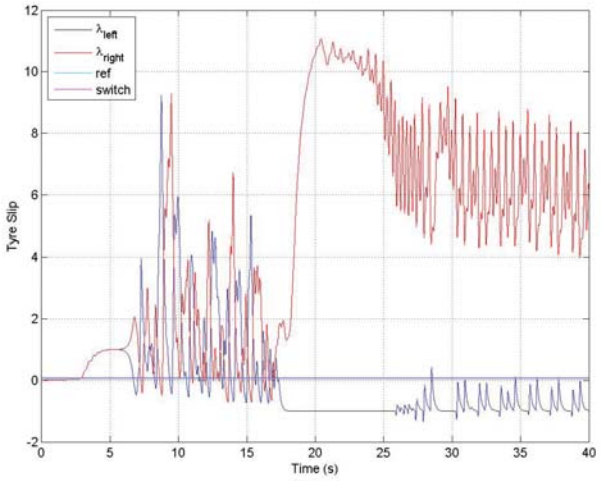

7.30(a) Model generated tyre slip

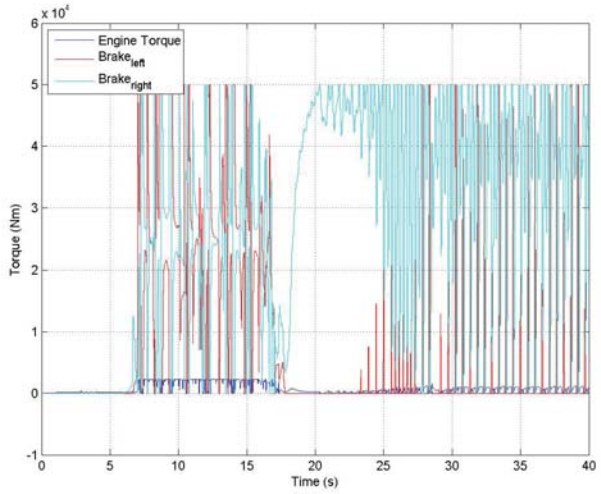

7.30(b) Manipulated variables

Figure 7.30: Simulation of controller with $\lambda_{ref_L} = \lambda_{ref_R} = 0.05$, with model linearized for the initial part of the slip curve.

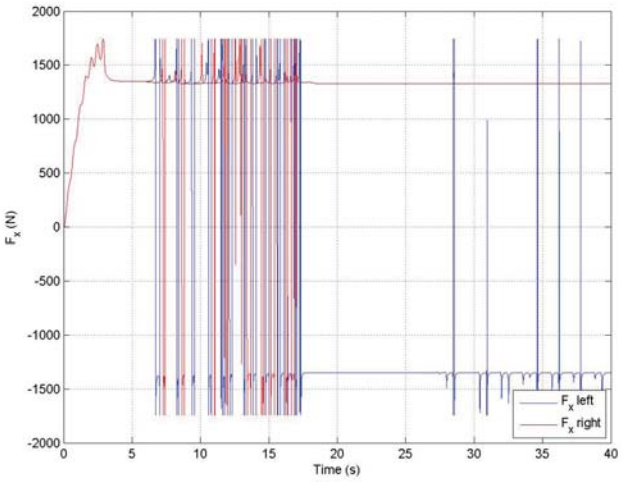

7.31(a) Tyre-road friction force

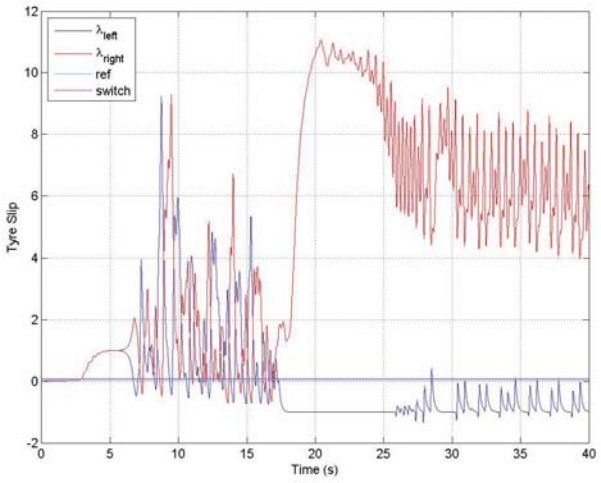

7.31(b) Model generated tyre slip

Figure 7.31: Simulation of controller with $\lambda_{ref_L} = \lambda_{ref_R} = 0.05$, with model linearized for the initial part of the slip curve

7.2.3 Controller 1 - a first attempt

With regards to the above considerations on weight assignments, a controller was designed. For a complete documentation of controller weights and constraints, see Appendix A. The results for the first simulation of the controller, denoted *Controller 1*, can be seen in Fig. 7.32-7.33. The set point has been chosen as $\lambda_{ref_L} = \lambda_{ref_R} = 0.06$, implying a point on the very edge of the stable part of the slip curve. The switch value, determining the point at which the controller being used is to be changed, i.e. the value for which it is assumed the linearization curves are changed from stable to unstable behaviour, is set to $\lambda_{max} = 0.08$.

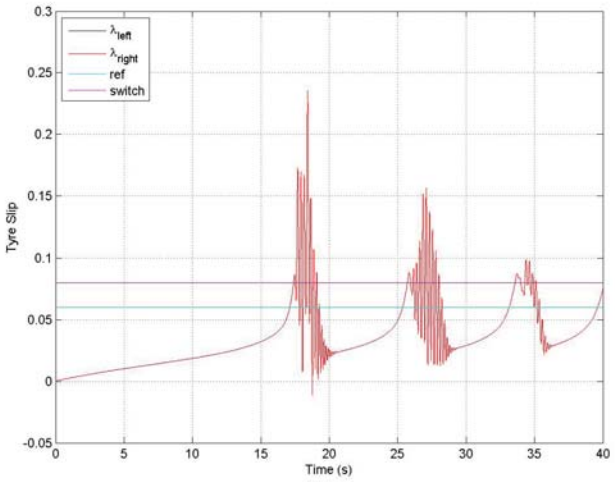

7.32(a) Model generated tyre slip

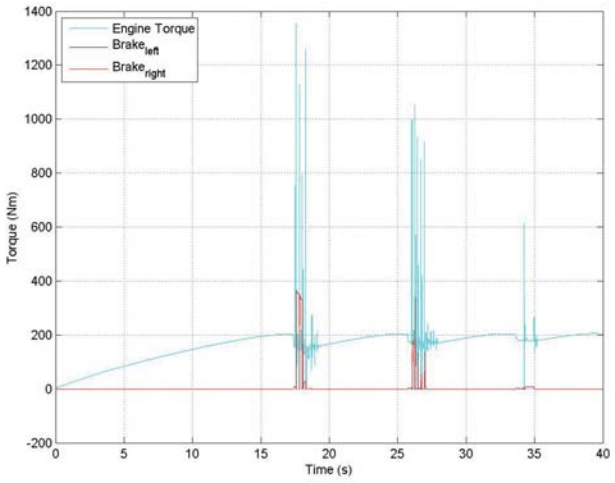

7.32(b) Manipulated variables

Figure 7.32: Simulation of Controller 1, with $\lambda_{ref_L} = \lambda_{ref_R} = 0.06$ and $\lambda_{max} = 0.08$

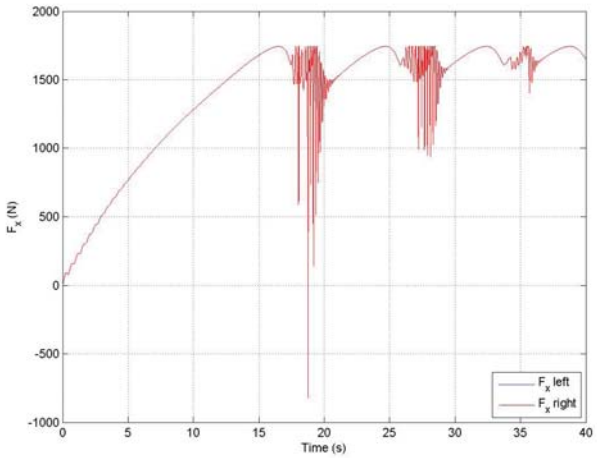

7.33(a) Tyre-road friction force

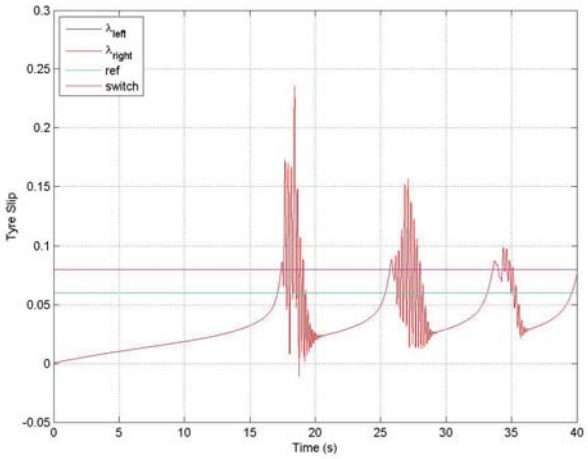

7.33(b) Model generated tyre slip

Figure 7.33: Simulation of Controller 1, with $\lambda_{ref_L} = \lambda_{ref_R} = 0.06$ and $\lambda_{max} = 0.08$

7.2.4 Controller 2 - a second attempt

The controller shown in Fig. 7.34-7.35 is for obvious reasons denoted *Controller 2*. To investigate the behavior if the engine torque is nonzero when the simulation i initiated, an initial value is set to 100 Nm. Simulations using the controller is done for both $\lambda_{ref_L} = \lambda_{ref_R} = 0.06$ and for a more stable point, $\lambda_{ref_L} = \lambda_{ref_R} = 0.05$.

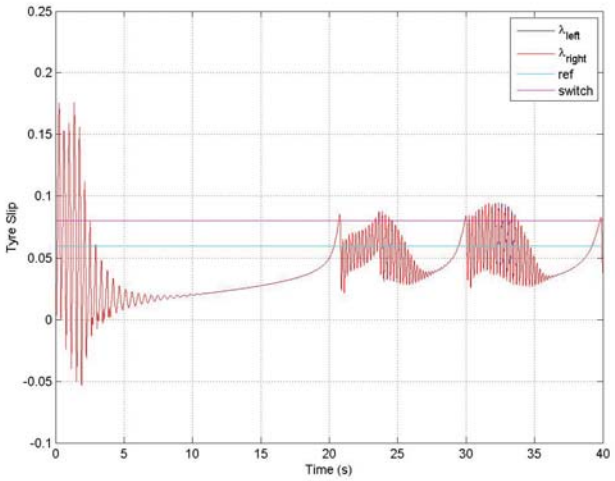

7.34(a) Model generated tyre slip

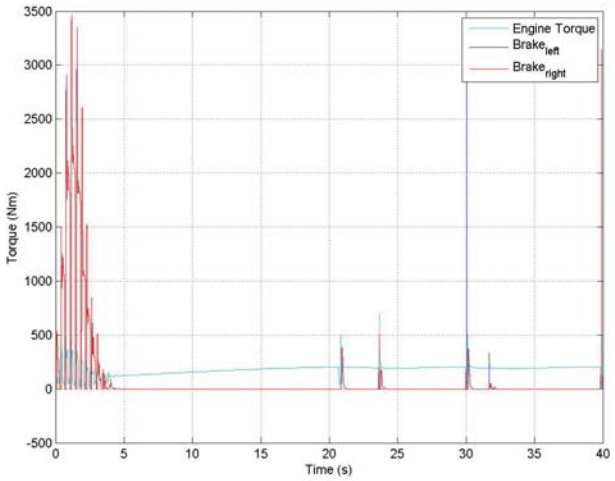

7.34(b) Manipulated variables

Figure 7.34: Simulation of Controller 2, with $\lambda_{ref_L} = \lambda_{ref_R} = 0.06$ and $\lambda_{max} = 0.08$

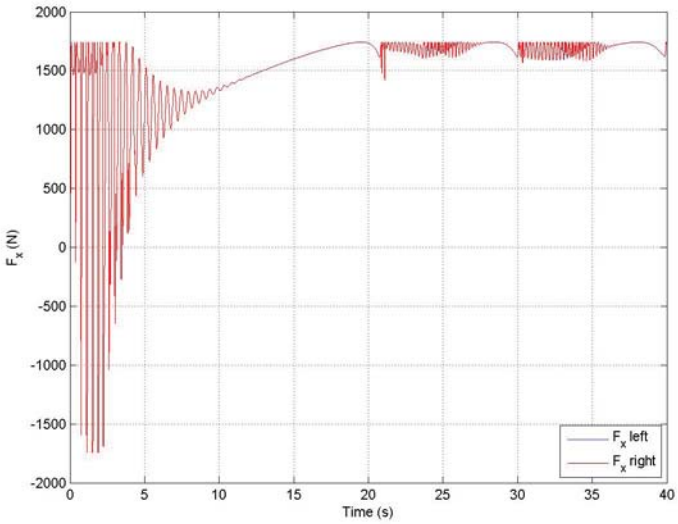

7.35(a) Tyre-road friction force

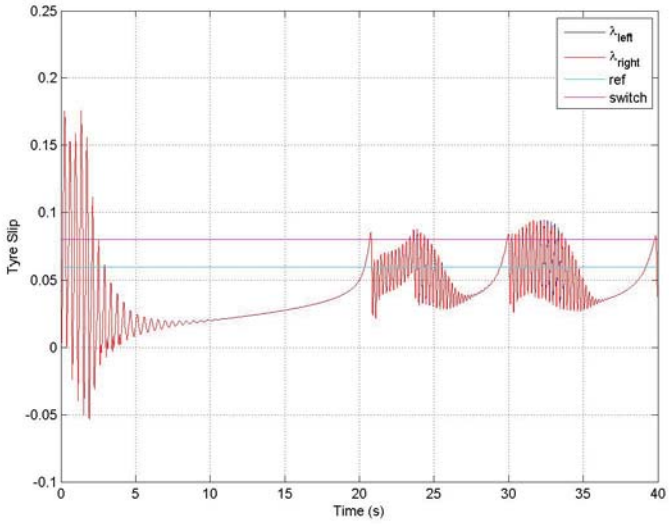

7.35(b) Model generated tyre slip

Figure 7.35: Simulation of Controller 2, with $\lambda_{ref_L} = \lambda_{ref_R} = 0.06$ and $\lambda_{max} = 0.08$

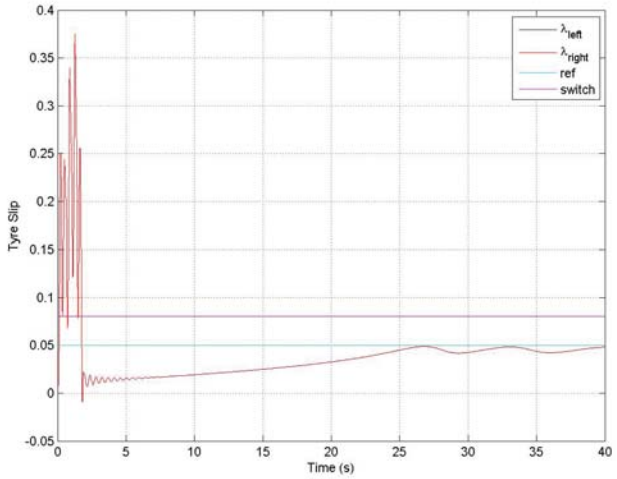

7.36(a) Model generated tyre slip

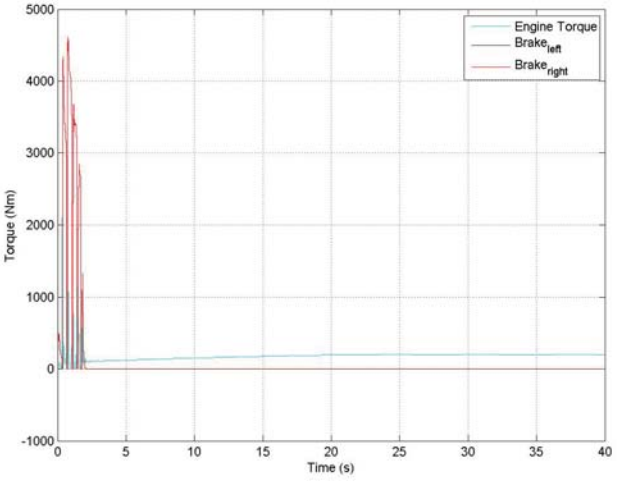

7.36(b) Manipulated variables

Figure 7.36: Simulation of Controller 2, with $\lambda_{ref_L} = \lambda_{ref_R} = 0.05$ and $\lambda_{max} = 0.08$

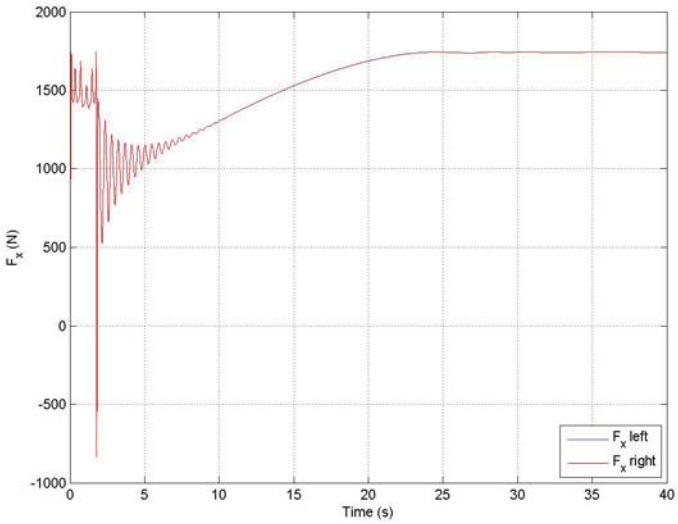

7.37(a) Tyre-road friction force

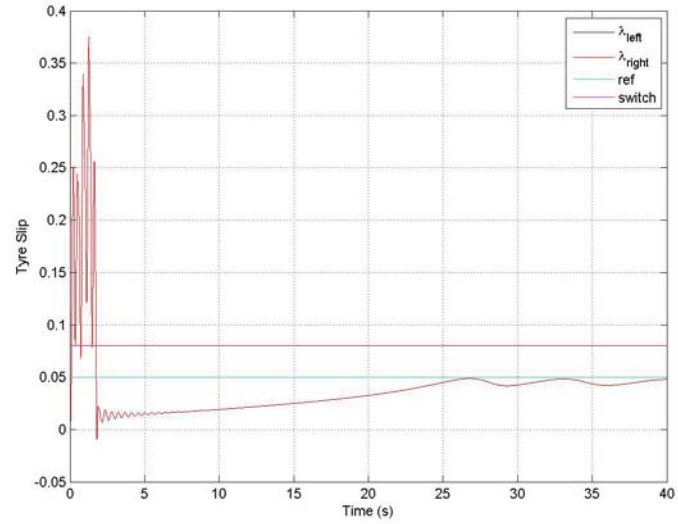

7.37(b) Model generated tyre slip

Figure 7.37: Simulation of Controller 2, with $\lambda_{ref_L} = \lambda_{ref_R} = 0.05$ and $\lambda_{max} = 0.08$

7.2.5 Controller 3 - a split slip controller

The behaviour of the split slip controllers, i.e. the US and SU controllers, can be seen in Fig. 7.38-7.39. The figures shows simulation results for a controller, *Controller 3* using a slightly different set of weights and linearization parameters compared to Controller 2.

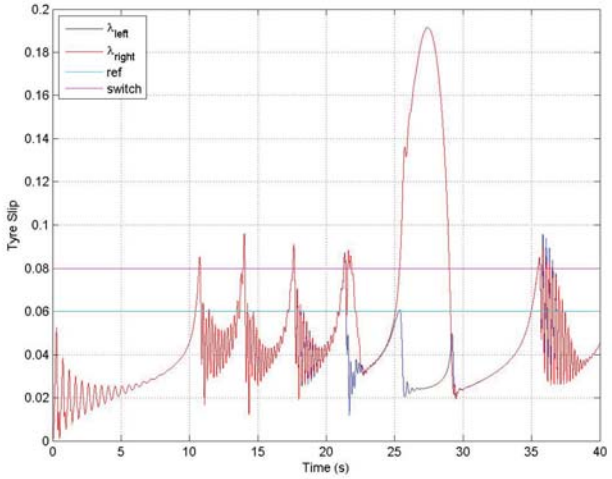

7.38(a) Model generated tyre slip

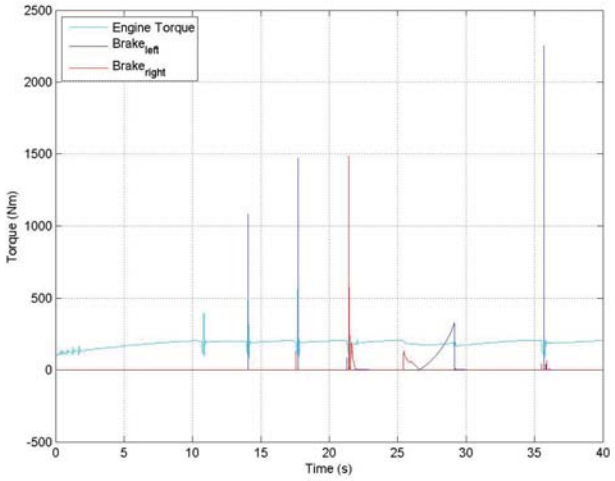

7.38(b) Manipulated variables

Figure 7.38: Simulation of Controller 3, with $\lambda_{ref_L} = \lambda_{ref_R} = 0.06$ and $\lambda_{max} = 0.08$

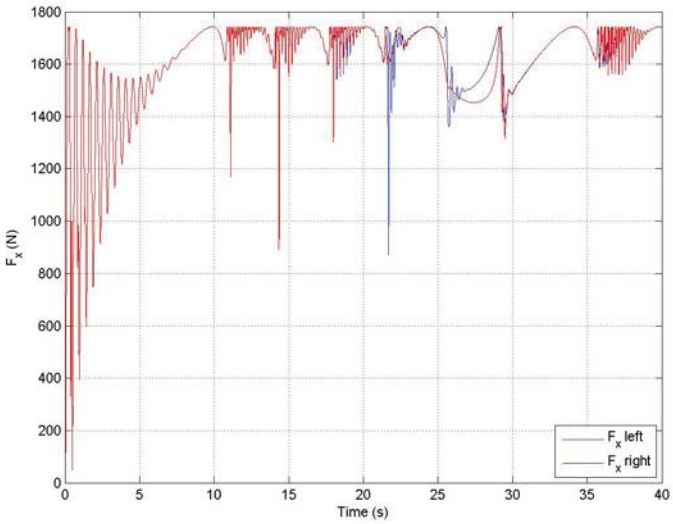

7.39(a) Tyre-road friction force

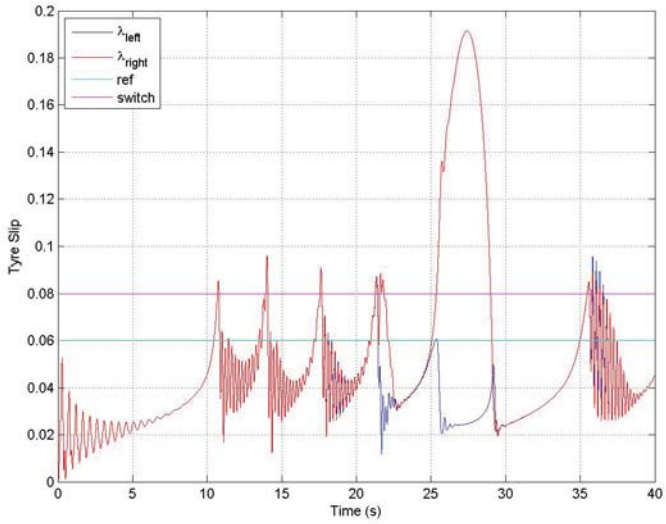

7.39(b) Model generated tyre slip

Figure 7.39: Simulation of Controller 3, with $\lambda_{ref_L} = \lambda_{ref_R} = 0.06$ and $\lambda_{max} = 0.08$

8 Discussion

8.1 Validation

8.1.1 Test 1

In Fig. 7.2-7.3 it can be observed that the model velocities match the actual velocities quite accurately. The large oscillations in the beginning of the model for both the left and the right wheels are due to the large offset, as the initial velocities of the model start at $0\ m/s$ while the actual velocities are almost $6\ m/s$ when the measurements are initiated. It is also visible that the velocities from the model are slightly higher compared to the actual velocities.

Implementing Coulomb friction and viscous friction affects the model slightly, see Fig. 7.5. Initially, the wheel velocities are low and the friction present is mainly Coulomb friction, not affecting the wheel velocities noticeable. However, increasing the velocity of the wheels and thus the velocity of the crown wheel, increases the viscous friction which results in a total friction affecting the model according to Fig. 7.5.

8.1.2 Test 2

For Test 2 it can be seen that the wheel velocities in Fig. 7.7-7.8 are quite similar in general. One of the most important physical phenomenon for an actual rear axle is that, due to the differential gear dynamics, the wheels often do not spin at the same time. In Fig. 4.8, i.e. for the measurement data, simultaneous spin occurs for the first two clusters of slip peaks, while the three following clusters initially show wheel spin for the right wheels. The left wheels do not spin until the right wheel spin have been suppressed by actuated brake torque. This phenomenon is captured for the last two clusters where it is visible that suppressing the spin for the right wheels results in spin for the left wheels.

Closer comparison of the figures is non instructive, prior to the consideration of a few problems. For instance, the third cluster of slip peaks in Fig. 7.10 is manifested in Fig. 7.9 by a large peak for the left wheels. This is most likely due to an error in the tyre-road friction coefficient. For ice and snow this value should be approximately $0.15 - 0.4$, if not specified the friction coefficient has been set to 0.3 for all plots in this section. However, the tests are performed in varying road surface conditions, thus, the wheels do not experience constant friction coefficient. To get good results, the model should at all times be provided with the correct friction coefficient, which is not available. Worth noting, however, is that the third cluster in Fig. 7.10 is described more accurately in Fig. 7.9 if the friction coefficient is adjusted properly.

Other possible problems are the actuated brake torques. The measurements are performed on a truck with an implemented traction controller, where the brakes are used when spin is initiated. In the model it is instead the braking of one wheel side of the differential that results in spin of the wheels on the other side, in combination with the road friction coefficient. Therefore, it is of great importance that the brake torques are actuated at exactly the right time. A small time discrepancy would account for the large peak for the left wheels in Fig. 7.9. Should, for example, the right wheels be subjected to a high

braking torque when excessive slip is in fact not present, the velocities of the left wheels would instead increase greatly due to differential gear dynamics.

When implementing both the Coulomb and viscous friction from Test 1 and the LuGre friction model some differences can be observed in Fig. 7.11-7.12. As mentioned for Test 1, the Coulomb friction and viscous friction effects are negligible and tests imply that the differences visible are due to the LuGre friction. Fig. 7.13 shows the actual impact of the LuGre friction on the planet gears. It may be expected that the friction should counteract the motion of the planet gears, however, as can be seen it sometimes causes an increase of the planet gear velocity. This is not necessarily a fault in the implementation of the friction, since the friction initially counteracts the velocities as expected, thus changing the states of the planet gears which may lead to unexpected results.

For Fig. 7.16-7.18 of the torques between planet gears and the side gears it is observed that when the torques changes sign, the model with backlash implemented is highly oscillatory compared to the model without backlash. In the other regions, however, the models coincide, as expected. However, considering the wheel velocities in Fig. 7.17-7.19 the effects when implementing the backlash seems to be minor although large oscillations are introduced.

When both friction and backlash are implemented in the model some problems occurs. Fast oscillations, like those generated by the backlash model, are problematic when using the LuGre friction model. The parameter σ_1 multiplies with the bristle deformation velocity to affect the friction, and with backlash implemented the deformations are very fast. To be able to use the model with both nonlinearities implemented, σ_1 should be zero, i.e. the friction model does not include the effect of frictional lag. Also, the fast changes causes model lag when viscous friction is implemented between the planet gear and side gears - however, since the velocities are small, the viscous friction can be neglected. Thus, the resulting parameters used can be seen in Table 8.1.

Name	Value
σ_{0_m}	50 m^{-1}
σ_{1_m}	0 s/m
α_{0_m}	0.4
α_{1_m}	0.16
α_{2_m}	0 Ns
v_{s_m}	0.1 m/s
μ_{C_m}	0.1
η_{v_m}	10 Nms

Table 8.1: Friction parameters

Both friction and backlash have some minor effect on the wheel velocities but considering the velocities in Fig. 7.9-7.10 the problem with the large peak for the left wheels remains. As previously discussed, this may be due to the road surface friction coefficient. Adjusting the values for the coefficient rendered Fig. 7.22 where it can be observed that the model is quite accurate for the last three clusters of peaks. However, initially there is still much oscillation, even though there is very little offset. The greatest difference between the

two first clusters compared with the last three is that in reality, both wheels are spinning at the same time. This is problematic for the model since the timing of the brakes with the input torque and the choice of the road surface friction coefficient must all be impeccable.

8.1.3 Test 3

Considering the third test, initially there is spin for both left and right wheels, see Fig. 7.23-7.24. The frequency of the actual wheel velocities during the spin is faster than that of the model and the fit in the figures are not perfect. However, the model is able to depict the presence of spin and adjusting the road surface friction coefficient can make the wheel velocities of the model more accurate. Fig. 7.25 for the interval is also interesting, since the actual wheels spin simultaneous which is difficult to model. Rather, it can be seen that the model result in wheel spin for one side of the differential only.

8.1.4 Step response

For the step inputs, initial wheel spin can be observed as the model adapts to the constant torque of 300 Nm, however, after a few seconds the outputs are stable. The step to 350 Nm after 10 s is insufficient to cause wheel spin, as can be seen in Fig. 7.1.4. Comparing with Fig. 7.1.4 it is interesting to see the response when the adhesive traction force reaches the maximum peak value, i.e. what happens when the wheels are spinning.

8.2 MPC results

8.2.1 Linearization points

Considering Fig. 7.28-7.29, the choice of parameters results in a less accurate description of the slip behaviour for very low slip. This accounts to some extent for the slow acceleration, requiring approximately 15 s to reach the reference value. However, using linearization parameters with regards to the initial slip behaviour, and using the same controller as for Fig. 7.28-7.29, results in a very aggressive controller, see Fig. 7.30-7.31. It should be noted that initially, when there is high spin, the controller does not act as expected. Except for the choice of linearization points, this could be due to efforts of the controller to prevent split slip, or concerns for controller constraints. This implies that the traction controller should be developed using linearization points in the vicinity of the slip peak. While the acceleration is slow in Fig. 7.28-7.29, it can be seen that the set point tracking in the vicinity of the reference values is good.

8.2.2 Weights and Constraints

When simulating the controllers, it was found that set point tracking was poor due to the differential gear dynamics, i.e. the controller did not take the dynamics into as much consideration as desired, resulting in an unstable controller. To solve this problem, a third set point, the difference in wheel velocity of the left and right side, was introduced. Obviously, an added set point results in a modified state-space model in Section 6.2. Adding the velocity difference improved the controller, since setting the reference value of the

velocity difference to zero causes the controller to be cautious with actions resulting in a split slip behaviour, i.e. different slip on the left and right side.
Introducing soft constraints on plant slip output proved to increase controller performance. Constraints were introduced for the SS, US and SU controllers, however, not for the UU controller. For the UU controller, the main concern should be to reduce the slip values to the stable side of the slip peak. While introducing constraints might improve this feature, it has shown to decrease the robustness of the UU controller due to the unstable behaviour of the UU model, often resulting in constraint violation. Thus, constraints on the UU controller has shown to reduce overall controller performance. The constraints should be soft, to discourage constraint violation, while not causing infeasibility of the optimization problem, as discussed in Section 5.3

8.2.3 Controller 1

Studying the results from the simulations in Fig. 7.32, it is clear that when switching controller, high oscillations were introduced. When the tyre slip reaches the switch value, i.e. when the wheels start to spin, the controller instantly decreases the engine torque. However, this results in a switch of controllers after which the engine torque is instantly increased to high values. Even though the oscillations eventually dampens, the controller performance is not to satisfaction. Thus, the controller weights needed tuning.

8.2.4 Controller 2

It was found that tuning the SS controller to be more robust, while increasing the engine torque weight of the UU controller while tuning it to be more robust as well, the overall controller performance was improved, see Fig. 7.34-7.35. As can be seen, the wheels instantly start to spin, and slip oscillations are introduced. The oscillations are dampened by the controller after which the controller accelerates the vehicle. As with the other controllers, acceleration is slow, however, the set point tracking, while oscillating, is good.

8.2.5 Controller 3

In Fig. 7.38 it can be seen that after approximately 20 s, a split slip situation occurs after which the split controllers are used to decrease the tyre slip of the spinning wheel. Due to the difference in linearization parameters compared to Controller 2, the acceleration is faster, however, the SS controller is slightly less robust causing the split situation. Controller 3 has not well-tuned SS and UU controllers, rather, it is presented here since it has the same US and SU controllers as Controller 2. Considering the peak in λ_{right} after approximately 25 s it is clear that the split slip controllers perform satisfactory.

8.2.6 Controller evaluation

The performance of the controllers discussed above is not as good as expected. This is most likely due to plant model inaccuracy. The tyre model provided by Haldex accounts for, among other tyre phenomena, the relaxation length of the tyre. The relaxation length is most easily described as a tyre compliance, see Fig. 8.1. The effects of the relaxation length was not made clear until late in the control design process. The wheel velocity obtained from the model as an output port, was used to calculate the slip according to Eq. (3.21). However, this velocity describes the rim of the wheel, rather than the actual

tyre. Due to the relaxation length, the rim velocity and the tyre velocity are only equal in steady-state. The relaxation length can be considered as a physical lowpass filter, i.e. rapid oscillatory changes in rim angular velocity might not affect the tyre angular velocity. Thus, the simplified plant model derived in Section 6.2 assumes measured *tyre slip* as output from the plant, while the actual output is in fact *rim slip*. The tyre slip represented in the figures in Section 7.2 is instead obtained from an internal state of the tyre model. Naturally, this is not a measurable signal from an actual truck, thus, it cannot be taken as plant output and used as input to the MPCs. To some extent, the performance of the controllers can be improved by lowpass filtering the measured signal, and use the filtered signal to control the switch, i.e. to control which MPC is to be used. It cannot be used, however, as plant output/MPC input, since the manipulated variables obtained from the MPCs will not affect the plant in a correct manner.

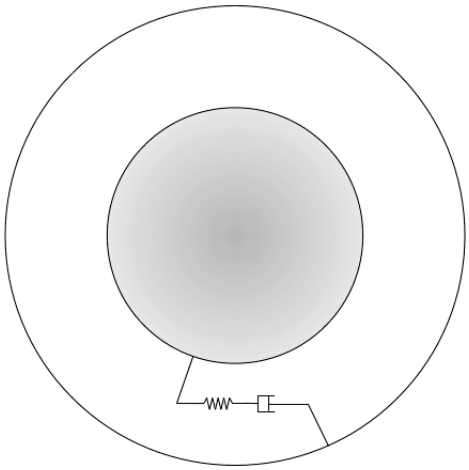

Figure 8.1: Simplified model of tyre relaxation

In addition, the linearization might be too crude, an approach using a piece-wise linear approximation with more than two linear curves, would most likely improve controller performance. The linearization approach also considers constant velocity, see Section 6.1 - using smaller velocity intervals might improve the accuracy of the linearized slip, which in turn might improve controller performance.

9 Conclusions

A model accurately describing important differential gear phenomena has been developed. One of the most important features of the differential gear to model, the transfer of spin to one side when using the brakes on the other side, has been implemented, improving model usability in traction control. The model wheel velocities has been shown to accurately match those of the measurement data. Nonlinearities have been thoroughly investigated and introduced, using a novel approach to implement backlash properties, as well as an advanced friction model. Implementing backlash and an advanced friction model have been shown to improve model results to some extent, however, due to extended simulation time, the model area of usage should determine what nonlinearites to implement.

A novel traction controller has been investigated and implemented. It has been found to present options desirable in traction control, such as constraints and prediction constraints. The controller has shown moderate results, yet an extended plant model would likely improve the behaviour.

10 Future work

Future work should include modeling of other rear axle components, such as suspensions. Internal gears of the differential will likely be affected by suspension movements, increasing for example friction. Several other components, such as bearings, introduces friction and the impacts from these should be investigated. Further, specified validation tests should be performed, to improve parameter choices for both friction and backlash.

The plant model used in the traction controller design should be improved to include tyre relaxation. The impact of linearization parameters as well as velocity regions for linearizing the slip, should be further investigated as should the possibilities of implementing an off line controller.

References

[1] Magnus Petterson, *Driveline modeling and Control*, Department of Electrical Engineering, Linköping University, Linköping, Sweden, 1997

[2] Uwe Kiencke, Lars Nielsen, *Automotive Control Systems - For engine, driveline and vehicle*, Springer, Berlin Heidelberg, 2005

[3] Kjell Melkersson, *Traction control of vehicles under varying road conditions*, Machine and Vehicle Design, Chalmers University of Technology, Gothenburg, Sweden, 1991

[4] Donald Margolis, *Bond Graph Model of a Multi-Plate Clutch in a Vehicle System Using Fixed Causality Slip-Stick Friction*, Department of Mechanical and Aeronautical Engineering, University of California, 2005

[5] Reza N. Jazar, *Vehicle Dynamics: Theory and Application*, Springer US, 2008

[6] Mattias Nordin, *Uncertain Systems with Backlash: Modeling, Identification and Synthesis*, Department of Mathematics, Royal Institute of Technology, Stockholm, Sweden

[7] Adam Lagerberg, *Control and Estimation of Automotive Powertrains with Backlash*, Department of Signals and Systems, Chalmers University of Technology, Gothenburg, Sweden, 2004

[8] T. D. Gillespie, *Fundamentals of Vehicle Dynamics*, Society of Automotive Engineers, Inc., 1992

[9] H. B. Pacejka, *Tyre and Vehicle Dynamics*, Elsevier, 2006

[10] J. Koppenaal, Tyre Module Specification, *Internal report, reg. no. 20046559*

[11] Fredrik Gustafsson, Slip-based Tire-Road Friction Estimation, *Automatica, vol 33, No. 6, pp.1087-1099*, 1997

[12] U. Eichhorn, F. Holzwarth, Non-contact sensors for road conditions, *Sensors and Actuators, A. Journal, 37-38, pp. 121-127*, 1993

[13] G. Erdogan, L. Alexander, R. Rajamani, A novel wireless piezoelectric tire sensor for the estimation of slip angle,*Measurement Science and Technology, 21*, 2010

[14] E. Rabinowicz, The nature of the static and kinetic coefficients of friction, emphJournal of Applied Physics, 22(11), pp. 1373-1379, 1951

[15] H. Olsson, *Control Systems with Friction*, Department of Automatic Control, Lund University, Lund, Sweden, 1996

[16] H. Olsson, K.J. Åström, C. Canudas de Wit, M. Gäfvert, P. Lischinsky, Friction Models and Friction Compensation, *Swedish Research Council for Engineering Sciences*, 1997

[17] C. Canudas de Wit, H. Olsson, K.J. Åström, P. Lischinsky, A New Model for Control of Systems with Friction, *IEEE Transactions on automatic control, vol. 40, No. 3, pp. 419-425*, 1995

[18] L. Vedmar, *Transmissioner*, Maskinelement, Lund University, Lund, Sweden, 2009

[19] R. Waiboer, R. Aarts, B. Jonker, Velocity dependence of joint friction in robotic manipulators with gear transmissions, *ECCOMAS Thematic Conference, Madrid, Spain*, 2005

[20] H. Xu, A. Kahraman, D.R. Houser, A Model to Predict Friction Losses of Hypoid Gears, *American Gear Manufacturers Association*, 2005

A Appendix A

A.1 Controller 1

Name	Weight	Rate Weight
Engine Torque	0	0.1
Brake Force left	1	0.1
Brake Force right	1	0.1
s left	1000	-
s right	1000	-
Ang vel diff	100	-
Prediction horizon (intervals)		25
Control horizon (intervals)		5
Overall weight		0.9

Table A.1: Weights and values Controller 1, SS

Name	Minimum	Maximum
λ_L	0.04	0.1
λ_R	0.04	0.1
Ang vel diff	-	-

Table A.2: Output constraints Controller 1, SS

Name	Weight	Rate Weight
Engine Torque	10	1
Brake Force left	0	0.1
Brake Force right	0	0.1
s left	1000	-
s right	1000	-
Ang vel diff	100	-
Prediction horizon (intervals)		15
Control horizon (intervals)		3
Overall weight		0.2

Table A.3: Weights and values Controller 1, US

Name	Minimum	Maximum
λ_L	0	1
λ_R	0	1
Ang vel diff	-	-

Table A.4: Output constraints Controller 1, US

Name	Weight	Rate Weight
Engine Torque	10	1
Brake Force left	0	0.1
Brake Force right	0	0.1
s left	1000	-
s right	1000	-
Ang vel diff	100	-

Prediction horizon (intervals)	15
Control horizon (intervals)	3
Overall weight	0.2

Table A.5: Weights and values Controller 1, SU

Name	Minimum	Maximum
λ_L	0	1
λ_R	0	1
Ang vel diff	-	-

Table A.6: Output constraints Controller 1, SU

Name	Weight	Rate Weight
Engine Torque	1	1
Brake Force left	0	1
Brake Force right	0	1
s left	1000	-
s right	1000	-
Ang vel diff	10	-

Prediction horizon (intervals)	15
Control horizon (intervals)	3
Overall weight	0.25

Table A.7: Weights and values Controller 1, UU

Name	Minimum	Maximum
λ_L	-	-
λ_R	-	-
Ang vel diff	-	-

Table A.8: Output constraints Controller 1, UU

k_1	1800
k_2	-480
λ_{max}	0.08

Table A.9: Values of linearization parameters, Controller 1

A.2 Controller 2

Name	Weight	Rate Weight
Engine Torque	0.1	1
Brake Force left	1	0.1
Brake Force right	1	0.1
s left	1000	-
s right	1000	-
Ang vel diff	100	-
Prediction horizon (intervals)		25
Control horizon (intervals)		5
Overall weight		0.3

Table A.10: Weights and values Controller 2, SS

Name	Minimum	Maximum
λ_L	0.04	0.08
λ_R	0.04	0.08
Ang vel diff	-	-

Table A.11: Output constraints Controller 2, SS

Name	Weight	Rate Weight
Engine Torque	10	1
Brake Force left	0	0.1
Brake Force right	0	0.1
s left	1000	-
s right	1000	-
Ang vel diff	100	-
Prediction horizon (intervals)		15
Control horizon (intervals)		3
Overall weight		0.4

Table A.12: Weights and values Controller 2, US

Name	Minimum	Maximum
λ_L	0	0.1
λ_R	0	0.1
Ang vel diff	-	-

Table A.13: Output constraints Controller 2, US

Name	Weight	Rate Weight
Engine Torque	10	1
Brake Force left	0	0.1
Brake Force right	0	0.1
s left	1000	-
s right	1000	-
Ang vel diff	100	-
Prediction horizon (intervals)		15
Control horizon (intervals)		3
Overall weight		0.4

Table A.14: Weights and values Controller 2, SU

Name	Minimum	Maximum
λ_L	0	0.1
λ_R	0	0.1
Ang vel diff	-	-

Table A.15: Output constraints Controller 2, SU

Name	Weight	Rate Weight
Engine Torque	50	0.1
Brake Force left	0	1
Brake Force right	0	1
s left	1000	-
s right	1000	-
Ang vel diff	10	-
Prediction horizon (intervals)		15
Control horizon (intervals)		3
Overall weight		0.3

Table A.16: Weights and values Controller 2, UU

Name	Minimum	Maximum
λ_L	-	-
λ_R	-	-
Ang vel diff	-	-

Table A.17: Output constraints Controller 2, UU

k_1	1800
k_2	-480
λ_{max}	0.08

Table A.18: Values of linearization parameters, Controller 2

A.3 Controller 3

Name	Weight	Rate Weight
Engine Torque	0	0.1
Brake Force left	1	0.1
Brake Force right	1	0.1
s left	1000	-
s right	1000	-
Ang vel diff	100	-
Prediction horizon (intervals)		25
Control horizon (intervals)		5
Overall weight		0.5

Table A.19: Weights and values Controller 3, SS

Name	Minimum	Maximum
λ_L	-	-
λ_R	-	-
Ang vel diff	-	-

Table A.20: Output constraints Controller 3, SS

Name	Weight	Rate Weight
Engine Torque	10	1
Brake Force left	0	0.1
Brake Force right	0	0.1
s left	1000	-
s right	1000	-
Ang vel diff	100	-
Prediction horizon (intervals)		15
Control horizon (intervals)		3
Overall weight		0.2

Table A.21: Weights and values Controller 3, US

Name	Minimum	Maximum
λ_L	0	1
λ_R	0	1
Ang vel diff	-	-

Table A.22: Output constraints Controller 3, US

Name	Weight	Rate Weight
Engine Torque	10	1
Brake Force left	0	0.1
Brake Force right	0	0.1
s left	1000	-
s right	1000	-
Ang vel diff	100	-
Prediction horizon (intervals)		15
Control horizon (intervals)		3
Overall weight		0.2

Table A.23: Weights and values Controller 3, SU

Name	Minimum	Maximum
λ_L	0	1
λ_R	0	1
Ang vel diff	-	-

Table A.24: Output constraints Controller 3, SU

Name	Weight	Rate Weight
Engine Torque	10	1
Brake Force left	0	1
Brake Force right	0	1
s left	100	-
s right	100	-
Ang vel diff	10	-
Prediction horizon (intervals)		15
Control horizon (intervals)		3
Overall weight		0.3

Table A.25: Weights and values Controller 3, UU

Name	Minimum	Maximum
λ_L	-	-
λ_R	-	-
Ang vel diff	-	-

Table A.26: Output constraints Controller 3, UU

k_1	1800
k_2	-480
λ_{max}	0.08

Table A.27: Values of linearization parameters, Controller 3